2017

Cortical Mechanisms Of Adaptation In Auditory Processing

Ryan Natan
University of Pennsylvania, rnatan@mail.med.upenn.edu

Cortical Mechanisms Of Adaptation In Auditory Processing

Abstract
Adaptation is computational strategy that underlies sensory nervous systems' ability to accurately encode stimuli in various and dynamic contexts and shapes how animals perceive their environment. Many questions remain concerning how adaptation adjusts to particular stimulus features and its underlying mechanisms. In Chapter 2, we tested how neurons in the primary auditory cortex adapt to changes in stimulus temporal correlation. We used chronically implanted tetrodes to record neuronal spiking in rat primary auditory cortex during exposure to custom made dynamic random chord stimuli exhibiting different levels of temporal correlation. We estimated linear non-linear model for each neuron at each temporal correlation level, finding that neurons compensate for temporal correlation changes through gain-control adaptation. This experiment extends our understanding of how complex stimulus statistics are encoded in the auditory nervous system. In Chapter 3 and 4, we tested how interneurons are involved in adaptation by optogenetically suppressing parvalbumin-positive (PV) and somatostatin-positive (SOM) interneurons during tone train stimuli and using silicon probes to record neuronal spiking in mouse primary auditory cortex. In Chapter 3, we found that inhibition from both PVs and SOMs contributes to stimulus-specific adaptation (SSA) through different mechanisms. SOM inhibition was stimulus-specific, suppressing responses to standard tones more strongly than responses to deviant tones, and increasing with standard tone repetition. PVs amplified SSA because inhibition was similar for standard and deviant tones and PV mediated inhibition was insensitive to tone repetition. PVs and SOMs themselves exhibit SSA, and a Wilson-Cowan dynamic model identified that PVs and SOMs can directly contribute to SSA in pyramidal neurons. In Chapter 4, we tested how SOMs and PVs inhibition is modulated with the dynamics of adaptation and across frequency tuning, during exposure to single frequency tone trains across the neuron's tuning curve. We found that the magnitude of SOM inhibition correlated with the magnitude of adaptive suppression, while PVs inhibition was largely insensitive to stimulus conditions. Together Chapters 3 and 4 implicate SOM inhibition in actively suppressing responses in a stimulus-specific manner while PV inhibition may passively enhance stimulus-specific suppression. These experiments inform the underlying principles and mechanisms of cortical sensory adaptation.

Degree Type
Dissertation

Degree Name
Doctor of Philosophy (PhD)

Graduate Group
Neuroscience

First Advisor
Maria N. Geffen

Keywords
Adaptation, Auditory, Cortex, Inhibition, Interneuron

CORTICAL MECHANISMS OF ADAPTATION IN AUDITORY PROCESSING

Ryan G Natan

A DISSERTATION

In

Neuroscience

Presented to the Faculties of the University of Pennsylvania

In

Partial Fulfillment of the Requirements for the
Degree of Doctor of Philosophy

2017

Supervisor of Dissertation

_____
Maria Neimark Geffen, PhD
Assistant Professor of Otorhinolaryngology

Graduate Group Chairperson

_____
Joshua I. Gold, PhD
Professor of Neuroscience

Dissertation Committee
Yale Cohen, Associate Professor of Otorhinolaryngology
Diego Contreras, Professor of Neuroscience
Christopher Fang-Yen, Assistant Professor of Neuroscience
Robert Froemke, Assistant Professor of Otolaryngology, Physiology & Neuroscience, NYU

This dissertation is dedicated to my family. I simply could not have achieved my goals without the boundless love and support of my mother, father, brother, and especially my wife Kathy.

Thanks, I love you!

ACKNOWLEDGMENTS

I would like to express my utmost gratitude to my advisor, Maria Neimark Geffen, for providing fantastic mentorship in my education, lab work and scientific career. It has been a wonderful experience to learn and grow under the guidance of a genuine friend and inspiring individual. Thanks to Yale Cohen, Diego Contreras, Chris Fang-Yen and Robert Froemke for serving on my thesis committee and helping me make the most of my graduate training. Thanks in addition to Mark Aizenberg, Jennifer Blackwell, John Briguglio, Isaac Carruthers, Laetitia Mwilambwe-Tshilobo, Winnie Rao, and current and former members of the Geffen Lab – it has been a great pleasure working with you. Thanks finally to the students, faculty and administration of the Neuroscience Graduate Group, who have cultivated a uniquely rewarding graduate training experience.

ABSTRACT

CORTICAL MECHANISMS OF ADAPTATION IN AUDITORY PROCESSING

Ryan G Natan

Maria Neimark Geffen

Adaptation is computational strategy that underlies sensory nervous systems' ability to accurately encode stimuli in various and dynamic contexts and shapes how animals perceive their environment. Many questions remain concerning how adaptation adjusts to particular stimulus features and its underlying mechanisms. In Chapter 2, we tested how neurons in the primary auditory cortex adapt to changes in stimulus temporal correlation. We used chronically implanted tetrodes to record neuronal spiking in rat primary auditory cortex during exposure to custom made dynamic random chord stimuli exhibiting different levels of temporal correlation. We estimated linear non-linear model for each neuron at each temporal correlation level, finding that neurons compensate for temporal correlation changes through gain-control adaptation. This experiment extends our understanding of how complex stimulus statistics are encoded in the auditory nervous system. In Chapter 3 and 4, we tested how interneurons are involved in adaptation by optogenetically suppressing parvalbumin-positive (PV) and somatostatin-positive (SOM) interneurons during tone train stimuli and using silicon probes to record neuronal spiking in mouse primary auditory cortex. In Chapter 3, we found that inhibition from both PVs and SOMs contributes to stimulus-specific adaptation (SSA) through different mechanisms. SOM inhibition was stimulus-specific, suppressing

responses to standard tones more strongly than responses to deviant tones, and increasing with standard tone repetition. PVs amplified SSA because inhibition was similar for standard and deviant tones and PV mediated inhibition was insensitive to tone repetition. PVs and SOMs themselves exhibit SSA, and a Wilson-Cowan dynamic model identified that PVs and SOMs can directly contribute to SSA in pyramidal neurons. In Chapter 4, we tested how SOMs and PVs inhibition is modulated with the dynamics of adaptation and across frequency tuning, during exposure to single frequency tone trains across the neuron's tuning curve. We found that the magnitude of SOM inhibition correlated with the magnitude of adaptive suppression, while PVs inhibition was largely insensitive to stimulus conditions. Together Chapters 3 and 4 implicate SOM inhibition in actively suppressing responses in a stimulus-specific manner while PV inhibition may passively enhance stimulus-specific suppression. These experiments inform the underlying principles and mechanisms of cortical sensory adaptation.

TABLE OF CONTENTS

LIST OF FIGURES

1. Introduction

In order to contain a detailed and accurate model of its sensory environment, an organism's sensory systems must operate in an extremely wide variety of sensory contexts to extract and encode a similarly wide variety of behaviorally relevant signals. Yet the computational capacity of neurons within any particular brain region is restricted by physiological limitations such as their number, connectivity patterns, and temporal constraints. Accordingly, the nervous system must employ strategies that increase the efficiency of sensory encoding and extract relevant stimulus features. Barlow proposed that adaptive processes, i.e. a sensory coding scheme sensitive to context, could circumvent these physiological limitations (Barlow, 1969). Further, adaptive models could simultaneously explain perceptual phenomena, such as visual after effects, and the underlying cortical spiking activity in response to particular visual stimuli (Blakemore, 1993). Since Barlow's work, a multitude of studies have demonstrated that adaptation is a canonical computation employed widely across species and sensory modalities (Solomon and Kohn, 2014). Despite our recognition that adaptation is ubiquitous in the sensory nervous system, we still lack a complete understanding of its range of sensitivity to stimulus context, functional purpose and underlying mechanisms. This is especially true for the mammalian sensory cortex, where adaptation can directly impact sensory perception and sensory guided behaviors.

Cortical adaptation is controlled by a combination of changes in synaptic connectivity and network level dynamics. In particular, the interplay of plasticity among excitatory and inhibitory neuron in the cortex has been proposed to control the many aspects of sensory adaptation (Schummers et al., 2005). The goal of this work is to discover the underlying principles and mechanism of adaptation. Observed in various forms throughout the brain, here we focus entirely on aspects of adaptation measureable from neuronal spiking rates in the primary auditory cortex. This approach allows us to observe the dynamics of cortical adaptation and then test models of adaptation, leading to a fuller understanding of the underlying mechanism. To introduce this topic, we will describe known forms and functions of sensory neuronal adaptation, and explore the known and potential underlying mechanisms.

The roles of adaptation in auditory sensation

Sensory adaptation is broadly defined as a stimulus-context dependent adjustment of neuronal responses to stimuli that improves sensory performance. In its simplest form, individual sensory neurons exhibit adaptive adjustment; after either a persistent increase or decrease in the intensity of a stimulus falling within a neuron's receptive field, the strength of its stimulus-evoked responses is either attenuated or enhanced, respectively. This means that neuronal stimulus-response transfer functions scale in an opposing direction to compensate for changes in the stimulus context. At this stage, the adaptive response matches the dynamic range of the stimulus, thereby

adjusting the resolution of neuronal stimulus encoding. Indeed, this phenomenon has been found in all sensory modalities and within every stage of sensory processing. In the auditory nervous system, dynamic range adaptation has been demonstrated starting from cochlear transduction (Ross, 1996) to the auditory nerve (Wen et al., 2012), the brainstem (Kawase et al., 1993) and the midbrain (Dean et al., 2008). Dynamic range adaptation is further observed in the auditory cortex: Phillips (1985) recorded spiking responses from auditory cortical neurons in the anesthetized cat, and measured a sigmoid response to center frequency tones over a range of intensities. The presence of broadband noise, overlapping the center frequency tone, attenuated responses across frequencies. Upon terminating the noise stimulus, sensitivity to tone intensity quickly recovered (Figure 1.1). Confirming the link between adaptation and expanding dynamic range, Simpson and Reiss (2013) produced a model showing that the neural codes at these different auditory stations adjust sensitivity to a wide range of absolute loudness,

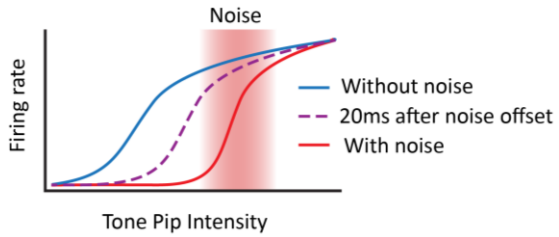

Figure 1.1. Dynamic range adaptation. In silence, the firing rate in response to a tone pip exhibits a sigmoidal increase with the pip's intensity (blue). In this regime, a range of low intensity pips evoke widely differential firing rate responses, but high intensities are saturated. If high intensity noise (shading) is played during tone pip presentation, the intensity-response curve (red) shifts rightward, so that high intensity sounds evoke differential firing rates (red). The temporal dynamics of adaptation are revealed by measuring an intermediate curve moments after noise offset, as adaptation is shifting from one regime to another (purple). Adapted from Phillips (Phillips, 1985).

and adaptation wide range of absolute loudness, and adaptation in downstream auditory brain regions further enhances sensitivity to small intensity changes over a wide dynamic range. Since adaptation is observed in the auditory cortex, it can directly shape auditory perception, compressing the experience of environmental sound. Analogous examples of dynamic range adaptation can be found in the visual (Fairhall et al., 2001; Ohzawa et al., 1982) and somatosensory (Adibi et al., 2013; Maravall et al., 2007) systems. These studies show that adaptation of the stimulus-response functions in single neurons enhances dynamic range and discriminability.

Further benefits to efficient stimulus encoding emerge from the ensemble activity of adapting neurons. Brain areas in the sensory pathway are comprised of individually feature-tuned units undergoing adaptation. It has been predicted that in order to maximize encoding efficiency, the set of neuronal tuning parameters should be distributed across units (Barlow et al., 1989). Building on these efficient coding principles, studies found that adaptation of individual neurons, coordinated over a population, can lead to improved sensory performance as measured neurometrically (Wark et al., 2007). For example, adaptation in a neuronal population may serve to sharpen acuity for particular stimulus features such as variance and contrast of sound intensity levels. In the inferior colliculus, changes in the distribution of sound intensity levels within a broadband stimulus led to adaptive adjustments of varied magnitude among intensity-tuned neurons. Calculating Fischer information across the population, Dean et al. (2005) demonstrated that distributed adaptation strengths maximize

encoding efficiency by increasing sensitivity to high probability sound levels. In the avian auditory forebrain, analogous to the mammalian auditory cortex, neurons differentially adapt to multiple dimensions of sound intensity thereby efficiently increasing stimulus information encoded by the population (Sharpee et al., 2011). Using broadband stimuli with rapidly varying intensity, these studies revealed gain-like input-response modulation across whole receptive field that improves dynamic range and population encoding.

In response to narrow band stimulus features, adaptation can also modulate the shape of the neuronal receptive field, especially in higher cortical areas, leading to improved sensory encoding. Stimulus-specific adaptation, or SSA in single neurons, refers to a selectively attenuated response to frequent stimuli (standard stimulus), whereas responses to rare stimuli remain unchanged or often enhanced. SSA exhibited within the receptive field of single neurons has been studied heavily throughout the auditory nervous system using oddball stimuli (Figure 1.2). Within the ascending lemniscal auditory pathway, the strength, prominence and complexity of SSA increases, and the primary auditory cortex is the first station in the auditory pathway exhibiting strong and widespread SSA (Khouri and Nelken, 2015). As measured in the primary auditory cortex, SSA is sensitive to various stimulus parameters such as tone frequency and intensity (Ulanovsky et al., 2003), time scale of repetition (Ulanovsky et al., 2004) and regularity (Yaron et al., 2012). SSA improves sensory encoding and underlies the detection of salient stimuli. By calculating discriminability between common and rare

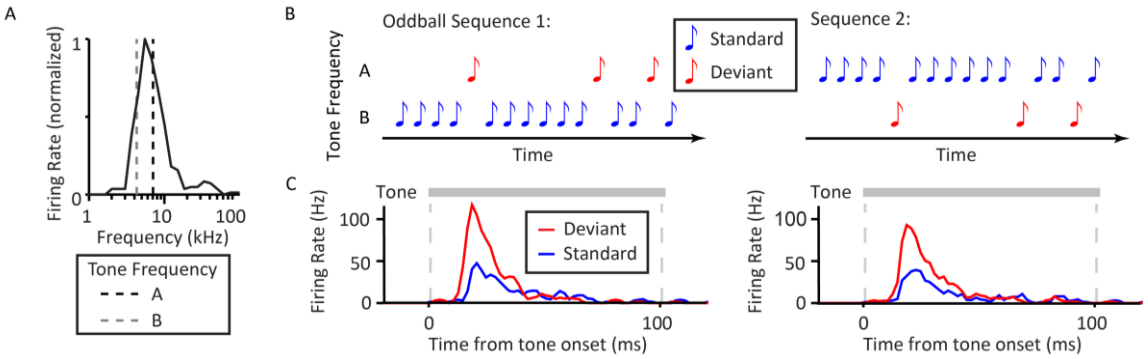

Figure 1.2. Stimulus-specific adaptation. A) Frequency-response curve of a neuron in primary auditory cortex. Dashed lines indicate the frequencies chosen to construct oddball stimuli. B) Oddball stimulus sequences. Left: Tone B is the standard tone, repeated more frequently than tone A, the deviant tone. Right: Tone probabilities are swapped. C) PSTH of the same neuron in A response to each sequence. Regardless of the frequency, the neuron responds more strongly to the deviant tone than to the standard tone. Adapted from Natan et al., 2015.

pure tones, Ulanovksy et al. (2003) showed that SSA in cortical neurons increases population sensitivity to small differences in frequency, thus improving frequency discrimination. Demonstrating that SSA in cortex resembles deviance detection, Taaseh et al. (2011) showed that the excitatory response to a rare stimulus is stronger when in the context of a standard tone as compared to many rare tones. SSA is an important part of sensory adaptation, which increases sensitivity to salient stimuli.

Adaptive modulations exhibited by the auditory cortex may underlie sensory perception and support sensory guided behaviors. Adaptation in auditory cortex parallels the perception of sound. A psychophysical phenomenon termed 'forward masking' describes the disrupted perception of a sound stimulus if it is presented immediately after a prior sound stimulus (Recanzone and Sutter, 2008). Resembling dynamic range adaptation, an analogous reduction in neuronal spiking response, termed

'forward suppression', has been measured along the auditory pathway, from the cochlear nucleus (Ingham et al., 2016), to the inferior colliculus (Nelson et al., 2009) and auditory cortex (Wehr and Zador, 2005). In parallel with psychophysical masking, neurometric masking specific to the auditory cortex extends to dynamic aspects of stimuli; Forward masking for sine amplitude modulated noise stimuli is more prominent in the auditory cortex (Wojtczak and Viemeister, 2005) than in the inferior colliculus (Wojtczak et al., 2011). Together, these studies show that modulations of stimulus-evoked responses in cortical activity due to stimulus context resemble and likely underlie features of sound perception.

Adaptive phenomena such as SSA may also directly shape perception. Repetition-dependent attenuation of specific frequency channels could describe a frequency-specific form of forward suppression. Indeed, forward masking also extends into the frequency modulation domain (Byrne et al., 2012), thus SSA may underlie this feature of perception as well. Since adaptation increases tuning acuity through stimulus-specific attenuation in cortical neurons, it could increase an animal's ability to discriminate between stimuli and simultaneously reduce the ability to detect weaker stimuli. This link between adaptation and perception guided behavior has been established in another modality; tactile stimulus repetition leading to attenuated somatosensory cortex responses lead to both improved stimulus discrimination and reduced stimulus detection both behaviorally and neurometrically (Musall et al., 2014; Zheng et al., 2015). While auditory SSA has not yet been directly linked to auditory

perception through behavioral assay, it is thought to underlie other neural correlates of perceived deviance detection such as the mismatch negativity (Grimm et al., 2012). Together, these findings point to SSA as a mechanism that improves stimulus perception in a context-dependent manner.

Adaptation in models of sensory encoding

In order to understand the biophysics and dynamics of adapting neurons, researchers have adopted a number of computational modeling approaches. Static models of neuronal response properties have informed our understanding of sensory encoding, but fail to predict responses to more complex stimuli. The linear non-linear model is popular framework for describing the response properties of sensory neurons, and consists of a linear spectro-temporal stimulus filter i.e., the receptive field, and a non-linearity i.e., an input-output transfer function (Eggermont et al., 1983). The basic model assumes a static linear filter and non-linearity that are fitted using a single spectro-temporal decomposition of the stimulus to the response, which can be used to predict responses to other stimuli (Figure 1.3). Such models provide qualitative descriptions of neuronal response properties, but spike train prediction accuracy declines rapidly in downstream stages of the auditory pathway, even between different cell types of the cochlear nucleus (Nelken et al., 1997). Downstream auditory areas are increasingly tuned to encode features of natural stimuli, containing spectro-temporal correlations (Escabi et al., 2003). Decorrelation methods have been applied to linear non-linear

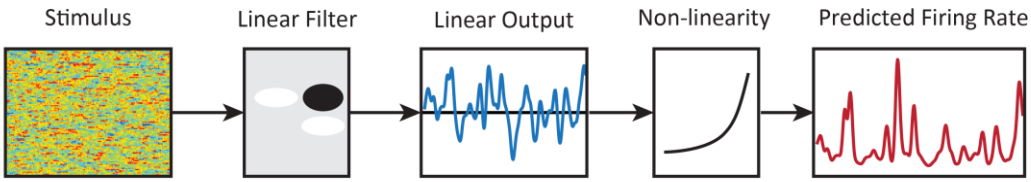

Figure 1.3. Linear non-linear model. A spectro-temporal decomposition of the stimulus (Stimulus) is convolved with the model's estimated spectro-temporal receptive field (Linear Filter), producing a prediction of the neuron's response intensity (Linear Output). The linear output is is passed through the model's estimated look-up table (non-linearity) to produce a predicted firing rate (Predicted Firing Rate).

model fitting in order to compensate for correlated stimulus features, only slightly improving the model's prediction quality (Machens et al., 2004; Carruthers et al., 2013). Static models of auditory neurons fail to capture the dynamics of sensory responses.

Models that include adaptive processes describe the response properties of auditory cortical neurons more accurately than static models. Auditory cortical neurons are able to encode stimuli exhibiting a wide range of broadband spectro-temporal contrast, yet models fitted to one level of stimulus contrast fail to accurately predict responses to other contrast levels. Comparing across models of neuronal responses fitted for each contrast level, the gain of the non-linearity is adjusted to compensate for changes in stimulus contrast (Rabinowitz et al., 2011). This adaptive adjustment in the non-linearity, referred to as gain control, confers sensitivity to broadband stimulus features and expands the encoded dynamic range. Adding to this adaptive functionality in Chapter 2, we describe how adaptive gain control of the non-linearity in linear non-linear models confers sensitivity to the broadband temporal correlation, another naturalistic stimulus feature. Incorporating adaptation in separate frequency specific

input channels further improves prediction quality, especially for natural sounds (Willmore et al., 2016). Rather than relying on a set of separate model parameters for each stimulus context, adaptation dynamically responds to naturalistic stimulus changes within the stimulus timecourse in a physiologically plausible manner. Each of these models incorporates adaptation that accounts for stimulus context and generate more accurate descriptions of neural activity, but what mechanism may underlie these modulations?

Synaptic depression has been proposed as a primary mechanism underlying adaptation. Some models of auditory response properties explicitly include adaptation analogous to synaptic depression by applying context dependent attenuation across an array of input channels (Wehr and Zador, 2005). In one such model, independent channels are defined by a range of depression latencies, and are better able to encode the temporal dynamics of a natural sound than a typical linear non-linear model (David and Shamma, 2013). Models that carefully replicate the dynamics of cortical synaptic depression in independent inputs display gain-control (Abbott et al., 1997). Stimulus-history dependent attenuation of individually frequency tuned inputs generates responses to oddball stimuli that resemble SSA (Mill et al., 2011). These models are physiologically plausible since cortical neurons receive narrowly tuned thalamocortical input which exhibit strong depression (Miller et al., 2001). However, these models fail to capture some critical features of SSA in auditory cortex (Nelken, 2014). Due to the constrained timescales of plasticity and channel independence, synaptic depression

models fail to replicate adaptation at multiple timescales (Ulanovsky et al., 2004), sensitivity to complex sequence irregularities (Yaron et al., 2012) or signatures of deviance detection (Hershenhoren et al., 2014). Whereas short-term synaptic plasticity accounts for some aspects of adaptation, the circuit-level properties can further contribute to our understanding of this phenomenon.

At the level of cortical excitatory-inhibitory circuits, adaptation may be supported by cortical inhibitory interneurons. Similar to synaptic depression, various inhibitory synapses are situated to provide a rectifying signal to compensate for changes in stimulus statistics. A common component among adaptive phenomena is compensatory scaling; both gain control and SSA each rely on a reduction in a neuron's stimulus-response function in response to prior high intensity stimulation. Inhibitory interneurons have been proposed as a possible mechanism of suppression in adaptation (Hershenhoren et al., 2014; Solomon and Kohn, 2014). Due to the variety of cortical interneurons, and the complexity of inhibitory circuitry, we are only beginning to understand the functional role of inhibitory interneurons in cortical sensory processing.

Inhibitory interneurons

Cortical interneurons take an enormous variety of forms. Recent technological developments have made it possible to label and target different classes of interneurons (Roux et al., 2014). Studies have converged on three broad but minimally overlapping classes of cortical interneurons: parvalbumin-positive (PV), somatostatin positive (SOM)

and vasoactive intestinal polypeptide-positive (VIP) neurons (Callaway, 2004; Rudy et al., 2011; Xu et al., 2010). Though PVs, SOMs and VIPs are each composed of several interneuronal subclasses, they are thought to express common characteristics within each class. These classes are differentiated by morphology, connectivity, and physiology (Figure 1.4). PVs, primarily composed of fast-spiking basket cells and chandelier cells, generally target the soma and proximal neurites of excitatory neurons and receive strongly depressing thalamocortical and pyramidal input (Ascoli et al., 2008). SOMs, primarily composed of late-spiking Martinotti cells, generally target the distal dendrites of excitatory neurons and receive input from facilitating synapses of pyramidal neurons (Rudy et al., 2011). VIPs, including regular-spiking bitufted interneurons, are notable for

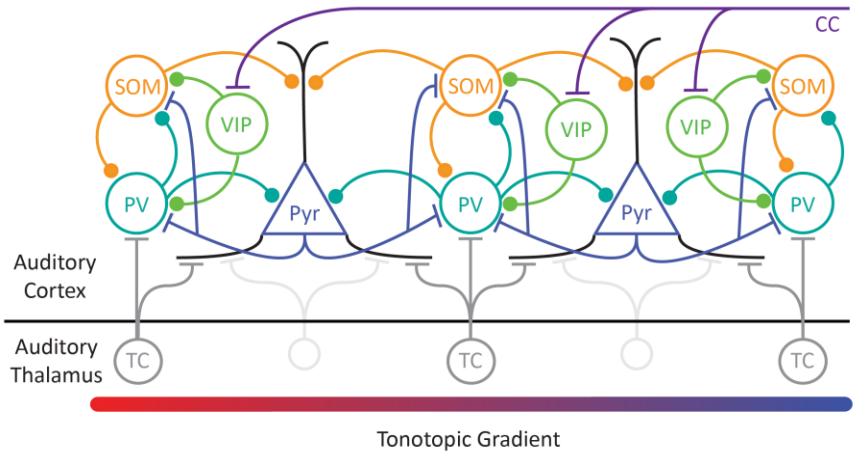

Figure 1.4. **Cortical connectivity between excitatory and inhibitory neurons in the auditory cortex.** Pyr: Excitatory neurons (blue), dendrites (black); PV: parvalbumin-positive interneurons (light blue); SOM: somatostatin-positive interneurons (orange); VIP: vasopressin-positive interneurons (Green); TC: Thalamo-cortical projection neurons (Gray). CC: Cortico-cortical projection (Purple) Flat lines: excitatory synapses; circles: inhibitory synapses.

primarily targeting other interneurons rather than pyramidal neurons and receiving strong cortico-cortical input (Acsady et al., 1996). Additionally, recent studies have also revealed a general hierarchy to inhibitory circuitry; PVs inhibit each other, SOMs strongly suppress PVs, while VIPs inhibit PVs and SOMs (Jiang et al., 2015; Pfeffer et al., 2013). While we lack a complete catalog of interneuronal subclasses, these differential attributes of PVs, SOMs, and VIPs hint at their unique functional roles.

Inhibitory interneurons are essential components of the cortex that shape auditory stimulus processing. Interneurons provide tuned inhibition to suppress stimulus-evoked responses in local pyramidal neurons. Intracellular recordings reveal that inhibitory inputs to cortical neurons are co-tuned with excitatory inputs (Volkov and Galuzjuk, 1992; Tan and Wehr, 2009; Wehr and Zador, 2003), although inhibition may be more broadly tuned in some pyramidal neurons (Wu et al., 2008). Such co-tuned inhibition shapes the dynamics of pyramidal neuron responses. Delayed stimulus-evoked inhibition restricts the stimulus input integration time-window (Gabernet et al., 2005), thus these interneurons truncate excitatory responses. Further, PVs, SOMs and VIPs are each driven by auditory stimuli and exhibit differential response properties. While SOM frequency tuning matches that of local pyramidal neurons, PVs and VIPs are more broadly tuned (Li et al., 2015; Mesik et al., 2015). Additionally, SOM and VIP sound evoked responses are delayed compared to those of PVs and pyramidal neurons. The extent of inhibitory and excitatory co-tuning can lead to sharpened frequency tuning among pyramidal neurons. Broadly tuned inhibition from PVs can increase spiking

thresholds across tuning, resulting in sharper frequency preference. The more sharply tuned SOMs, on the other hand, may drive sharpened tuning by suppressing specific subsets of inputs. Consistent with both of these possibilities, optogenetic activation of either PVs or SOMs lead to either subtractive, divisive or mixed modulations of pyramidal neuron tuning curves (Seybold et al., 2015). By modulating responses to sound, interneurons can effect auditory guided behavior. Aizenberg et al. (2015) showed that activating or suppressing PVs not only modulated neurometric frequency selectivity, but also modulated behavioral performance in a frequency discrimination task. PVs and SOMs are also central components of disinhibitory circuits that regulate auditory fear conditioning (Letzkus et al., 2011) and reinforcement learning (Pi et al., 2013). Since PVs and SOMs directly shape the dynamics and tuning of auditory-evoked responses in cortex, it is possible that inhibition also plays a role in adaptation.

Inhibition in adaptation

There are a variety of circuit configurations that could, in principle, enable inhibitory neurons to generate adaptation. Feedforward inhibition, in which stimulus-evoked signals are carried upstream by both excitatory and inhibitory neurons, could mediate fatigue-like adaptation similar to synaptic depression. Monosynaptic feedforward inhibition in the auditory pathway, mediated by GABAergic projections from the cochlear nucleus (Cant and Benson, 2003) or inferior colliculus (Winer et al., 1996), could carry an adaptive signal in parallel with excitation. In the cortex, however,

thalamocortical projections are exclusively excitatory (Lee and Sherman, 2008), so a disynaptic feed-forward pathway mediated by local inhibitory interneurons is the minimal circuit necessary to carry an inhibitory adaptive signal. PVs are most likely to underlie disynaptic feedforward inhibition in auditory cortex because PVs in all cortical layers receive strong and widespread thalamocortical input while SOMs and VIPs receive weaker thalamocortical input and only in layer 4 (Ji et al., 2016). Completing the feed-forward circuit, these neurons, especially PVs and SOMs, inhibit local thalamorecipient pyramidal neurons (Jiang et al., 2015; Pfeffer et al., 2013). By simply relaying and reversing the excitatory input signal, feedforward inhibition represents the most direct route for inhibition mediated adaptation.

Another possible inhibitory circuit configuration capable of mediating adaptation is local feedback inhibition. Signals drive excitation in pyramidal neurons which drive inhibition in turn, which recursively inhibits those same pyramidal neurons. There is physiological evidence for such reciprocal circuits in the auditory cortex especially for putative PV interneurons (Otsuka and Kawaguchi, 2009; Zaitsev and Lewis, 2013). SOMs and PVs are ideal candidates for mediating adaptive signaling through feedback or feedforward inhibition.

Lastly, top down inhibition provides a highly flexible circuit configuration for mediating complex forms of context dependent adaptation. PVs, SOMs and VIPs in auditory cortex are strongly modulated by corticocortical projections (Pi et al., 2013; Schneider et al., 2014), and may also be subject to multimodal modulation.

Neuromodulatory projections also strongly modulate PV, SOM and VIP interneurons during changes in stimulus and behavioral contexts (Kuchibhotla et al., 2016). Together, these three circuit motifs provide a variety of potential mechanisms through which inhibition may underlie stimulus dependent adaptive modulations.

Interneurons are capable of generating adaptive signals, as evidenced by their ability to modulate sensory responses. Both PVs and SOMs can impose subtractive and divisive modulation on local pyramidal neurons (Seybold et al., 2015; Phillips and Hasenstaub, 2016). Thus when integrated into feed forward or feedback circuit motifs, interneurons could reasonably underlie stimulus history specific modulations of stimulus-evoked responses such as gain-control. Adaptation generated by feedforward inhibition would resemble the modulatory properties of synaptic depression and are, therefore, similarly unable explain complex phenomena such as cortical SSA (Nelken, 2014). However, the inhibitory feedback motif provides interneurons with more complex adaptive mechanism. Additionally, PVs, SOMs, VIPs and their interneuron subclasses each exhibit differential short-term synaptic plasticity characteristics. SOMs, for example, uniquely exhibit strongly facilitating recurrent synaptic activity (Hoy et al., 2016). Circuits involving multiple levels of synaptic plasticity allow for increasingly non-linear stimulus response properties. In somatosensory cortex, inhibitory post-synaptic potentials recover from adaptation more slowly than excitatory which leads to facilitation after adaptation (Cohen-Kashi Malina et al., 2013). Even if synaptic strengths are held static, adaptation can arise from highly recurrent inhibitory and excitatory

cortical connections (Del Mar Quiroga et al., 2016). Thus it could be possible that differential response timings produce adaptation over different time scales. Stimulus-specific inhibitory facilitation or recurrent connectivity may underlie the unique properties that define cortical SSA.

Recent experimental findings directly implicate cortical inhibition in SSA. In intracellular recordings from pyramidal neurons in primary auditory cortex, the stimulus-specific modulations of postsynaptic inhibitory potentials suggest that PV and SOM mediated local inhibition both adapt to repeated tones (Chen et al., 2015). Interestingly, while both PVs and SOMs could mediate some portion of the adaptive effect, SOM inhibition displays signatures of true deviance detection. We postulated that PV or SOM inhibition underlies SSA. In Chapter 3, we test use optogenetic manipulation to test how PVs and SOMs inhibit deviant versus standard tones. In chapter 4, we test the role of SOM and PV inhibition in generalized adaptation across auditory tuning curves.

Given the central role adaptation plays in perception and behavior, and our lack of understanding its underlying mechanisms, we have investigated the extent of adaptive responses and the strongest candidates for mediation of adaptation. In an effort to more clearly understand the role of context specific adaptation in sensory coding, we focused on adaptation in the primary auditory cortex due to these well-established adaptation paradigms. Our findings herein help illuminate suppressive mechanisms

underlying cortical sensory adaptation and shape future models of sensory processing of complex stimuli.

Bibliography

Abbott, L.F., Varela, J.A., Sen, K., Nelson, S.B., 1997. Synaptic depression and cortical gain control. Science 275, 220-224.

Acsady, L., Gorcs, T.J., Freund, T.F., 1996. Different populations of vasoactive intestinal polypeptide-immunoreactive interneurons are specialized to control pyramidal cells or interneurons in the hippocampus. Neuroscience 73, 317-334.

Adibi, M., McDonald, J.S., Clifford, C.W., Arabzadeh, E., 2013. Adaptation improves neural coding efficiency despite increasing correlations in variability. J Neurosci 33, 2108-2120.

Aizenberg, M., Mwilambwe-Tshilobo, L., Briguglio, J.J., Natan, R.G., Geffen, M.N., 2015. Bidirectional Regulation of Innate and Learned Behaviors That Rely on Frequency Discrimination by Cortical Inhibitory Neurons. PLoS Biol 13, e1002308.

Barlow, H.B., 1969. Trigger Features, Adaptation and Economy of Impulses, in: Leibovic, K.N. (Ed.), Information Processing in The Nervous System: Proceedings of a Symposium held at the State University of New York at Buffalo 21st–24th October, 1968. Springer Berlin Heidelberg, Berlin, Heidelberg, pp. 209-230.

Barlow, H.B., Kaushal, T.P., Mitchison, G.J., 1989. Finding minimum entropy codes. Neural Comput 1, 412-423.

Blakemore, C., 1993. Vision: Coding and Efficiency. Cambridge University Press.

Byrne, A.J., Wojtczak, M., Viemeister, N.F., 2012. Forward masking of frequency modulation. J Acoust Soc Am 132, 3375-3386.

Callaway, E.M., 2004. Feedforward, feedback and inhibitory connections in primate visual cortex. Neural Netw 17, 625-632.

Cant, N.B., Benson, C.G., 2003. Parallel auditory pathways: projection patterns of the different neuronal populations in the dorsal and ventral cochlear nuclei. Brain Res Bull 60, 457-474.

Carruthers, I.M., Natan, R.G., Geffen, M.N., 2013. Encoding of ultrasonic vocalizations in the auditory cortex. J Neurophysiol 109, 1912-1927.

Chen, S.X., Kim, A.N., Peters, A.J., Komiyama, T., 2015. Subtype-specific plasticity of inhibitory circuits in motor cortex during motor learning. Nat Neurosci 18, 1109-1115.

Cohen-Kashi Malina, K., Jubran, M., Katz, Y., Lampl, I., 2013. Imbalance between excitation and inhibition in the somatosensory cortex produces postadaptation facilitation. J Neurosci 33, 8463-8471.

David, S.V., Shamma, S.A., 2013. Integration over multiple timescales in primary auditory cortex. J Neurosci 33, 19154-19166.

Dean, I., Harper, N.S., McAlpine, D., 2005. Neural population coding of sound level adapts to stimulus statistics. Nat Neurosci 8, 1684-1689.

Dean, I., Robinson, B.L., Harper, N.S., McAlpine, D., 2008. Rapid neural adaptation to sound level statistics. J Neurosci 28, 6430-6438.

Del Mar Quiroga, M., Morris, A.P., Krekelberg, B., 2016. Adaptation without Plasticity. Cell Rep 17, 58-68.

Eggermont, J.J., Johannesma, P.M., Aertsen, A.M., 1983. Reverse-correlation methods in auditory research. Q Rev Biophys 16, 341-414.

Escabi, M.A., Miller, L.M., Read, H.L., Schreiner, C.E., 2003. Naturalistic auditory contrast improves spectrotemporal coding in the cat inferior colliculus. J Neurosci 23, 11489-11504.

Fairhall, A.L., Lewen, G.D., Bialek, W., de Ruyter Van Steveninck, R.R., 2001. Efficiency and ambiguity in an adaptive neural code. Nature 412, 787-792.

Gabernet, L., Jadhav, S.P., Feldman, D.E., Carandini, M., Scanziani, M., 2005. Somatosensory integration controlled by dynamic thalamocortical feed-forward inhibition. Neuron 48, 315-327.

Grimm, S., Recasens, M., Althen, H., Escera, C., 2012. Ultrafast tracking of sound location changes as revealed by human auditory evoked potentials. Biol Psychol 89, 232-239.

Hershenhoren, I., Taaseh, N., Antunes, F.M., Nelken, I., 2014. Intracellular correlates of stimulus-specific adaptation. J Neurosci 34, 3303-3319.

Hoy, J.L., Yavorska, I., Wehr, M., Niell, C.M., 2016. Vision Drives Accurate Approach Behavior during Prey Capture in Laboratory Mice. Curr Biol.

Ingham, N.J., Itatani, N., Bleeck, S., Winter, I.M., 2016. Enhancement of forward suppression begins in the ventral cochlear nucleus. Brain Res 1639, 13-27.

Ji, X.Y., Zingg, B., Mesik, L., Xiao, Z., Zhang, L.I., Tao, H.W., 2016. Thalamocortical Innervation Pattern in Mouse Auditory and Visual Cortex: Laminar and Cell-Type Specificity. Cereb Cortex 26, 2612-2625.

Jiang, X., Shen, S., Cadwell, C.R., Berens, P., Sinz, F., Ecker, A.S., Patel, S., Tolias, A.S., 2015. Principles of connectivity among morphologically defined cell types in adult neocortex. Science 350, aac9462.

Kawase, T., Delgutte, B., Liberman, M.C., 1993. Antimasking effects of the olivocochlear reflex. II. Enhancement of auditory-nerve response to masked tones. J Neurophysiol 70, 2533-2549.

Khouri, L., Nelken, I., 2015. Detecting the unexpected. Curr Opin Neurobiol 35, 142-147.

Kuchibhotla, K.V., Gill, J.V., Lindsay, G.W., Papadoyannis, E.S., Field, R.E., Sten, T.A., Miller, K.D., Froemke, R.C., 2016. Parallel processing by cortical inhibition enables context-dependent behavior. Nat Neurosci.

Lee, C.C., Sherman, S.M., 2008. Synaptic properties of thalamic and intracortical inputs to layer 4 of the first- and higher-order cortical areas in the auditory and somatosensory systems. J Neurophysiol 100, 317-326.

Letzkus, J.J., Wolff, S.B., Meyer, E.M., Tovote, P., Courtin, J., Herry, C. and Lüthi, A., 2011. A disinhibitory microcircuit for associative fear learning in the auditory cortex. Nature 480, 331-335.

Li, L.Y., Xiong, X.R., Ibrahim, L.A., Yuan, W., Tao, H.W., Zhang, L.I., 2015. Differential Receptive Field Properties of Parvalbumin and Somatostatin Inhibitory Neurons in Mouse Auditory Cortex. Cereb Cortex 25, 1782-1791.

Machens, C., Wehr, M., Zador, A., 2004. Linearity of cortical receptive fields measured with natural sounds. J Neurosci 24, 1089-1100.

Maravall, M., Petersen, R.S., Fairhall, A.L., Arabzadeh, E., Diamond, M.E., 2007. Shifts in coding properties and maintenance of information transmission during adaptation in barrel cortex. PLoS Biol 5, e19.

Mesik, L., Ma, W.P., Li, L.Y., Ibrahim, L.A., Huang, Z.J., Zhang, L.I., Tao, H.W., 2015. Functional response properties of VIP-expressing inhibitory neurons in mouse visual and auditory cortex. Front Neural Circuits 9, 22.

Mill, R., Coath, M., Wennekers, T., Denham, S.L., 2011. Abstract stimulus-specific adaptation models. Neural Comput 23, 435-476.

Miller, L.M., Escabi, M.A., Read, H.L., Schreiner, C.E., 2001. Functional convergence of response properties in the auditory thalamocortical system. Neuron 32, 151-160.

Musall, S., von der Behrens, W., Mayrhofer, J.M., Weber, B., Helmchen, F., Haiss, F., 2014. Tactile frequency discrimination is enhanced by circumventing neocortical adaptation. Nat Neurosci 17, 1567-1573.

Nelken, I., 2014. Stimulus-specific adaptation and deviance detection in the auditory system: experiments and models. Biol Cybern.

Nelken, I., Kim, P.J., Young, E.D., 1997. Linear and non-linear spectral integration in type IV neurons of the dorsal cochlear nucleus. II. Predicting responses with the use of non-linear models. J Neurophysiol 78, 800-811.

Nelson, P.C., Smith, Z.M., Young, E.D., 2009. Wide-dynamic-range forward suppression in marmoset inferior colliculus neurons is generated centrally and accounts for perceptual masking. J Neurosci 29, 2553-2562.

Ohzawa, I., Sclar, G., Freeman, R.D., 1982. Contrast gain control in the cat visual cortex. Nature 298, 266-268.

Otsuka, T., Kawaguchi, Y., 2009. Cortical inhibitory cell types differentially form intralaminar and interlaminar subnetworks with excitatory neurons. J Neurosci 29, 10533-10540.

Ascoli, G.A., Alonso-Nanclares, L., Anderson, S.A., Barrionuevo, G., Benavides-Piccione, R., Burkhalter, A., Buzsaki, G., Cauli, B., Defelipe, J., Fairen, A., Feldmeyer, D., Fishell, G., Fregnac, Y., Freund, T.F., Gardner, D., Gardner, E.P., Goldberg, J.H., Helmstaedter, M., Hestrin, S., Karube, F., Kisvarday, Z.F., Lambolez, B., Lewis, D.A., Marin, O., Markram, H., Munoz, A., Packer, A., Petersen, C.C., Rockland, K.S., Rossier, J., Rudy, B., Somogyi, P., Staiger, J.F., Tamas, G., Thomson, A.M., Toledo-Rodriguez, M., Wang, Y., West, D.C., Yuste, R., 2008. Petilla terminology: nomenclature of features of GABAergic interneurons of the cerebral cortex. Nat Rev Neurosci 9, 557-568.

Pfeffer, C.K., Xue, M., He, M., Huang, Z.J., Scanziani, M., 2013. Inhibition of inhibition in visual cortex: the logic of connections between molecularly distinct interneurons. Nat Neurosci 16, 1068-1076.

Phillips, D.P., 1985. Temporal response features of cat auditory cortex neurons contributing to sensitivity to tones delivered in the presence of continuous noise. Hear Res 19, 253-268.

Phillips, E.A., Hasenstaub, A.R., 2016. Asymmetric effects of activating and inactivating cortical interneurons. Elife 5.

Pi, H.J., Hangya, B., Kvitsiani, D., Sanders, J.I., Huang, Z.J., Kepecs, A., 2013. Cortical interneurons that specialize in disinhibitory control. Nature 503, 521-524.

Rabinowitz, N.C., Willmore, B.D., Schnupp, J.W., King, A.J., 2011. Contrast gain control in auditory cortex. Neuron 70, 1178-1191.

Recanzone, G.H., Sutter, M.L., 2008. The biological basis of audition. Annu Rev Psychol 59, 119-142.

Ross, S., 1996. A functional model of the hair cell-primary fiber complex. J Acoust Soc Am 99, 2221-2238.

Roux, L., Stark, E., Sjulson, L., Buzsaki, G., 2014. In vivo optogenetic identification and manipulation of GABAergic interneuron subtypes. Curr Opin Neurobiol 26, 88-95.

Rudy, B., Fishell, G., Lee, S., Hjerling-Leffler, J., 2011. Three groups of interneurons account for nearly 100% of neocortical GABAergic neurons. Dev Neurobiol 71, 45-61.

Schneider, D.M., Nelson, A., Mooney, R., 2014. A synaptic and circuit basis for corollary discharge in the auditory cortex. Nature 513, 189-194.

Schummers, J., Sharma, J., Sur, M., 2005. Bottom-up and top-down dynamics in visual cortex. Prog Brain Res 149, 65-81.

Seybold, B.A., Phillips, E.A., Schreiner, C.E., Hasenstaub, A.R., 2015. Inhibitory Actions Unified by Network Integration. Neuron 87, 1181-1192.

Sharpee, T., Atencio, C., Schreiner, C., 2011. Hierarchical representations in the auditory cortex. Curr Opin Neurobiol.

Simpson, A.J., Reiss, J.D., 2013. The dynamic range paradox: a central auditory model of intensity change detection. PLoS One 8, e57497.

Solomon, S.G., Kohn, A., 2014. Moving sensory adaptation beyond suppressive effects in single neurons. Curr Biol 24, R1012-1022.

Taaseh, N., Yaron, A., Nelken, I., 2011. Stimulus-specific adaptation and deviance detection in the rat auditory cortex. PLoS One 6, e23369.

Tan, A.Y., Wehr, M., 2009. Balanced tone-evoked synaptic excitation and inhibition in mouse auditory cortex. Neuroscience 163, 1302-1315.

Ulanovsky, N., Las, L., Farkas, D., Nelken, I., 2004. Multiple time scales of adaptation in auditory cortex neurons. J Neurosci 24, 10440-10453.

Ulanovsky, N., Las, L., Nelken, I., 2003. Processing of low-probability sounds by cortical neurons. Nat Neurosci 6, 391-398.

Volkov, I.O., Galazyuk, A.V., 1992. Peculiarities of inhibition in cat auditory cortex neurons evoked by tonal stimuli of various durations. Exp Brain Res 91, 115-120.

Wark, B., Lundstrom, B.N., Fairhall, A., 2007. Sensory adaptation. Curr Opin Neurobiol 17, 423-429.

Wehr, M., Zador, A.M., 2003. Balanced inhibition underlies tuning and sharpens spike timing in auditory cortex. Nature 426, 442-446.

Wehr, M., Zador, A.M., 2005. Synaptic mechanisms of forward suppression in rat auditory cortex. Neuron 47, 437-445.

Wen, B., Wang, G.I., Dean, I., Delgutte, B., 2012. Time course of dynamic range adaptation in the auditory nerve. J Neurophysiol 108, 69-82.

Willmore, B.D., Schoppe, O., King, A.J., Schnupp, J.W., Harper, N.S., 2016. Incorporating Midbrain Adaptation to Mean Sound Level Improves Models of Auditory Cortical Processing. J Neurosci 36, 280-289.

Winer, J.A., Saint Marie, R.L., Larue, D.T., Oliver, D.L., 1996. GABAergic feedforward projections from the inferior colliculus to the medial geniculate body. Proc Natl Acad Sci U S A 93, 8005-8010.

Wojtczak, M., Nelson, P.C., Viemeister, N.F., Carney, L.H., 2011. Forward masking in the amplitude-modulation domain for tone carriers: psychophysical results and physiological correlates. J Assoc Res Otolaryngol 12, 361-373.

Wojtczak, M., Viemeister, N.F., 2005. Forward masking of amplitude modulation: basic characteristics. J Acoust Soc Am 118, 3198-3210.

Wu, G.K., Arbuckle, R., Liu, B.H., Tao, H.W., Zhang, L.I., 2008. Lateral sharpening of cortical frequency tuning by approximately balanced inhibition. Neuron 58, 132-143.

Xu, X., Roby, K.D., Callaway, E.M., 2010. Immunochemical characterization of inhibitory mouse cortical neurons: three chemically distinct classes of inhibitory cells. J Comp Neurol 518, 389-404.

Yaron, A., Hershenhoren, I., Nelken, I., 2012. Sensitivity to complex statistical regularities in rat auditory cortex. Neuron 76, 603-615.

Zaitsev, A.V., Lewis, D.A., 2013. Functional properties and short-term dynamics of unidirectional and reciprocal synaptic connections between layer 2/3 pyramidal cells and fast-spiking interneurons in juvenile rat prefrontal cortex. Eur J Neurosci 38, 2988-2998.

Zheng, H.J., Wang, Q. and Stanley, G.B., 2015. Adaptive shaping of cortical response selectivity in the vibrissa pathway. J Neurophysol 113, 3850-3865.

2. Gain Control in the Auditory Cortex Evoked by Changing Temporal Correlation of Sounds.

Abstract

Natural sounds exhibit statistical variation in their spectro-temporal structure. This variation is central to identification of unique environmental sounds and to vocal communication. Using limited resources, the auditory system must create a faithful representation of sounds across the full range of variation in temporal statistics. Imaging studies in humans demonstrated that the auditory cortex is sensitive to temporal correlations. However, the mechanisms by which the auditory cortex represents the spectro-temporal structure of sounds and how neuronal activity adjusts to vastly different statistics remain poorly understood. In this study, we recorded responses of neurons in the primary auditory cortex of awake rats to sounds with systematically varied temporal correlation, to determine whether and how this feature alters sound encoding. Neuronal responses adapted to changing stimulus temporal correlation. This adaptation was mediated by a change in the firing rate gain of neuronal responses rather than their spectro-temporal properties. This gain adaptation allowed neurons to maintain similar firing rates across stimuli with different statistics, preserving their ability to efficiently encode temporal modulation. This dynamic gain control mechanism may underlie comprehension of vocalizations and other natural sounds under different

contexts, subject to distortions in temporal correlation structure via stretching or compression. **Published as Natan, R.G., Carruthers, I.M., Mwilambwe-Tshilobo, L., Geffen, M.N. (2016) Gain Control in the Auditory Cortex Evoked by Changing Temporal Correlation of Sounds. Cerebral Cortex, pii: bhw083.**

Introduction

Sounds in the natural world exhibit variations in their temporal statistical structure. Different acoustic scenes are composed of sounds with temporal modulations under variable statistical constraints and this variation in the temporal correlation (TC) statistics serves as a cue for discrimination and identification of natural sounds (Attias and Schreiner, 1997; Escabi et al., 2003; Geffen et al., 2011; Gervain et al., 2014; McDermott et al., 2013; McDermott and Simoncelli, 2011; Singh and Theunissen, 2003). The correlation of amplitude modulations over time determines a highly salient qualitative property of sound: the slowly changing howl of wind blowing through an open window has a high TC, whereas the rapidly changing rustle of wind blowing though leaves exhibits a relatively low TC. Communication sounds, including speech, contain important components across a range of temporal scales (Poeppel, 2003; Rosen, 1992). In particular, the temporal structure of human vocalizations plays a role in speech comprehension: degrading temporal, but not spectral information impairs speech comprehension (Remez et al., 1981; Shannon et al., 1995). Therefore, it is critical to identify how neurons in the auditory stream encode and represent sounds across

varying TC statistics in order to elucidate the neuronal mechanisms for hearing both environmental and communication sounds.

Our present knowledge of neuronal mechanisms of encoding of the vast range of sounds at different TCs remains limited. Human brain imaging studies found that sounds with different temporal modulation properties differentially activated regions of the auditory cortex, suggesting a hierarchical scheme of sensitivity to TC in sounds. In Heschl's gyrus, containing the primary auditory cortex, studies have identified sensitivity to sounds with increasingly rapid modulations (Schonwiesner et al., 2005; Zatorre and Belin, 2001). The superior temporal sulcus, containing higher-order auditory cortices, exhibited sensitivity to sounds with lower temporal modulations (Boemio et al., 2005). Further, areas downstream of the auditory cortex, including the superior temporal gyrus and auditory association cortex, but not the primary auditory areas, exhibited differential activation by sounds with varying TC (Overath et al., 2008). The goal of our study was to identify the neuronal coding strategies in the primary auditory cortex for sounds with varying TC using electrophysiological recordings in rodents to isolate spiking activity.

As the BOLD signal is thought to be driven by elevation of the average neuronal activity over large populations of neurons (Logothetis and Wandell, 2004), a number of coding strategies in the primary auditory cortex would be consistent with the imaging results. While exhibiting on average uniform activity across all neurons, subpopulations of neurons in the auditory cortex may preserve information about TC of sounds leading

to differential activation in downstream areas. Just as neurons have been found to adapt with the statistical distribution of sound intensity and contrast (Dean et al., 2005; Dean et al., 2008; Rabinowitz et al., 2011; Watkins and Barbour, 2011), they may also adapt with to the TC structure of the stimuli thereby maximizing the dynamic range for their responses and providing information about TCs to downstream areas. Alternatively, different neurons may be tuned to stimuli with specific TC structure, resulting in uniform responses when averaged across neurons. Here, we tested whether and how neurons in the auditory cortex responded to sounds with varying temporal correlation and whether they exhibited adaptation in response to such variation.

To determine the mechanisms of sensitivity and responsiveness to sounds with varying temporal correlation TC, we recorded the activity of A1 neurons in awake rats while presenting dynamic chord stimuli with varying TC. We designed these stimuli to preserve the spectral complexity found in natural scenes, while permitting systematic variation in temporal statistics (Overath et al., 2008). Consistent with human imaging studies, we found that varying TC of sounds did not change the overall response of A1 in terms of the mean population firing rate. As an underlying mechanism of this stability, we revealed that A1 neurons adapted to increasing stimulus TC by decreasing stimulus-response gain. Expanding on prior findings on gain control of stimulus intensity and spectro-temporal contrast (Rabinowitz et al., 2011), these results show that gain control in A1 compensates for a wider range of sound statistics and identifies the mechanisms

for sensitivity to sounds with varying TC structure, that are likely essential in natural sound processing.

Methods

Animals. All procedures were approved by the Institutional Animal Care and Use Committee of the University of Pennsylvania. Subjects in all experiments were adult male Long-Evans rats. Rats were housed in a temperature- and humidity-controlled vivarium on a reversed 24-h light-dark cycle with food and water provided ad libitum.

Surgery. Adult male Long-Evans rats (N = 7, 12–21 wk) were implanted with a chronic custom-built six-tetrode drive as previously described (Blackwell et al., 2015; Carruthers et al., 2015; Carruthers et al., 2013; Otazu et al., 2009). Briefly, rats were anesthetized with a mixture of ketamine (60 mg/kg body wt, IP) and dexmedetomidine (0.25 mg/kg, IP). Buprenorphine (0.1 mg/kg, SC) was used as an operative analgesic, with ketoprofen (5 mg/kg, SC) as postoperative analgesic. The animal's head was secured in a stereotactic frame, and the temporal muscle was recessed. Craniotomy and durotomy were performed over A1. Eight tetrodes, housed in a custom-built microdrive were lowered in the brain, and the microdrive was attached to the skull with dental cement (Metabond) and dental acrylic. Each tetrode consisted of four polyimide-coated nichrome wires (Kanthal Palm Coast, wire diameter of 12 µm) twisted together and was controlled independently with a turn of a screw. Two screws (one reference and one ground) were inserted in the skull at a location distal from the craniotomy. The tetrodes were positioned 4.0–6.0 mm posterior to bregma and 7.0 mm left of the midline and

covered with agar solution (3.5%). During the recording, the microdrive was connected via a custom-built interface board to a headstage (Neuralynx). The electrodes were gradually advanced below the brain surface in daily increments of 40–50 μm to ensure recorded units were unique. Targeting of the electrodes to the primary auditory cortex (A1) was verified on the basis of their position in relation to brain surface blood vessels, stereotaxic coordinates, and histological reconstruction of the electrode tracks, and confirmed by identifying the frequency response function of the recorded units as previously described (Carruthers et al., 2013) (Figure 2.1A). The recorded units' best frequency (frequency of the tone that elicited the highest firing rate) and tuning width spanned the range of rat hearing (n = 118, Figure 2.1B) and was consistent with previous studies on the response properties of units in A1 (Carruthers et al., 2015; Carruthers et al., 2013; Polley et al., 2007; Sally and Kelly, 1988).

Stimulus Construction. All stimuli were created in Matlab (MathWorks) and sampled at 400k Hz and 32-bit resolution. A set of temporally correlated dynamic random chord stimuli (CDRC) (Linden et al., 2003) was constructed similarly to stimuli in previous studies (Overath et al., 2008), adapted to the rat hearing range (Figure 2.1C). This stimulus was designed to measure the spectro-temporal receptive field of neurons under different statistical regimes by fitting a linear-non-linear model (Figure 2.3B). 100 amplitude modulated pure tones, of logarithmically spaced frequencies from 400 Hz to 70k Hz, were superimposed. The amplitude envelope was generated as following: For the uncorrelated (low TC, $r = 0$) stimulus, the amplitude modulations of each frequency

were drawn independently from a normal distribution over 5ms time frames. For the correlated (medium TC and high TC) stimuli, the amplitude within each successive frame was generated to ensure correlation with the previous frame, according to the Pearson's correlation coefficient of r = 0.67 for medium TC or r = 0.90 for high TC (Figure 2.1C). To generate the frequency amplitude envelope matrix, the first column at time 0 was generated with a random set of values drawn from a Gaussian distribution (mean = 40dB, standard deviation = 8.7dB). Each subsequent frame was generated as follows:

$$(1)\ S_i = S_{i-1} * p + g(1-p^2)^{0.5}$$

where S_{i-1} is a vector of the amplitude values of the previous frame, p is r/10, and g is a vector of random values drawn from the same Gaussian distribution. After generating each frame, the correlation coefficient between the adjacent frames was calculated to ensure that it was r+/-0.01. Frames that violated this condition were rejected and recalculated with a new g. Likewise, frames were also rejected if they contained values >3 standard deviations in order to prevent sound clipping. The final matrix S was rescaled to an average of 65 and standard deviation of 15 dB. Each frequency amplitude envelope was resampled to 400 kHz with linear spline interpolation in order to smooth amplitude transitions. Respective amplitude envelopes were multiplied by sine-waves of each frequency and added together to produce the final signal. For all TC values, the stimuli had the same average intensity and standard deviation of the amplitudes within each spectral band. A 5ms cosine squared ramp was applied to the beginning and end of each stimulus. The correlation coefficients used correspond to the window-length of 5,

20, or 80 ms for a correlation reduction to r = 0.2. These values were chosen to be smaller, similar or greater than a typical temporal width of a spectro-temporal receptive field of the recorded neurons.

Using the method described above, three sets of stimuli were created: short, long and alternating. Short and long stimuli consisted of a single CDRC stimulus at each TC level, 10 s and 10 min long, respectively. Alternating stimuli consisted of a sequence of CDRC stimuli, at 2 TC levels (low/medium, medium/high, and low/high), alternating every 2 s. For each alternating stimulus, an amplitude envelope matrix was created in which r changed between 2 selected values every 200 frames (2 s). In order to ensure that amplitude power was sampled evenly across frequencies at each time frame, one vector from the matrix was time shifted by a 4 s interval and applied to each frequency.

Stimulus delivery. Acoustic stimuli were output from the computer via a National Instruments 16-bit high sampling rate data card (NIDAQ model NI PCIe-6353), pre-amplified and delivered via a magnetic speaker (MF-1, Tucker-Davis Technologies) positioned above the recording chamber. The speaker output was calibrated using a Bruel and Kjaer 1/4-inch free-field microphone type 4939 positioned at the location of the animal's ear. The microphone was used to record speaker output of repeated white noise bursts and tone pips between 400 and 80,000 Hz. From these measurements, the speaker transfer function and its inverse were computed. The input to the microphone was adjusted using the inverse of the transfer functions previously described (Carruthers et al., 2013), such that the speaker output 70-dB sound pressure level

relative to 20 μPa (SPL) tones within 3 dB between 400 and 80,000 Hz. Spectral and temporal distortion products were found to be >50 dB below the SPL of the fundamental. All stimuli were presented at 400-kHz sampling rate. The narrow recording chamber was custom-designed to minimize acoustic distortions. The chamber was positioned inside a sound-proof acoustically isolated double-walled room.

Experimental design. The rat was implanted with an electrode microdrive and was trained to sit still in the recording chamber. Animals were monitored via video recording for their level of arousal, following methods previously developed in the laboratory (Aizenberg, 2013; Aizenberg et al., 2015; Blackwell et al., 2015; Carruthers et al., 2015; Carruthers et al., 2013; Mwilambwe-Tshilobo et al., 2015). The chronically implanted microdrive was connected via a cable to the Neuralynx digital acquisition system. The rat was exposed to stimuli for < 4h and given a 15 min break to drink water every 1.5 h. A stimulus designed to map the frequency response function of the recorded units, consisting of 50 tones, each 50 ms long, between 400 and 80,000 Hz, logarithmically spaced, at 70 dB, was presented first. The same set of stimuli was played in the following order: 1 repeat of a long CDRC stimulus at each TC, 50 repeats of each short CDRC stimulus at each TC, 1 repeat of each alternating CDRC stimulus. After stimulus presentation, each tetrode was advanced by 40 μm.

Neural signals were acquired from the 24 implanted electrodes with a Neuralynx Cheetah system. The neuronal signal was filtered between 0.6 kHz and 6.0 kHz, digitized, and recorded at 32 kHz rate. Spikes were clustered into single-unit and multi-

unit clusters with Plexon Offline Spike Sorter software. Single units were isolated using a stringent set of criteria as previously described (Aizenberg, 2013; Aizenberg et al., 2015; Blackwell et al., 2015; Carruthers et al., 2015; Carruthers et al., 2013; Natan et al., 2015): Single-unit clusters contained <1% of spikes within a 1.0 ms interspike interval, and the spike waveforms had to form a visually identifiable distinct cluster in a projection onto a three-dimensional subspace (Bizley et al., 2010; Brasselet et al., 2012; Otazu et al., 2009).

Mean firing rate. To avoid drift effects, the mean firing rate was measured from responses to the alternating TC stimuli, between 1 to 2 s after TC transition, and pooled across 900 TC alternation cycles per stimulus. To test for changes in firing rate between different TC levels for each neuron, we compared the mean firing rate across TC cycles across neurons, using the paired sign rank test to assay the significance ($\alpha = 0.05$).

Linear non-linear model. To compute the spectro-temporal receptive field and the instantaneous non-linearity, the neuronal responses at steady state (at least 200 ms following stimulus onset) to the 10m long stimulus were fitted to a linear-non-linear model (Figure 2.3B). The linear-non-linear model consisted of a linear component, corresponding to the spectro-temporal receptive field (STRF), followed by a static rectifying non-linearity (Baccus and Meister, 2002; Carruthers et al., 2013; Geffen et al., 2007; Linden et al., 2003; Woolley et al., 2005). The linear output (LO) is given by:

(2) $$LO(t) = \sum_{f'=0}^{F-1} \sum_{t'=0}^{M-1} STRF(f', t') s(f', t = t')$$

and the predicted firing rate by:

(3) $R(t) = N[LO(t)]$

where STRF is an M by F matrix; F is the number of frequency bins, and M is the number of temporal bins; and $N(x)$ is the instantaneous non-linearity. The standard deviation of the linear output (SD_{LO}) is computed by taking the standard deviation of *LO(t)* over time.

STRF parameters. STRFs were estimated as the optimal linear filter between the spiking response and the frequency amplitude envelope. Ridge regression was applied to normalize the filter by the stimulus auto-correlation function (Baccus and Meister, 2002; Escabi et al., 2003; Geffen et al., 2007; Theunissen et al., 2001), after which the filter was smoothed by applying a two-dimensional Gaussian filter with standard deviation of 1.5 bins (7.5ms and 0.15 octaves in the temporal and spectral domains, respectively). STRF was denoised, by setting all values outside of a significant positive cluster of pixels to 0. Negative clusters were not included in the analysis because including them did not improve firing rate prediction accuracy and did not appear to systematically change with TC. To determine the significance of the cluster, the z-score of pixels was computed relative to the baseline values from a STRF generated with scrambled spike trains, using Stat4ci toolbox (Chauvin et al., 2005). From STRF, the center time, duration, center frequency and bandwidth of the positive cluster were measured (Schneider and Woolley, 2010; Shechter and Depireux, 2007; Woolley et al., 2006). To measure temporal parameters of the receptive field, the positive portion of the cluster corrected STRF over the positive lobe was averaged across frequencies, and fitted with a one-dimensional Gaussian. Because we only examine the positive lobe of the STRF and not

the entire STRF, we assumed that the positive lobe of the STRF was linearly separable in frequency and time. Center time and duration were defined as the center and twice the standard deviation of the Gaussian fit to the temporal STRF profile, respectively. Likewise, to measure spectral parameters, STRF was averaged across time over the positive lobe, and fitted with a one-dimensional Gaussian. Center frequency and bandwidth were defined as the center and 2x standard deviation of the Gaussian fit, respectively.

Non-linearity. The non-linear component of the linear-non-linear model was computed as the transfer function between the linear prediction from the cluster-corrected STRF and the actual firing rate (Baccus and Meister, 2002; Carruthers et al., 2013; Geffen et al., 2007) and fitted to exponential or logistic functions, $N(x)$:

(4) $N_1(x) = a + b * e^{x*c}$

(5) $N_2(x) = \frac{L}{1+e^{-k(x-x_0)}}$

Where *a*, *b*, *c*, *L*, *k* and x_0 are free variables. Firing rate offset was defined as the firing rate at the average linear output ($N_1(x)$ = 0) along the exponential non-linearity fit. Gain was defined as the slope between two points along the exponential (Equation 4): One point at the average linear output and the other at the linear output 2 standard deviations greater than the average, thus the slope between $N_1(x)$ = 0 and 2. Steepness was defined as the variable *k* (Equation 5).

Fano factor. The Fano factor was defined as the firing rate variance divided by the mean firing rate (Marguet and Harris, 2011). The Fano factor was measured from responses to the alternating stimulus, at 1 to 2 s after TC transition for each TC level.

Signal to noise ratio. Signal was defined as the variance of the firing rate over time, averaged over trials. Noise was defined as the variance of the firing rate over trials, averaged over time (Geffen et al., 2009). The signal to noise ratio was measured from responses to the alternating stimulus, at 1 to 2 s after TC transition for each TC level.

Prediction quality of the linear-non-linear model. The prediction quality of the model was measured as the correlation coefficient between the predicted firing rate from the linear-non-linear model and the measured firing rate. The model was fitted on responses to the long stimulus, and tested for prediction quality on responses to the repeated short stimulus.

Adaptation time constant. Two post-stimulus time histograms (PSTH), one for each TC level, were computed from the mean firing rate over time between TC transitions (every other 2s) for each alternating TC stimulus (Asari and Zador, 2009). PSTHs were smoothed with a Gaussian filter with a standard deviation of 50 ms (10 frames). A decaying exponential function was fitted from the peak of the absolute value of the initial response (between 25 and 250ms), to the end of the PSTH as:

$$y(t) = c + k * e^{\frac{-t}{\tau}} \quad (6)$$

Where *c* is the adapted firing rate, *k* is the magnitude of the initial response, and τ is the adaptation time constant.

Neuron selection criteria for analysis. Out of 180 single units recorded, 118 displayed measurable tuning properties (Figure 2.1). Only those with demonstrable stimulus response to each TC level (mean signal to noise ratio greater than 0.22 across low, medium and high TC) were included for analysis of firing rate, signal to noise ratio, fano factor, and non-linearity slope, steepness and offset (n = 45, Figure 2.s 2-5, and 8; n = 37, Figure 2.6). Only units with a minimally stable STRF (at least one shared significant positive pixel between STRFs generated from low, medium and high TC) were included in analysis of STRFs (n = 30, Figure 2.7). To measure adaptation, only units with demonstrable adaptation (variance differing significantly between the initial 25-250 ms and final 500ms after both transitions, unpaired one-tailed t-test, $\alpha = 0.001$) were included (n = 51, Figure 2.9).

Statistical Tests. The correlation coefficient (*r*) and correlation p-values were computed as Pearson's correlation coefficient following a standard MATLAB routine. The index of change, Δ (index), was used to compute differences between lower and higher TC levels for several parameters:

$$\Delta = \frac{TC_h - TC_l}{TC_h + TC_l} \quad (7)$$

Where TC_h and TC_l represent the parameter value during the lower and higher of two stimulus TC levels. Significant differences and p-values of these parameters between

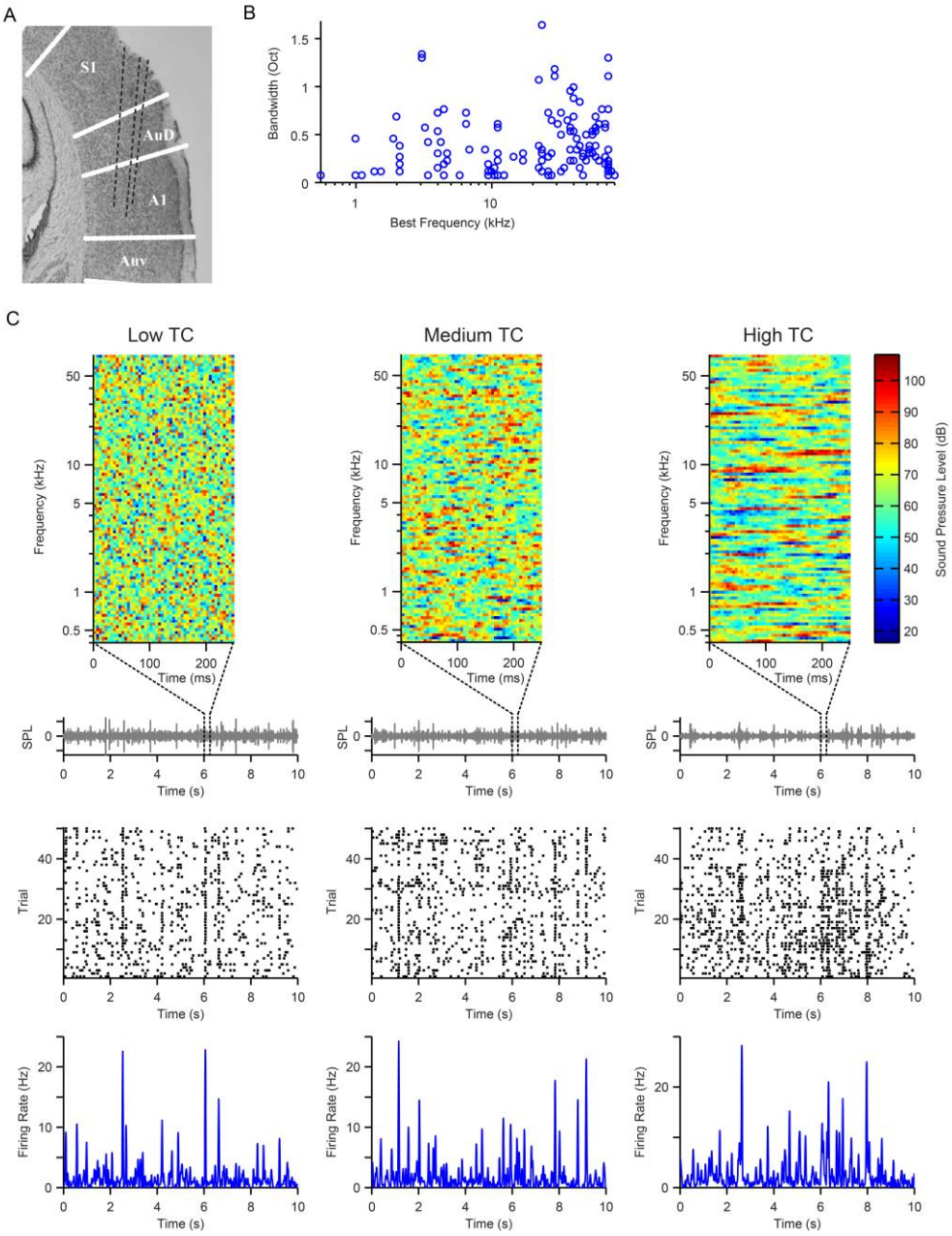

Figure 2.1. **Recording neuronal spiking activity from primary auditory cortex (A1).** A. Reconstruction of primary auditory cortex showing tetrode traces in black dashed lines and cortical area borders in white lines. B. Distribution of the best frequency and bandwidth of recorded units. C. Top row: 100 ms sample of the amplitude envelope across each frequency for each stimulus TC level. Below, waveforms of the repeated 10 s stimuli, from which each sample is extracted. Center row: Spike raster from a single neuron in response to 50 repeats of each stimulus TC level. Bottom row: Mean firing rate PSTH of response to each stimulus TC level. Left column: low TC. Center column: medium TC. Right column: high TC.

stimulus TC levels were reported based on the index of change as calculated using single sample Student's t-test (unless noted otherwise) with standard MATLAB routines. In calculating population mean percent changes, outliers were removed if they exceeded the sample mean +/- 5 standard deviations. Mean +/- standard error of the mean was reported unless stated otherwise.

Results

Neurons in A1 are sensitive to the temporal modulation rate in the acoustic structure of sounds, but how this sensitivity is affected by the overall statistics of the stimulus is unknown. Here, we tested the effect of changes in the range of temporal modulation statistics on encoding of temporally modulated sounds by neurons in A1. We presented a series of spectro-temporally complex acoustic stimuli to awake rats and recorded the responses of neurons in their primary auditory cortex. The stimuli consisted of a library of correlated dynamic random chords (CDRC) with different temporal correlation structure (Figure 2.1C), presented either separately for each TC level, or in alternating block design (TC level changed every 2 s). Each CDRC was composed of 100 tones, and the amplitude of each tone varied over time. In the uncorrelated (low TC, r = 0) stimulus, the amplitude of each tone within the chord was chosen at random every 5 ms. For the intermediate and high TC stimuli, the amplitude of tones in a chord depended on the amplitude in the preceding chords, according to the correlation coefficient of that CDRC (r = 0.67 and r = 0.9, respectively). Stimuli with

different TC values (low, medium and high) evoked precise time-locked responses in A1 neurons (Figure 2.1C).

Adaptation in A1 neurons to changed TC of the stimulus. Upon transition to a different TC value of the stimulus, A1 neurons typically responded by a brief increase or a decrease in their mean firing rate, followed by relaxation to a steady firing rate. The responses of three representative neurons to an alternating high-to-low TC stimulus are depicted in Figure 2.2. In the stimulus, TC level alternates every 2 s. Note that upon transition from low TC to high TC, the firing rate consistently increased, and then gradually decreased to a steady-state level; whereas upon transition from high to low TC level, there was a transient decrease in the firing rate following by a gradual increase (Figure 2.2A, B). These firing rate profiles are characteristic of neurons undergoing adaptation to a statistical change in the stimulus (Chen et al., 2010; Dean et al., 2005; Dean et al., 2008; Hosoya et al., 2005; Rabinowitz et al., 2011). Interestingly, not only did the firing rate adapt between TC levels, but also the spectro-temporal receptive field remained constant during isolated stimuli of different TC levels (Figure 2.2C). Such adaptation is thought to facilitate efficient coding in neuronal circuits, by bringing the dynamic range of the response closer to the dynamic range of the stimulus (Barlow, 1961). We next investigated whether over the recorded neuronal population, the responses of neurons exhibited adaptation to stimulus TC, and if so, what mechanism might be responsible for it.

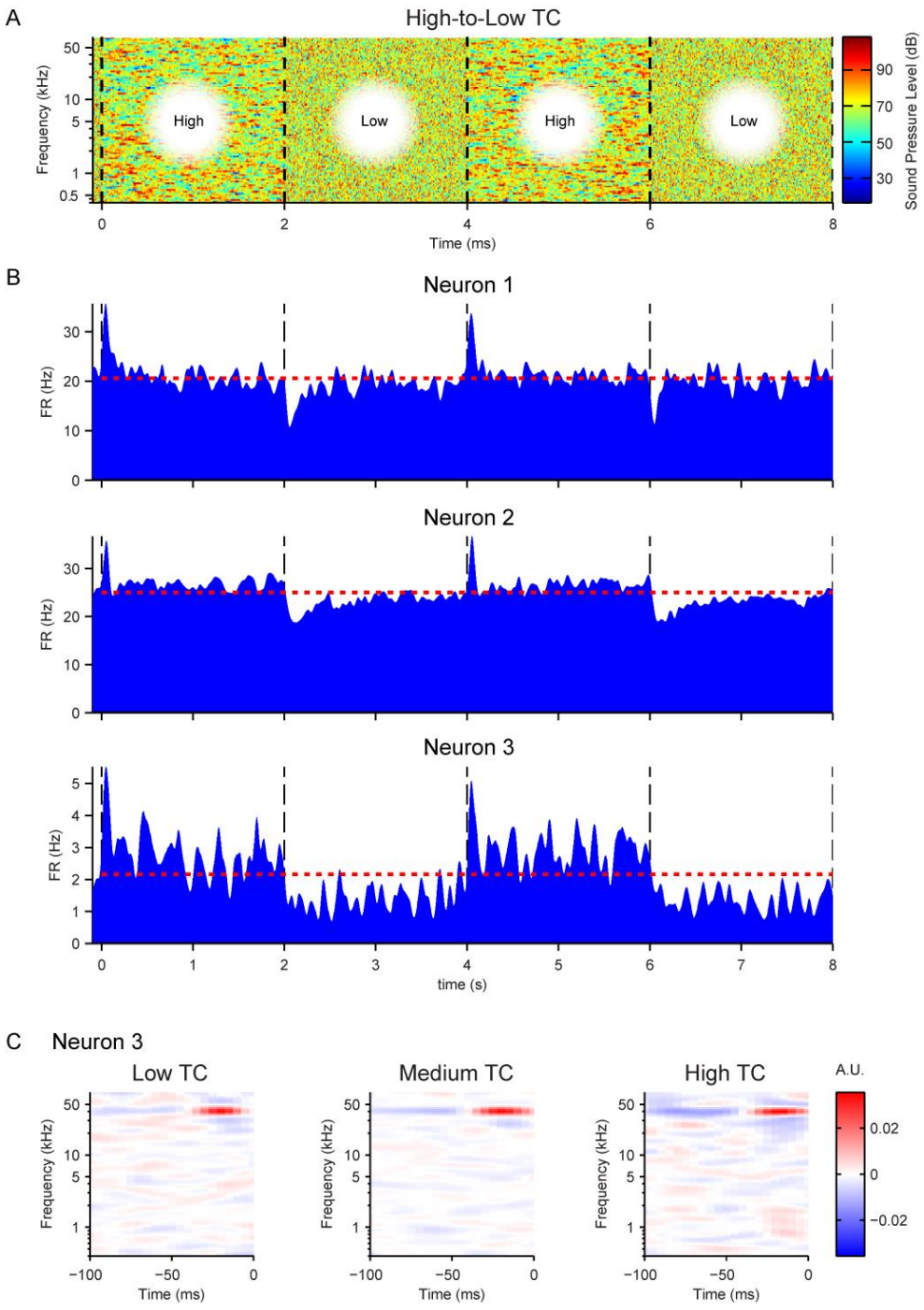

Figure 2.2. **Properties of neuronal spiking in response to varied TC levels.** A. Top: 8 s sample of the stimulus amplitude envelope for the alternating low-to-high TC stimulus. Transitions between TC levels occurred every 2 seconds (black dashed lines). B. Below, mean firing rate PSTHs from three representative neurons aligned to the TC level transitions every 8s. C. STRFs from neuron 3 in response to low, medium and high TC levels.

Expectation for an increase in neuronal responses to stimuli with higher temporal correlation. Neuronal responses to CDRC in A1 are typically modeled by a linear non-linear model, which consists of a linear term that takes into account the stimulus history, and an instantaneous non-linearity, which rectifies the output. Under the linear-non-linear model, the linear component of the neuronal response is modeled as the spectro-temporal receptive field (STRF, Figure 2.3B). Prior to non-linear rectification, the convolution of the stimulus with the STRF generates an estimate of the stimulus input strength to the model, termed the linear output (Equation 2). The non-linear component is the instantaneous transfer function from the STRF's linear output to the observed firing rate of the neuron (Figure 2.3C). We designed the stimuli using a random composition of the signal within each frequency band, which allowed for fitting stimulus responses to the linear-non-linear model. To establish an expectation for how response properties would change without gain control, we used the linear-non-linear model fits estimate the change in mean and standard deviation of the firing rate in response to low and high TC stimuli. Under the linear-non-linear model, the dynamic range of the linear prediction for each neuron can be characterized by the standard deviation of the linear output (Equation 2, SD_{LO}). We found that between low and high TC, SD_{LO} increased by a factor of 2.8 (difference 183 +/- 20%, p = 5.6e-19, n = 45, Figure 2.3D). An implementation of the full linear-non-linear model, fitted on the response to the low TC stimulus (Equation 3), also predicted a 1.5-fold increase in the mean firing rate and a 6-fold increase in the standard deviation of the firing rate (SD_{FR}) as compared to the responses to low TC stimulus (FR: difference 53 +/- 17%, p = 1.42e-5; SD_{FR}:

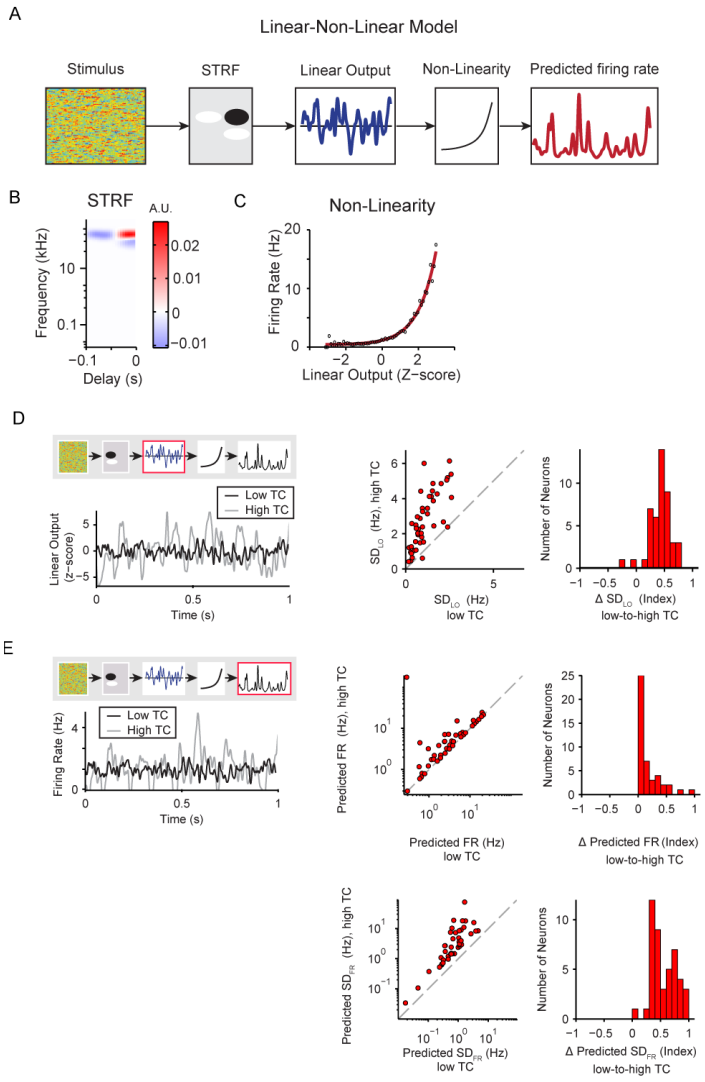

Figure 2.3. **Predicted increase in neuronal responses with increased stimulus TC.** A. Linear-non-linear model diagram illustrating how the model predicts the firing rate in response to input stimulus: Amplitude modulation envelope of the stimulus is convolved with the linear filter (STRF) to produce the linear output**,** (Equation 2), which is subject to a transfer function (exponential fit to the non-linearity) to generate the predicted firing rate for the neuron (Equation 3). B. Sample STRF. C. Sample non-linearity (red: exponential fit, black: data). D, E. Model predictions for responses to low or high stimulus TC levels. Left panels: Example of model outputs fitted to a single neuron's TC stimulus response properties. The red box in the model diagram highlights the feature being analyzed. Middle: Single neuron responses. Right: Population histogram of the change in predicted response with increased stimulus TC. D. Standard deviation of the linear output (SD_{LO}, Equation 2) of the low TC model in response to low or high TC stimuli. E. Predicted mean firing rate (top) and standard deviation (bottom) (Equation 3) of the low TC model in response to low versus high TC stimuli. Fit to low TC responses: black; fit to high TC responses: gray. Here and below: unity line: gray dashed.

difference 497+/- 110%, p = 5.1e-21; n = 45, Figure 2.3E, SD_{FR} reflects the dynamic range of the response). Therefore, we expected a dramatic increase in the range of the firing rate of neurons in response to the high TC stimulus.

Change in the temporal correlation of the stimulus evokes gain control in A1 neurons. Analysis of the recorded neuronal responses to stimuli with varying TC levels (Figure 2.4, A) revealed that changes in the firing rate and its standard deviation were much lower than those predicted by the linear-non-linear model, pointing to an adaptation process. For the low-to-high TC level transition (between 1-2 s after TC transition), there were no significant changes in the mean firing rate (p = 0.95, n = 45, Figure 2.4B), and there was only a small difference in SD_{FR} (-26 +/- 6%, p = 1.9e-4, Figure 2.4C). These changes in FR were significantly smaller than would have been expected from predicted SD_{LO} (p = 1.7e-12, Figure 2.4D, left) or predicted FR (p = 0.025, Figure 2.4D, right). Likewise, the observed changes in the SD_{FR} were significantly smaller than expected from predicted SD_{LO} (p = 4.0e-13, Figure 2.4E, left) or SD_{FR} (p = 3.2e-15, Figure 2.4E, right). These results support the hypothesis that A1 neurons adapt to the temporal dynamic range of the inputs, thus preserving the ability to efficiently encode stimuli under varying statistical constraints without changing the activity level.

Next we wanted to understand which parameters of neuronal responses contributed to the preservation of the firing rate and SD_{FR} over time. The gain of the non-linearity has been previously shown to be involved in the firing rate adaptation to acoustic contrast and amplitude (Rabinowitz et al., 2011). We predicted that in order

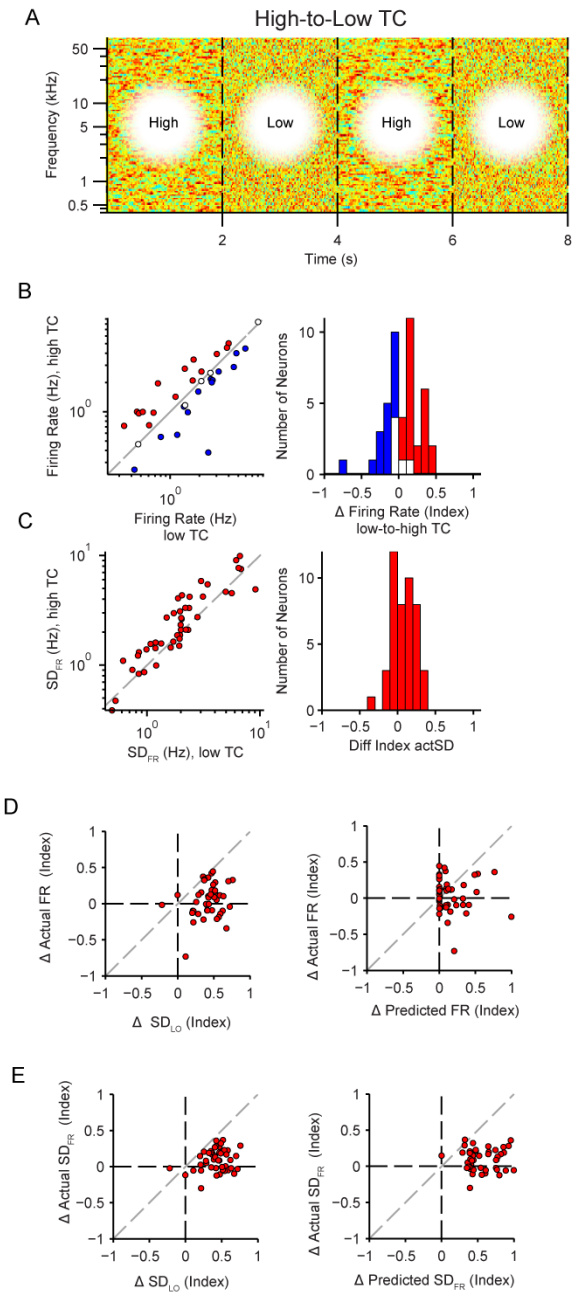

Figure 2.4. **Adaptation in neuronal responses to stimuli with increased temporal correlation.** A. Stimulus amplitude envelope, as in Figure 2.1C, for the alternating high-low TC stimulus. B. Mean neuronal firing rate to high TC versus low TC stimulus. Left: single neuron responses, right: histogram of population responses (blue: significant decrease, red: significant increase; white: not significant). C. Standard deviation of the firing rate to high TC versus low TC stimulus. Panels same as in B. D. Actual versus predicted change in the mean firing rate. Left: prediction based on standard deviation of the linear output. Right: prediction based on full linear – non-linear model. E. Actual versus predicted change in standard deviation of the firing rate. Panels same as in D.

reduce or eliminate a change in firing rate following change in stimulus TC, the gain should decrease with higher TC in order to fully or partly compensate for the increased synaptic input, as predicted by SD_{LO}. We independently estimated the linear-non-linear model to responses to either low or high TC stimuli, fitting an exponential function (Equation 4) to the non-linearity (Figure 2.5A). Indeed, across the population, the gain was significantly lower for higher TC stimuli (-31 +/- 9%, p = 1.4e-5, n = 45, Figure 2.5B). The change in gain exhibited significant positive correlation with the change in firing rate (r = 0.54, p = 1.3e-4) and change in SD_{FR} (r = 0.30, p = 0.048), i.e. neurons that displayed no change or reduced firing rate or standard deviation for higher stimulus TC exhibited stronger gain reductions (Figure 2.5C). Fitting the non-linearity with a logistic function (Figure 2.5D), preserved the results: the parameter controlling the steepness of the slope of the non-linearity, *k*, decreased with higher TC of the stimulus (-28 +/- 10%, p = 8.2e-7, n = 45, Figure 2.5E). The change in steepness also correlated with the change in SD_{FR} (r = 0.37, p = 0.012), although not the change in firing rate (p = 0.33) (Figure 2.5F). When we re-fitted the model on responses to the higher TC stimulus, thereby incorporating the gain changes, the firing rate and SD_{FR} did not change from low to high TC (FR: p = 0.42; SD_{FR}: p = 0.27; Figure 2.5G, H). Also, there was no longer a discrepancy between the change in predicted versus actual firing rate magnitude and standard deviation (FR: not significant, p = 0.44; SD_{FR}: not significant, p = 0.35). Furthermore, the correlation between the predicted and expected changes in the firing rate and its standard deviation were improved (FR: r = 0.47, P = 0.0012; SD_{FR}: r = 0.33, p = 0.027 Figure 2.5G, H) as compared to non-significant correlation between the prediction of the

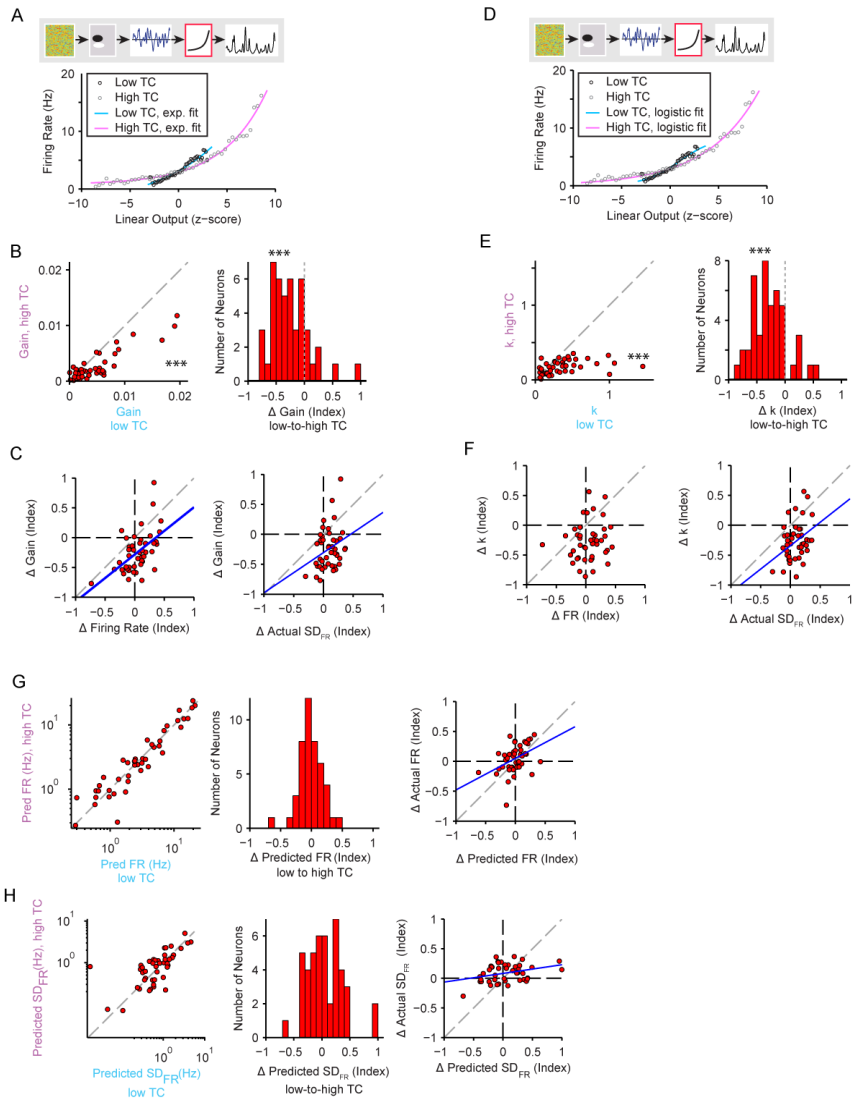

Figure 2.5. **Gain adaptation in neuronal responses to stimuli with increased temporal correlation.** A. Exponential non-linearity fitted to the actual firing rate response to low versus high TC stimuli. Gain is measured through a linear fit to the exponential. Cyan: low TC fit, Magenta: high TC fit. Responses to low TC stimulus: black circles; responses to high TC stimulus: gray circles. B. Gain measurements for high versus low TC stimuli. Left: individual neurons, right: histogram of change in the gain. Stars indicate that gain was higher for low TC than for high TC stimuli (left panel) and that gain decreased upon transition from high to low TC stimuli (right panel). C. Change in the gain versus the change in the firing rate (left) or the standard deviation of the firing rate (right). D, E, and F. Same as in A, B, C but with logistic non-linearity fit. Gain is measured as the steepness parameter *k* in equation 5. G. Predictions for the firing rate based on models fitted to high versus low TC stimulus. Left: Individual neurons. Center: histogram of the index of change of the predicted firing rate with increasing TC. Right: Actual versus predicted change in firing rate. H. Predictions for the standard deviation of the firing rate based on models fitted to high versus low TC stimulus. Panels same as in G.

model based on low TC responses, which lacked gain adaptation (Figure 2.4D, E). Together these results suggest that changes in gain reflect adaptation in neuronal responses.

We examined the changes in the firing rate offset of the non-linearity as an analog for a shift in baseline firing rate between TC conditions. If the observed effects were due primarily to gain adaptation, we would not expect the non-linearity offset to change significantly across conditions. Indeed, across the neuronal population, offset did not change between lower and higher TC stimuli ($p = 0.42$). Since the baseline firing rate does not change across the population, it is unlikely to contribute to compensation for increased SD_{LO}. However, changes in offset were correlated with changes in firing rate ($r = 0.40$, $p = 0.0058$). For individual neurons, underlying offset firing may explain some of the change in firing rate exhibited upon stimulus TC transitions.

Transitions from low TC to medium TC, and from medium TC to higher TC led to similar adaptation in FR and its standard deviation (Figure 2.6). There was no difference in the mean firing rate or its standard deviation for low-to-medium transitions (FR: $p = 0.50$; SD_{FR}: $p = 0.13$; $n = 37$, Figure 2.6A). For medium-to-high transitions, there was no change in firing rate (FR: $p = 0.84$) and a small change in SD_{FR} (SD_{FR}: 16+/-5%, $p = 0.011$, $n = 37$, Figure 2.6B). We note that individual neurons exhibited significant changes in their firing rates, with some neurons increasing and some decreasing their responses to higher TC stimuli. The firing rate changes between responses for low-to-medium and

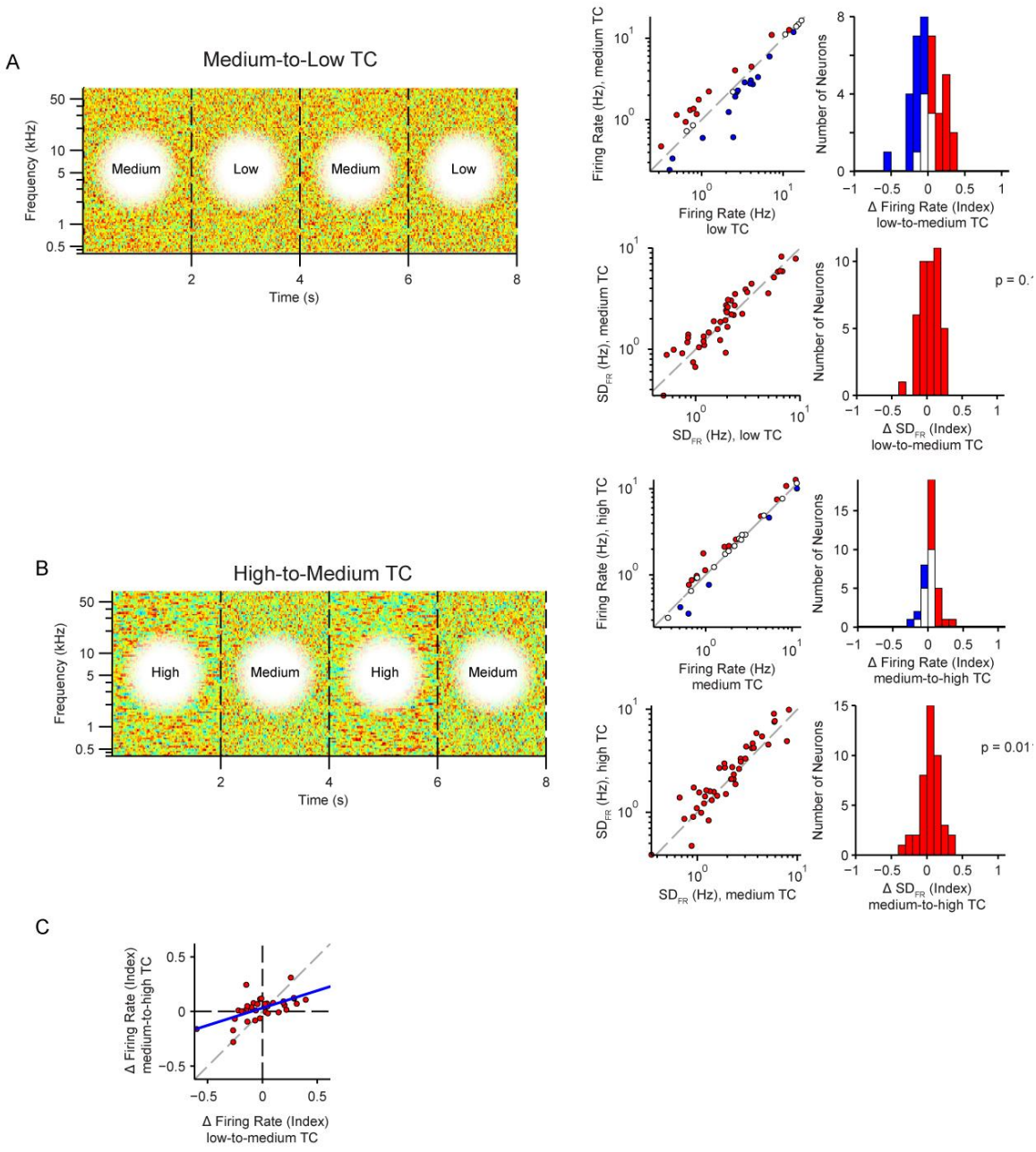

Figure 2.6. **Neuronal firing rates in response to intermediate TC level changes.** A: Transition from low to medium TC. B. Transition from medium to high TC. A, B. Left: Stimulus envelope, as in Figure 2.5A. Right: Change in mean firing rate (top) and standard deviation of the firing rate (bottom) from low to high TC stimulus. Axes and colors same as in Figure 2.4B, C. C. Correlation between change in mean firing rate for medium-to-low and high-to-medium TC stimuli.

medium-to-high TC transitions were correlated (n = 37, r = 0.60, p = 7.5e-5, Figure 2.6C), suggesting that firing rate responses to TC level changes are monotonic with TC level.

Our results thus far demonstrate that neurons in the primary auditory cortex exhibit adaptation to changes in temporal correlation of the stimulus. The mean firing rate does not change significantly and its standard deviation increases only slightly upon transition from low to high temporal correlation, whereas a large change would have been expected on the basis of the spectro-temporal receptive field of these neurons. The measured adaptation in the firing rate can primarily be attributed to the change in the slope of the non-linear response function, corresponding to the gain of neuronal responses.

Spectro-temporal dynamics of neuronal responses are unaffected by stimulus TC. Changes in the gain of neurons due to adaptation are commonly accompanied by changes in the receptive fields of neurons (Baccus and Meister, 2002; Nagel and Doupe, 2006). For example, in the visual system, the time course of the receptive fields of ganglion cells becomes slower with a decrease in contrast (Baccus and Meister, 2002). The spectro-temporal density of tone pips in an auditory stimulus has also been shown to affect the receptive fields of neurons in the inferior colliculus (Blake and Merzenich, 2002; Kvale and Schreiner, 2004). Changes in the receptive field shape and size could potentially modulate the neurons response properties. Therefore, in order to determine if the changes in the receptive field explain differences in the firing rate between different temporal correlation levels, we quantified four aspects of the recorded STRFs

under each condition (Figure 2.7A): peak response time, temporal duration, center frequency and frequency bandwidth. Only units containing a significant positive cluster-corrected lobe in the STRF for both low and high TC models, that spatially overlapped, were included in this analysis.

Interestingly, we found no systematic changes in the temporal or spectral profile of STRFs with an increase in TC. There were no significant changes in the bandwidth, center frequency, and duration of the STRF positive lobe ($p = 0.14$, $p = 0.32$, and $p = 0.28$, respectively, $n = 30$), nor were there significant correlations between the change in these parameters and changes in firing rate ($p = 0.68$, $p = .74$, $p = 0.051$, respectively) (Figure 2.7B-D). Although there was a small reduction in the time-to-peak (-2.3 +/ 1.3 ms, $p = 0.018$, Figure 2.7E), this change was smaller than the 5ms time frame of acoustic envelope modulation. In addition, changes in time-to-peak were not correlated with changes in firing rate ($p = 0.99$), Taken together, we did not find a systematic change in the receptive field that can explain the pattern of change in the firing rate with an increasing temporal correlation.

Adaptation to temporal correlation leads to more efficient information processing. The efficient coding hypothesis posits that matching the stimulus response dynamic range to the dynamic range of the stimulus improves the efficiency of coding (Barlow, 1961; Fairhall et al., 2001; Schwartz and Simoncelli, 2001; Vinje and Gallant, 2002). We hypothesized that the gain modulation observed above serves to maintain encoding efficiency under different TC conditions. We quantified encoding efficiency using three

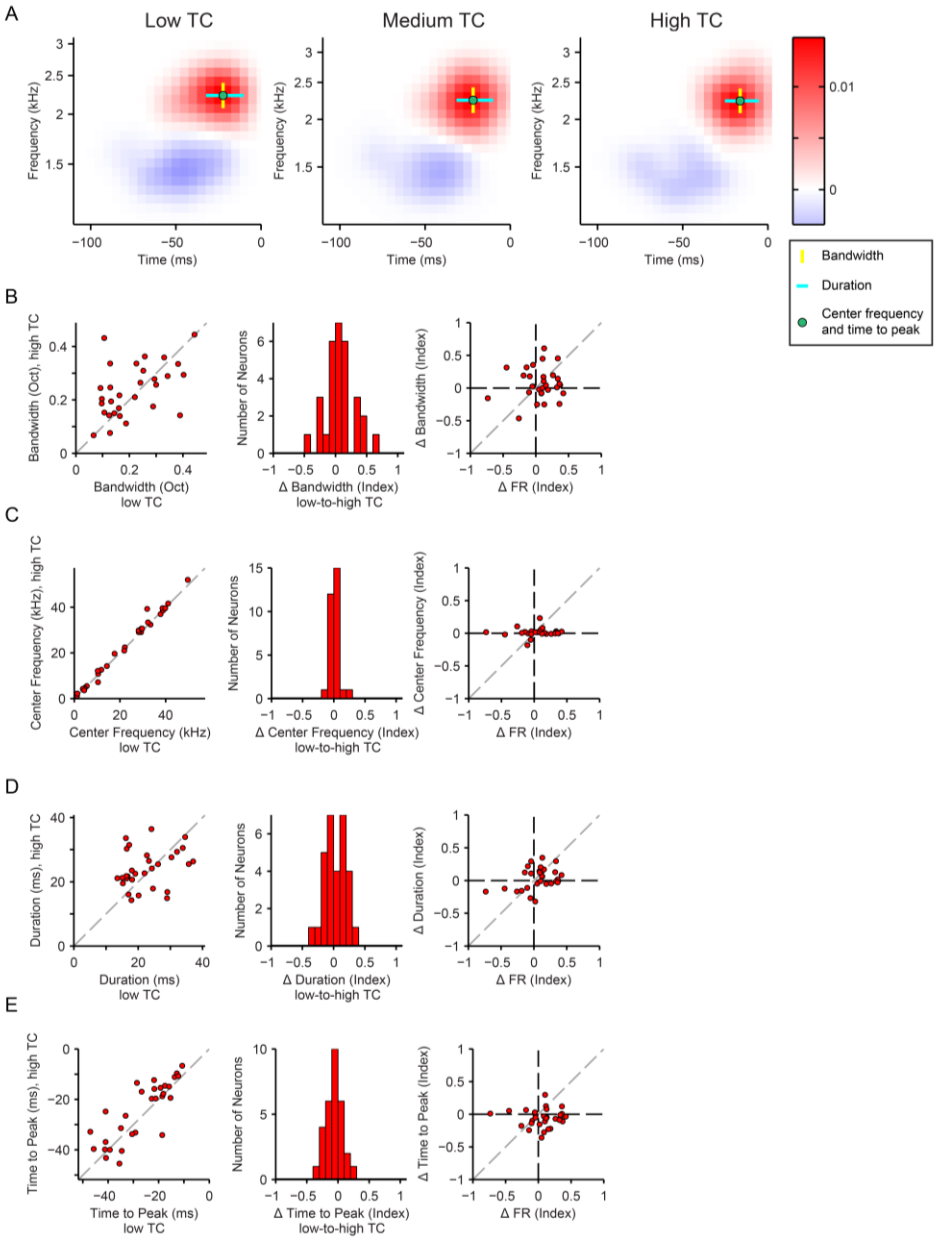

Figure 2.7. **Neuronal spectro-temporal receptive fields remain stable across varying temporal correlation levels.** A. Spectro-temporal receptive field (STRF) of a neuron in response to low (left), medium (middle), and high (right) stimulus TC levels. Excitatory lobe: red, inhibitory lobe: blue. Excitatory lobe bandwidth: yellow line. Excitatory lobe duration: cyan line. Center frequency and peak response time: green filled circle. B-E. Analysis of model parameters (positive lobe of the linear filter) in response to high-to-low stimulus TC levels for each neuron. B. Frequency Bandwidth. C. Center frequency. D. Duration. E. Time to peak. B-E. Left: Single neuron data. Center: Population histogram. Right: Correlation between the change in the STRF parameter versus the change in the firing rate with increased TC.

measures: the signal to noise ratio, the Fano factor, and prediction quality, and compared them for different TC levels.

The Fano Factor provides a quantification of the variability in neuronal responses to the stimulus (Churchland et al., 2011). An effect of adaptation, consistent with the efficient coding hypothesis, would result in a decrease in the Fano factor. In fact, we found that the Fano factor decreased with increased TC (-5.1+/-3.6%, p = 0.029, n = 45, Figure 2.8A). Changes in Fano factor were also significantly correlated with changes in firing rate (r = 0.52, p = 2.8e-4).

The signal to noise ratio (SNR) gives a measure of how strongly the response variability is used to encode the stimulus (Geffen et al., 2009). Consistent with the efficient coding hypothesis, an effect of adaptation should be an increase in SNR (Baccus and Meister, 2002). Indeed we found that SNR increased between low and high TCs (13 +/- 3.1%, p = 3.1e-4, n = 45), and changes in SNR were not correlated with changes in firing rate (p = 0.10) (Figure 2.8B). This suggests that populations of A1 neurons encode stimuli of higher TC with less noise.

The prediction quality is a measure of how well the linear-non-linear model captures the response properties of each neuron (Carruthers et al., 2013; Schneider and Woolley, 2010; Woolley et al., 2005). It can be affected by the dynamic range of the stimulus, as well as the precision and variability of the response. We compared the prediction quality of the linear-non-linear model for responses to the low, medium and high TC stimuli (n = 30, Figure 2.8C-E). Over the population, prediction quality was

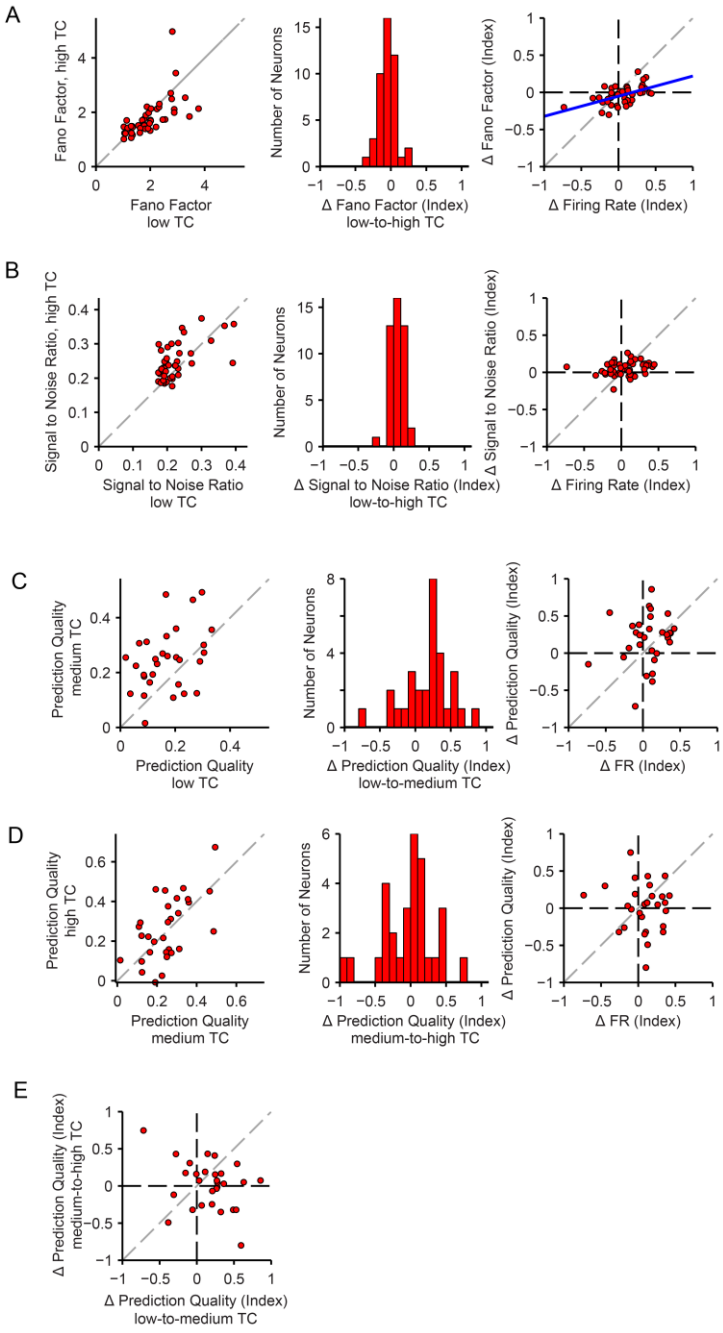

Figure 2.8. **Improved encoding efficiency with increases in temporal correlation.** A. Fano factor of each neuron for low versus high stimulus TC. B. Signal-to-noise ratio of each neuron for low versus high stimulus TC. C. Prediction quality of each neuron for low versus medium stimulus TC. D. Prediction quality of each neuron for medium versus high stimulus TC. Left, middle and right panels as in Figure 2.6B-D. E. Index of change in prediction quality from low-to-medium stimulus TC versus medium-to-high stimulus TC for each neuron. Plot axes as in D, left right panel.

lowest for low TC stimuli, and highest for medium and high TC stimuli (prediction quality = 0.17+/-0.02, 0.24+/-0.02, 0.26+/-0.03, respectively). Between the two lowest TC levels, prediction quality was significantly greater for medium TC stimuli (108 +/- 43%, p = 0.0062, Figure 2.8C). Comparing medium to high stimulus TC, there was no significant change in prediction quality (p = 0.076, Figure 2.8D). Neither prediction quality comparison (low-to-medium or medium-to-high) showed correlation with firing rate changes associated with different TC levels (p = 0.33, 0.87, respectively, Figure 2.8C-D). Together, these results show that increasing the TC of the stimulus improves encoding. However, prediction quality does not continue to increase with increased TC. In fact, across the population, there is no correlation between increased prediction quality from low to medium TC versus medium to high TC (p = 0.073, Figure 2.8E).

Interestingly, the correlation time window (Overath et al., 2008) of the medium TC stimulus (20ms) most closely matches the temporal duration of the STRF (22+/-1ms). Therefore, the typical spectro-temporal response properties of A1 neurons, at least in rats, may be best suited to encode amplitude fluctuations occurring within the medium TC stimuli and contributes to more efficient encoding for this TC level. Furthermore, this implies that the time course of adaptation likely scales with encoding time of cortical neurons, and neurons with different encoding times (such as found in other cortical auditory fields (Polley et al., 2007)) may adapt to different TC stimuli.

Dynamics of firing rate adaptation to changes in temporal correlation. Examining the time course of firing rate change after a transition in the stimulus temporal correlation

can be informative about the neuronal mechanism that underlies the firing rate adaptation (Asari and Zador, 2009). We averaged the neuronal responses to a non-repeating sequence of CDRCs, whose TC alternated between high and low, triggered on the low-to-high or high-to-low transitions and examined the dynamics of the firing rate over several hundred milliseconds following the transition. Upon transition to a higher or lower TC regime, neurons (34% of recorded neurons) displayed either a transient increase (peak) or decrease (dip) in their firing rate over about 100 ms. If neurons followed the linear-non-linear model and used gain adaptation, they would uniformly exhibit a peak in firing rate upon transition to higher TC, and a dip upon transition to low TC. In contrast, all combinations of initial responses were observed: peaks for both transition (Peak-Peak, Figure 2.9A), dips for both transition (Dip-Dip, Figure 2.9B) and peak for one and dip for another (Dip-Peak or Peak-Dip, Figure 2.9C-D, also see Figure 2.2A), as characterized by the z-score of their initial response. Across the population (n = 51), there is some correlation with each neuron's adaptation profile and its changes in adapted firing rate (represented by c in the adaptation model, Figure 2.9E): All Dip-Dip neurons exhibit decreased firing rate in response to higher TC. Also, most Dip-Peak neurons exhibit increased firing rate in response to higher TC. However, the Dip-Peak and Peak-Peak populations did not exhibit a consistent change in responses to stimuli with different TC.

Our results demonstrate substantial heterogeneity in the initial response to a transition between high and low TCs. Similar heterogeneity was observed in the time

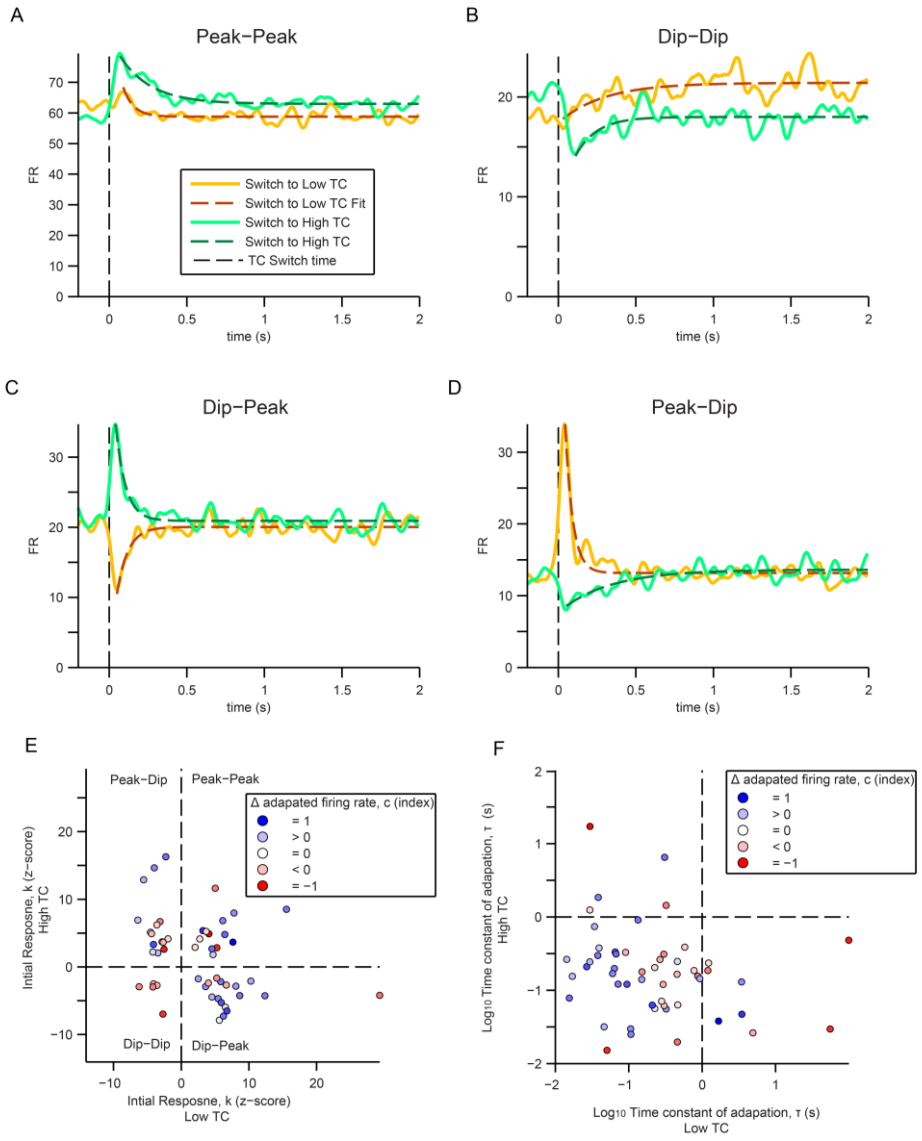

***Figure 2.9*. Heterogeneous responses to abrupt changes in stimulus TC.** A-D. Example PSTHs of the average firing rate of neurons with the transition from one TC level to another centered at time 0. Transitions from high to low TC and its adaptation fit (decaying exponential function, Equation 6) are in orange and dashed dark orange lines, respectively. Transitions from low to high TC and its adaptation fit are in green and dashed dark green lines, respectively. A. A neuron that displays a peak in firing rate after either transition. B. A neuron that displays a dip in firing rate after either transition. C. A neuron that displays a dip in firing rate after transition to low TC and a peak in firing rate after transition to high TC. D. A neuron that displays a peak in firing rate after transition to low TC and a dip in firing rate after transition to high TC. E. Z-score of the initial response (k) after transition to low versus high TC. Each neuron is represented by a circle and its fill color indicates the index of change in adapted firing rate (c). F. Time constant (τ) of the firing rate adaptation after the initial response to the low versus to the high stimulus TC. Each neuron is represented as in E.

constants that characterize the time scale of the adaptation of the baseline firing rate from the peak to baseline (Figure 2.9F). For the majority of cells, the time constants fell below 1 s (Figure 2.9F), which is consistent with previously observed timecourse for gain control in both the inferior colliculus and the auditory cortex (Dean et al., 2008; Rabinowitz et al., 2011). Neurons that increased their firing rate in response to high TC had shorter time constants of adaptation. This suggests that there are multiple processes in place that determine the initial response to TC transition, and that these processes are in some cases distinct from those determining the baseline firing rate change.

Combined, we found that over the neuronal population, there was no significant change in the neuronal steady state firing rates with increase in TC. A prediction for the response strength of neurons to these stimuli was that neurons would exhibit higher firing rates to stimuli with higher TC. Analysis of specific response components revealed that the firing rate adaptation could be attributed to the change in the neuronal stimulus-driven non-linear response gain rather than neuronal spectro-temporal receptive fields. The change in the gain was part of an active adaptation mechanism, triggered by the transition in the stimulus to an increased or decreased TC.

Discussion

Dynamic gain control is ubiquitous in neuronal systems (Baccus and Meister, 2002; Brown and Masland, 2001; Chander and Chichilnisky, 2001; Chen et al., 2010;

Chung et al., 2002; Dean et al., 2005; Dean et al., 2008; Kohn and Movshon, 2003; Kvale and Schreiner, 2004; Nagel and Doupe, 2006; Rabinowitz et al., 2011; Shapley and Victor, 1978; Smirnakis et al., 1997). From the point of view of efficiency of neuronal coding, dynamic gain control permits increased information transmission by matching the dynamic range of responses to the dynamic range of the stimulus (Barlow, 1961; Fairhall et al., 2001; Schwartz and Simoncelli, 2001; Vinje and Gallant, 2002). Neurons in the auditory cortex exhibit tuning to the temporal modulation structure of acoustic stimuli (Linden et al., 2003; Lu et al., 2001; Miller et al., 2002; Ter-Mikaelian et al., 2007; Woolley et al., 2005). This tuning, however, has previously been measured using stimuli with fixed temporal correlation structure. We found that changes in the temporal correlation of a broadband acoustic signal evoked gain control in neuronal responses in the primary auditory cortex. This gain control mechanism affected the non-linear component of the response, improving stimulus encoding. Interestingly, unlike in other sensory modalities (Baccus and Meister, 2002), the temporal response parameters of neurons were not affected by the temporal statistics of the stimulus.

Cortical contribution to temporal gain control. Gain adaptation has previously been observed in the auditory cortex in response to sounds with varying intensity and contrast (Rabinowitz et al., 2011), as well as to transitions between different types of sounds (Asari and Zador, 2009). Responses of neurons in the inferior colliculus have also been shown to exhibit adaptation to sound contrast (Blake and Merzenich, 2002; Dean et al., 2005; Dean et al., 2008; Kvale and Schreiner, 2004). Gain adaptation to stimulus

contrast in the auditory cortex is therefore likely a combination of processing that takes place at the more peripheral processing stages as well as within the cortex, at the level of inhibitory-excitatory neuronal circuits. The dynamic gain control in response to temporal correlation observed in the present study may be driven by a similar mechanism as the previously observed gain control to changes in sound contrast (Chen et al., 2010; Rabinowitz et al., 2011). Indeed, when the stimulus is projected on the receptive field of the neuron, despite its normalization for intensity and standard deviation, it produces signals with increasing dynamic range for higher TCs (Figure 2.5A). As the spectro-temporal receptive field can be thought of as approximating processing performed prior to integration of the inputs by the A1 neuron, the stimulus with an increased TC provides higher dynamic range of inputs to the A1 neuron, much like a stimulus with an increased intensity contrast. This is due to the specific properties of the temporal integration time course of the spectro-temporal receptive fields of A1 neurons. Therefore, the observed gain control likely extends to a range of higher-order statistics beyond the lower-order features, such as intensity, contrast and temporal correlation.

We observed that for some neurons, responses increased with increasing TC (Figure 2.4) – therefore, gain control did not lead to complete adaptation, preserving information about TC in the mean firing rate of the neurons. These effects are consistent with those observed previously in response to an increase in sound contrast, where the firing rate of neurons increases with contrast, but is subject to incomplete

gain control (Rabinowitz et al., 2011). Interestingly, the effects of gain control for changes from high to low TC, and vice versa, were heterogeneous for a subpopulation of neurons. Some neurons that lowered their firing rate to low TC exhibited a transient increase in firing rate upon transition to high TC (Figure 2.9). The non-linear component of the linear-non-linear model is thought to reflect the spiking non-linearity at the level of cortical neurons. Therefore, this observation supports the argument for contribution of intra-cortical mechanisms to gain adaptation, at least in some of the neurons (in which the sign of firing rate change upon transition is inconsistent with the prediction of the linear-non-linear model). Remarkably, we did not find a significant effect on the timing and spectral bandwidth of the receptive fields of the neurons. A circuit that uses synaptic depression or facilitation in implementing gain control would likely result in a change in temporal response properties of the neurons (Abbott et al., 1997; Chance et al., 1998), and therefore is not supported by the present observations. Furthermore, the measured time scale of gain control in A1, with time constants of adaptation below 1 s for most neurons (Figure 2.9F), is greater than the time course of adaptation measured in the inferior colliculus, corresponding to the time constants of tens of milliseconds (Dean et al., 2008). Therefore, while a major component of adaptation may be inherited from earlier auditory areas to the cortex, intra-cortical mechanisms also seem to play an important role.

Relation to previous studies. Neurons in A1 have been shown to exhibit both time-locked and sustained responses to sounds that were modulated at different temporal

rates: neurons responded to fast sounds with a sustained response, encoding the click rate in their mean firing rate; and to slower temporal fluctuation with synchronized spiking discharges, phase-locked to the modulations (Lu et al., 2001). In the present study, we did not observe such a dichotomy in responses; the change from time-locked to sustained responses would have been reflected in a change in the temporal component of the neuronal spectro-temporal receptive field. Here, we did not identify a systematic change in the temporal component of the STRF (Figure 2.6). This inconsistency may be due to the difference in stimuli between different studies: we implemented a novel approach to examining the effect of temporal fluctuation rates on A1 responses by systematically changing the statistical structure of the broadband stimulus. It is plausible that the time scales of the stimulus modulation that were used in this study differed from those used previously. Furthermore, using a spectro-temporally more complex stimulus decreased the synchronization versus firing rate dichotomy, as the responses were likely driven by an integration of onset and sustained acoustic cues.

Our results provide for a potential link between two earlier studies in humans: one identifying differential activation in the human auditory cortex by stimuli with varying temporal modulation rates (Boemio et al., 2005) and the other using a similar stimulus design to ours that found differential activation of the areas downstream in the auditory cortex, including the superior temporal gyrus and auditory association cortex. (Overath et al., 2008). The BOLD signal may average out the heterogeneous changes in the neuronal spiking responses (Logothetis and Wandell, 2004). Our findings provide

support for this explanation for two reasons. The momentarily high responses that are produced at the transition from low to high temporal correlation are likely too fast to be detected by the BOLD signal that integrates the inputs over hundreds of seconds. The gain control mechanism that we observed may normalize the responses that the BOLD signal picks up. At the same time, since some neurons are inhibited by the increase in TC, while others are excited, the averaged population activity is also less affected. In contrast, the downstream areas may convert the heterogeneous changes in the firing rates of A1 neurons into an increase in their firing activity, and therefore, their responsiveness may be detected by the BOLD signal.

Consequences for processing of speech and communication signals. Temporal modulations at different time scales have been shown to correspond to different aspects of the speech signal (Hickok and Poeppel, 2007; Poeppel, 2003; Rosen, 1992). The faster fluctuations denote the fine structure of speech, while the slower fluctuations refer to periodicity and envelope (Rosen, 1992). Signals at different temporal scales contribute information about different aspects of segmental and prosodic cues in speech perception. Our results suggest that at the level of A1, the neuronal resources devoted to any single scale are equalized, as the neuronal firing rates are stable across a range of TCs.

Furthermore, the auditory system shows remarkable invariance to temporal stretching and compressing of acoustic signals: compressing speech up to two-fold does not lead to an impairment in speech comprehension (Ahissar et al., 2001; Beasley et al.,

1980). The neuronal mechanisms that would enable such invariance have been hypothesized to produce a code that also stretches and compresses with changes in the stimulus statistics. Our results do not support such transformation, as the receptive fields of neurons do not change with temporal correlation of the stimulus. Therefore, they are expected to produce differential responses to sounds that are stretched or compressed, consistent with our previous measurements of responses to rat vocalizations and emergent properties of invariant representation within the auditory cortex (Carruthers et al., 2015; Carruthers et al., 2013).

To summarize, we found that neurons in the primary auditory cortex exhibited gain control to changes in the temporal correlation statistics of acoustic stimuli. This adaptation allows neurons to maintain their mean firing rates under different stimulus regimes, while increasing or preserving the information that neurons can transmit about the stimulus.

Bibliography

Abbott, L.F., Varela, J.A., Sen, K., Nelson, S.B., 1997. Synaptic depression and cortical gain control. Science 275, 220-224.

Ahissar, E., Nagarajan, S., Ahissar, M., Protopapas, A., Mahncke, H., Merzenich, M.M., 2001. Speech comprehension is correlated with temporal response patterns recorded from auditory cortex. Proc Natl Acad Sci U S A 98, 13367-13372.

Aizenberg, M., Geffen, M.N., 2013. Bidirectional effects of auditory aversive learning on sensory acuity are mediated by the auditory cortex. Nat Neurosci 16, 994-996.

Aizenberg, M., Mwilambwe-Tshilobo, L., Briguglio, J.J., Natan, R.G., Geffen, M.N., 2015. Bidirectional Regulation of Innate and Learned Behaviors That Rely on Frequency Discrimination by Cortical Inhibitory Neurons. PLoS Biol 13, e1002308.

Asari, H., Zador, A., 2009. Long-lasting context dependence constrains neural encoding models in rodent auditory cortex. J Neurophysiol 102, 2638-2656.

Attias, H., Schreiner, C., 1997. Temporal low-order statistics of natural sounds. Advances in Neural Information and Processing Systems 9, 27-33.

Baccus, S.A., Meister, M., 2002. Fast and slow contrast adaptation in retinal circuitry. Neuron 36, 909-919.

Barlow, H.B., 1961. Possible principles underlying the transformation of sensory messages, in: Rosenblith, W. (Ed.), Sensory Communication. MIT Press, Cambridge, MA, pp. 217-234.

Beasley, D.S., Bratt, G.W., Rintelmann, W.F., 1980. Intelligibility of time-compressed sentential stimuli. J Speech Hear Res 23, 722-731.

Bizley, J.K., Walker, K.M., King, A.J., Schnupp, J.W., 2010. Neural ensemble codes for stimulus periodicity in auditory cortex. J Neurosci 30, 5078-5091.

Blackwell, J.M., Taillefumier, T.O., Natan, R.G., Carruthers, I.M., Magnasco, M.O., Geffen, M.N., 2015. Stable encoding of sounds over a broad range of statistical parameters in the auditory cortex. Eur J Neurosci, 10.1111/ejn.13144.

Blake, D.T., Merzenich, M.M., 2002. Changes of AI receptive fields with sound density. J Neurophysiol 88, 3409-3420.

Boemio, A., Fromm, S., Braun, A., Poeppel, D., 2005. Hierarchical and asymmetric temporal sensitivity in human auditory cortices. Nat Neurosci 8, 389-395.

Brasselet, R., Panzeri, S., Logothesis, N.K., Kayser, C., 2012. Neurons with Stereotyped and Rapid Responses Provide a Reference Frame for Relative Temporal Coding in Primate Auditory Cortex. Journal of neuroscience 32, 2998-3008.

Brown, S.P., Masland, R.H., 2001. Spatial scale and cellular substrate of contrast adaptation by retinal ganglion cells. Nat Neurosci 4, 44-51.

Carruthers, I.M., Laplagne, D.A., Jaegle, A., Briguglio, J.J., Mwilambwe-Tshilobo, L., Natan, R.G., Geffen, M.N., 2015. Emergence of invariant representation of vocalizations in the auditory cortex. J Neurophysiol 114, 2726-2740.

Carruthers, I.M., Natan, R.G., Geffen, M.N., 2013. Encoding of ultrasonic vocalizations in the auditory cortex. J Neurophysiol 109, 1912-1927.

Chance, F.S., Nelson, S.B., Abbott, L.F., 1998. Synaptic depression and the temporal response characteristics of V1 cells. J Neurosci 18, 4785-4799.

Chander, D., Chichilnisky, E.J., 2001. Adaptation to temporal contrast in primate and salamander retina. J Neurosci 21, 9904-9916.

Chauvin, A., Worsley, K.J., Schyns, P.G., Arguin, M., Gosselin, F., 2005. Accurate statistical tests for smooth classification images. J Vis 5, 659-667.

Chen, T.L., Watkins, P.V., Barbour, D.L., 2010. Theoretical limitations on functional imaging resolution in auditory cortex. Brain Res 1319, 175-189.

Chung, S., Li, X., Nelson, S.B., 2002. Short-term depression at thalamocortical synapses contributes to rapid adaptation of cortical sensory responses in vivo. Neuron 34, 437-446.

Churchland, A.K., Kiani, R., Chaudhuri, R., Wang, X.J., Pouget, A., Shadlen, M.N., 2011. Variance as a signature of neural computations during decision making. Neuron 69, 818-831.

Dean, I., Harper, N.S., McAlpine, D., 2005. Neural population coding of sound level adapts to stimulus statistics. Nat Neurosci 8, 1684-1689.

Dean, I., Robinson, B.L., Harper, N.S., McAlpine, D., 2008. Rapid neural adaptation to sound level statistics. J Neurosci 28, 6430-6438.

Escabi, M.A., Miller, L.M., Read, H.L., Schreiner, C.E., 2003. Naturalistic auditory contrast improves spectrotemporal coding in the cat inferior colliculus. J Neurosci 23, 11489-11504.

Fairhall, A.L., Lewen, G.D., Bialek, W., de Ruyter Van Steveninck, R.R., 2001. Efficiency and ambiguity in an adaptive neural code. Nature 412, 787-792.

Geffen, M.N., Broome, B.M., Laurent, G., Meister, M., 2009. Neural encoding of rapidly fluctuating odors. Neuron 61, 570-586.

Geffen, M.N., de Vries, S.E., Meister, M., 2007. Retinal ganglion cells can rapidly change polarity from Off to On. PLoS Biol 5, e65.

Geffen, M.N., Gervain, J., Werker, J.F., Magnasco, M.O., 2011. Auditory perception of self-similarity in water sounds. Front Integr Neurosci 5, 15.

Gervain, J., Werker, J.F., Geffen, M.N., 2014. Category-specific processing of scale-invariant sounds in infancy. PLoS One 9, e96278.

Hickok, G., Poeppel, D., 2007. The cortical organization of speech processing. Nat Rev Neurosci 8, 393-402.

Hosoya, T., Baccus, S.A., Meister, M., 2005. Dynamic predictive coding by the retina. Nature 436, 71-77.

Kohn, A., Movshon, J.A., 2003. Neuronal adaptation to visual motion in area MT of the macaque. Neuron 39, 681-691.

Kvale, M., Schreiner, C., 2004. Short-term adaptation of auditory receptive fields to dynamic stimuli. J Neurophysiol 91, 604-612.

Linden, J.F., Liu, R.C., Sahani, M., Schreiner, C.E., Merzenich, M.M., 2003. Spectrotemporal structure of receptive fields in areas AI and AAF of mouse auditory cortex. J Neurophysiol 90, 2660-2675.

Logothetis, N.K., Wandell, B.A., 2004. Interpreting the BOLD signal. Annual review of physiology 66, 735-769.

Lu, T., Liang, L., Wang, X., 2001. Temporal and rate representations of time-varying signals in the auditory cortex of awake primates. Nat Neurosci 4, 1131-1138.

Marguet, S.L., Harris, K.D., 2011. State-dependent representation of amplitude-modulated noise stimuli in rat auditory cortex. J Neurosci 31, 6414-6420.

McDermott, J.H., Schemitsch, M., Simoncelli, E.P., 2013. Summary statistics in auditory perception. Nat Neurosci 16, 493-498.

McDermott, J.H., Simoncelli, E.P., 2011. Sound texture perception via statistics of the auditory periphery: evidence from sound synthesis. Neuron 71, 926-940.

Miller, L.M., Escabi, M.A., Read, H.L., Schreiner, C.E., 2002. Spectrotemporal receptive fields in the lemniscal auditory thalamus and cortex. J Neurophysiol 87, 516-527.

Mwilambwe-Tshilobo, L., Davis, A.J., Aizenberg, M., Geffen, M.N., 2015. Selective Impairment in Frequency Discrimination in a Mouse Model of Tinnitus. PLoS One 10, e0137749.

Nagel, K.I., Doupe, A.J., 2006. Temporal processing and adaptation in the songbird auditory forebrain. Neuron 51, 845-859.

Natan, R.G., Briguglio, J.J., Mwilambwe-Tshilobo, L., Jones, S.I., Aizenberg, M., Goldberg, E.M., Geffen, M.N., 2015. Complementary control of sensory adaptation by two types of cortical interneurons. eLife 4, pii: e09868.

Otazu, G.H., Tai, L.H., Yang, Y., Zador, A.M., 2009. Engaging in an auditory task suppresses responses in auditory cortex. Nat Neurosci 12, 646-654.

Overath, T., Kumar, S., von, K., Katharina, Griffiths, T.D., 2008. Encoding of spectral correlation over time in auditory cortex. J Neurosci 28, 13268-13273.

Poeppel, D., 2003. The analysis of speech in different temporal integration windows: cerebral lateralization as asymmetric sampling in time. Speech Communication 41, 245-255.

Polley, D.B., Read, H.L., Storace, D.A., Merzenich, M.M., 2007. Multiparametric auditory receptive field organization across five cortical fields in the albino rat. J Neurophysiol 97, 3621-3638.

Rabinowitz, N.C., Willmore, B.D., Schnupp, J.W., King, A.J., 2011. Contrast gain control in auditory cortex. Neuron 70, 1178-1191.

Remez, R.E., Rubin, P.E., Pisoni, D.B., Carrell, T.D., 1981. Speech perception without traditional speech cues. Science 212, 947-949.

Rosen, S., 1992. Temporal information in speech: acoustic, auditory and linguistic aspects. Philos Trans R Soc Lond B Biol Sci 336, 367-373.

Sally, S., Kelly, J., 1988. Organization of auditory cortex in the albino rat: sound frequency. J Neurophysiol 59, 1627-1638.

Schneider, D.M., Woolley, S.M., 2010. Discrimination of communication vocalizations by single neurons and groups of neurons in the auditory midbrain. J Neurophysiol 103, 3248-3265.

Schonwiesner, M., Rubsamen, R., von Cramon, D.Y., 2005. Hemispheric asymmetry for spectral and temporal processing in the human antero-lateral auditory belt cortex. Eur J Neurosci 22, 1521-1528.

Schwartz, O., Simoncelli, E.P., 2001. Natural signal statistics and sensory gain control. Nat Neurosci 4, 819-825.

Shannon, R.V., Zeng, F.G., Kamath, V., Wygonski, J., Ekelid, M., 1995. Speech recognition with primarily temporal cues. Science 270, 303-304.

Shapley, R.M., Victor, J.D., 1978. The effect of contrast on the transfer properties of cat retinal ganglion cells. J Physiol 285, 275-298.

Shechter, B., Depireux, D.A., 2007. Stability of spectro-temporal tuning over several seconds in primary auditory cortex of the awake ferret. Neuroscience 148, 806-814.

Singh, N., Theunissen, F., 2003. Modulation spectra of natural sounds and ethological theories of auditory processing. J Acoust Soc Am 114, 3394-3411.

Smirnakis, S.M., Berry, M.J., Warland, D.K., Bialek, W., Meister, M., 1997. Adaptation of retinal processing to image contrast and spatial scale. Nature 386, 69-73.

Ter-Mikaelian, M., Sanes, D.H., Semple, M.N., 2007. Transformation of temporal properties between auditory midbrain and cortex in the awake Mongolian gerbil. J Neurosci 27, 6091-6102.

Theunissen, F.E., David, S.V., Singh, N.C., Hsu, A., Vinje, W.E., Gallant, J.L., 2001. Estimating spatio-temporal receptive fields of auditory and visual neurons from their responses to natural stimuli. Network 12, 289-316.

Vinje, W.E., Gallant, J.L., 2002. Natural stimulation of the nonclassical receptive field increases information transmission efficiency in V1. J Neurosci 22, 2904-2915.

Watkins, P.V., Barbour, D.L., 2011. Level-tuned neurons in primary auditory cortex adapt differently to loud versus soft sounds. Cereb Cortex 21, 178-190.

Woolley, S., Fremouw, T., Hsu, A., Theunissen, F., 2005. Tuning for spectro-temporal modulations as a mechanism for auditory discrimination of natural sounds. Nat Neurosci 8, 1371-1379.

Woolley, S., Gill, P., Theunissen, F., 2006. Stimulus-dependent auditory tuning results in synchronous population coding of vocalizations in the songbird midbrain. J Neurosci 26, 2499-2512.

Zatorre, R.J., Belin, P., 2001. Spectral and temporal processing in human auditory cortex. Cereb Cortex 11, 946-953.

3. Complementary control of sensory adaptation by two types of cortical interneurons.

Abstract

Reliably detecting unexpected sounds is important for environmental awareness and survival. By selectively reducing responses to frequently, but not rarely, occurring sounds, auditory cortical neurons are thought to enhance the brain's ability to detect unexpected events through stimulus-specific adaptation (SSA). The majority of neurons in the primary auditory cortex exhibit SSA, yet little is known about the underlying cortical circuits. We found that two types of cortical interneurons differentially amplify SSA in putative excitatory neurons. Parvalbumin-positive interneurons (PVs) amplify SSA by providing non-specific inhibition: optogenetic suppression of PVs led to an equal increase in responses to frequent and rare tones. In contrast, somatostatin-positive interneurons (SOMs) selectively reduce excitatory responses to frequent tones: suppression of SOMs led to an increase in responses to frequent, but not to rare tones. A mutually coupled excitatory-inhibitory network model accounts for distinct mechanisms by which cortical inhibitory neurons enhance the brain's sensitivity to unexpected sounds. **Published as Natan, R.G., Briguglio, J.J., Mwilambwe-Tshilobo, L., Jones, S.I., Aizenberg, M., Goldberg, E.M., Geffen, M.N., (2015). Complementary control of sensory adaptation by two types of cortical interneurons. eLife 4, pii: e09868**

Introduction

Across sensory modalities, cortical neurons exhibit adaptation, attenuating their responses to redundant stimuli (Asari and Zador, 2009; Das and Gilbert, 1999; Garcia-Lazaro et al., 2007; Khatri et al., 2009; Ulanovsky et al., 2003). Adaptation to stimulus context is thought to increase efficiency of sensory coding under the constraints of limited resources (Barlow, 1961). Yet the neuronal-circuit mechanisms that facilitate adaptation in the cortex remain poorly understood. In the primary auditory cortex, the vast majority of neurons exhibit stimulus-specific adaptation (SSA, Figure 3.1). When presented with a sequence of two tones, one of which occurs frequently (termed "standard") and another rarely (termed "deviant"), the neuron's response to the standard becomes weaker, but the response to the deviant remains strong (Farley et al., 2010; Fishman and Steinschneider, 2012; Szymanski et al., 2009; Ulanovsky et al., 2003). Whereas SSA has also been found in sub-cortical structures, e.g. in the auditory midbrain (Malmierca et al., 2009; Thomas et al., 2012; Zhao et al., 2011) and the auditory thalamus (Anderson et al., 2009; Antunes et al., 2010; Bauerle et al., 2011; Kraus et al., 1994), it is weak in the lemniscal areas, which project to A1, and stronger in those non-lemniscal areas that receive feedback from A1 (Duque et al., 2012; Perez-Gonzalez et al., 2005; Ulanovsky et al., 2004). Therefore, cortical circuits are proposed to contribute to and amplify SSA in A1 (Bauerle et al., 2011; Escera and Malmierca, 2014; Fishman and Steinschneider, 2012; Szymanski et al., 2009; Ulanovsky et al., 2003),

through a combination of plastic modulation of thalamocortical inputs and intra-cortical inhibitory circuits, which would allow for selective suppression of neuronal responses to specific stimuli (Nelken, 2014). Our study tests whether and how inhibitory neurons contribute to cortical SSA.

Auditory cortex, like other sensory cortices, contains morphologically and physiologically diverse inhibitory interneurons, which form dense interconnected networks with excitatory neurons (DeFelipe, 2002; Douglas and Martin, 2004). While different interneuron types have been hypothesized to carry out specialized complementary functions in sensory processing (DeFelipe, 2002; Isaacson and Scanziani, 2011; Kepecs and Fishell, 2014; Markram et al., 2004; Marlin et al., 2015), their function in driving changes in dynamic auditory processing has not been previously established. We hypothesized that the two most common types of interneurons in the cortex, parvalbumin- (PVs) and somatostatin-positive cells (SOMs) (Rudy et al., 2011; Xu et al., 2010), facilitate SSA in excitatory neurons of A1 in a complementary fashion. PVs, a subset of which receive direct thalamic inputs (Staiger et al., 1996), may amplify SSA in excitatory neurons by providing a constant inhibitory drive; equally strong inhibitory drive would attenuate the weak response to standard tones relatively more than the strong response to deviant tones, leading to a greater differential between standard versus deviant tone spiking response. SOMs, which target distal dendrites of pyramidal cells (Gentet et al., 2012; McGarry et al., 2010), receive excitatory synapses that exhibit facilitation upon repetitive stimulation (Reyes et al., 1998; Silberberg and Markram,

2007). Therefore, inputs from SOMs may exert a stimulus-specific increase in suppression of excitatory neurons that is selective to the standard and does not generalize to the deviant. Alternatively, they may contribute to selective adaptation in excitatory neurons through differential post-synaptic integration.

To tease apart the function of different inhibitory types in SSA, we tested whether optogenetic suppression of either PV or SOM interneurons during sound presentation reduced SSA in putative excitatory neurons in the auditory cortex (Hamilton et al., 2013; Pi et al., 2013; Weible et al., 2014). We found that both types of interneurons contribute to SSA in the cortex, with PVs providing constant inhibition, and SOMs increasing their effect with repeated tones.

Results

Nearly all neurons in A1 exhibit SSA. We recorded spiking activity of neurons as well as local field potentials in A1 in head-fixed mice under light isoflurane anesthesia. SSA was measured from the firing rate of neurons in response to tones presented as a series of "oddball" stimuli. Each oddball stimulus consisted of a sequence of tone pips at one of two frequencies (tones A and B). In each oddball stimulus, one tone was presented as the rare (deviant) tone while the other was presented as the frequent (standard) tone (A to B ratio of 90:10 or 10:90, Figure 3.1a). A third stimulus was also presented (equal stimulus), with tones A and B being presented equally often (50:50). The frequencies of tone A and B were selected at 0.39 octave interval, below the typical tuning bandwidth

of A1 neurons (Guo et al., 2012; Hackett et al., 2011; Kanold et al., 2014), such that they activated the majority of recorded neurons on each session (Figure 3.1b).

As expected, for a representative neuron recorded in A1, the mean firing rate (FR) in response to a tone was lower when the tone was presented as the standard than as the deviant (Figure 3.1c), exhibiting SSA. To quantify the level of adaptation for each neuron, we computed the index of the change in FR to the same tone when it was presented as the deviant versus the standard (SSA index). SSA index is 1 when adaptation is complete i.e., no response to the standard, and significant response to the deviant, and 0 when there is no adaptation i.e., the response to the standard and deviant are equal. Almost all neurons recorded in A1 exhibited significant SSA (Figure 3.1d, standard tone-evoked FR significantly lower than the deviant tone-evoked FR in N = 138 out of 147 neurons, Wilcoxon rank sum test $p < 0.05$).

Contribution of thalamocortical inputs to SSA. We first tested whether SSA is present in inputs from the thalamus. Current source density analysis has been extensively used to quantify inputs from the thalamus (Happel et al., 2014; Kaur et al., 2005; Metherate and Cruikshank, 1999; Szymanski et al., 2009). We used a linear probe to record local field potentials using electrodes spaced 50 microns apart inserted perpendicularly to brain surface in the primary auditory cortex. The multi-electrode probe is 775 µm long, spanning layers 1-6 of mouse A1. Current source density is computed as the second spatial derivative of the LFPs across the depth of the cortex (Figure 3.1e, Figure 3.1—Figure supplement 1a, 20 sessions, 15 mice). Typically, in response to tones, CSD

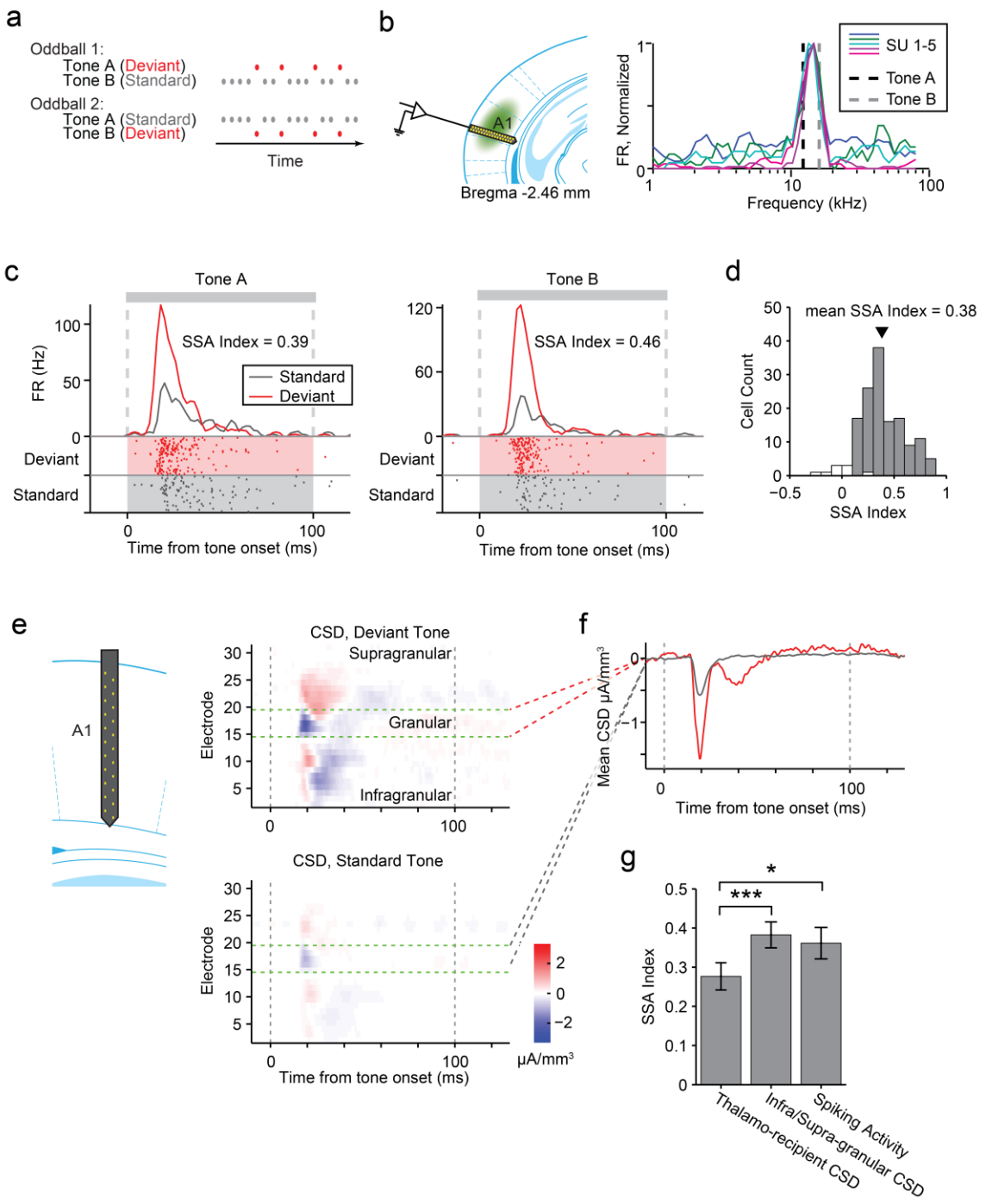

Figure 3.1. Nearly all recorded A1 neurons exhibit stimulus-specific adaptation. (**a**) Diagrams of oddball stimuli; Oddball stimuli are composed of a 2.5 Hz train of 100ms long sine-wave tone pips separated by 300ms of silence (gray and red dots). Each tone pip is at one of two frequencies, tone A or B. In oddball stimulus 1, 10% of all pips are tone A and 90% of pips are tone B. In oddball stimulus 2, the tone probabilities are reversed. The less frequent tone is referred to as the deviant tone (red dots). The more frequent tone is

referred to as the standard (gray dots). (**b**) Left: Diagram of recording. Electrode was lowered perpendicular to the brain surface. Virus was injected in A1. Right: The frequencies of tones A and B (dashed black and gray lines) are selected based on the frequency response functions of neurons of interest. Mean firing rate of 5 co-tuned neurons (colored lines) recorded simultaneously in a single session in response to 65dB tone pips at 50 frequencies logarithmically spaced from 1 to 80k Hz. FR is normalized to the peak response of each neuron. (**c**) A representative neuron exhibited suppressed responses to a tone presented as a standard (gray raster and PSTH) compared to the same tone presented as a deviant (red raster and PSTH). Left: Responses to tone A, presented as a deviant in oddball stimulus 1, and a standard in oddball stimulus 2. Right: Responses to tone B. Shaded regions indicate standard (gray) and deviant (red) tones trials. Gray dashed lines indicate tone onset and offset times. (**d**) Population histogram of SSA index exhibited by all neurons included in the analysis. Gray and white bars indicate neurons expressing significant and non-significant SSA, respectively. Spike count for response to deviant tones was significantly greater than for response to standard tones (Wilcoxon rank sum test, one tail, $p < 0.05$). The black marker indicates the population average SSA index. (**e**) Left: Diagram of electrode spanning A1. Right: Representative peri-stimulus CSD. Top: Mean response to deviant tones. Bottom: Mean response to standard tones. Gray dashed lines indicate tone onset and offset. Green dashed lines indicate the location of the granular layer. Negative CSD values (blue) indicate current sinks, while positive CSD values (red) indicate current sources. (**f**) Mean CSD collected from the thalamo-recipient layer, in response to standard (gray) and deviant (red) tones. Gray dashed lines indicate tone onset and offset. (**g**) Mean SSA index across sessions measured from thalamo-recipient granular layer CSD, infra- and supra-granular layer cortical CSD and mean neuronal spiking activity SSA index averaged over sessions.

exhibits a negative basin, termed sink, within a short delay of tone onset, localized to electrodes in thalamo-recipient layer (Figure 3.1f, Figure 3.1—Figure supplement 1b) (Kaur et al., 2005; Szymanski et al., 2009). The amplitude of current in the sink was taken as a measure of the combined strength of post-synaptic inputs onto layer 4 neurons, which should reflect the strength of the thalamic inputs to the cortex (Happel et al., 2014; Kaur et al., 2005; Metherate and Cruikshank, 1999; Szymanski et al., 2009).

We compared the amplitude of the CSD sink for each tone when presented as a deviant or standard, and computed their ratio (Figure 3.1 f). The sink amplitude was lower for the standard as compared to the deviant tones (Figure 3.1f, g), suggesting that excitatory signals produced by thalamo-cortical inputs exhibit stimulus-specific

adaptation, consistent with previous findings (Szymanski et al., 2009). This finding supports the "adaptation in narrowly tuned inputs" model, which postulates that stimulus-specific adaptation in broadly tuned neurons in A1 reflects adaptation in either thalamocortical inputs, or at the stage of integration of thalamocortical inputs, specific to inputs tuned to the standard tone (Mill et al., 2011; Nelken, 2014; Taaseh et al., 2011). Importantly, across sessions, the SSA index of the granular layer CSD sinks was significantly lower than that of either the non-thalamo-recipient layers (Δ = -28%, p-value from one-sided test after correction (p1) = 6e-4, z = -3.4, Bonferroni corrected for 2 tests (C = 2)) or the SSA index of the mean spiking activity of A1 neurons (Δ = 23%, p1 = 0.029, z = -2.1, C = 2) in each session (N = 20 sessions in 15 mice, Figure 3.1g), suggesting that additional intra-cortical mechanisms may contribute to SSA in the cortex.

Suppression of either PVs or SOMs decreases SSA in putative excitatory neurons. We next tested whether cortical inhibitory interneurons may contribute to stimulus-specific adaptation. Since different inhibitory neuronal subtypes can differentially affect sensory responses of putative excitatory neurons (Cottam et al., 2013b; Lee et al., 2012; Wilson et al., 2012), we separately tested the role of PVs and SOMs. We used targeted viral delivery in the auditory cortex of mice to drive Archaerhodopsin (Arch) expression, which hyperpolarizes neurons when stimulated by light, in either PVs or SOMs (Chow et al., 2010). A modified adeno-associated virus (AAV) encoding anti-sense code for Arch and a fluorescent reporter, under the FLEX cassette, was injected into PV-Cre or SOM-Cre mice (Boyden et al., 2005; Cardin et al., 2010; Deisseroth, 2011; Sohal et al., 2009;

Zhang et al., 2010) (Figure 3.2a). Two weeks following virus injection, Arch was expressed selectively in PVs or SOMs in auditory cortex at expected levels (Kvitsiani et al., 2013) (Figure 3.2b, c PV-Cre: N = 250 neurons in 4 mice, specificity = 92 ± 1%, efficiency = 73 ± 5%. SOM-Cre: N = 149 neurons in 5 mice, specificity = 95 ± 2%, efficiency = 86 ± 5%). To activate Arch, a light guide was positioned to cast 180mW/mm^2 532 nm light onto A1 surface, perpendiular to cortical layers. *In vitro* intracellular recordings from optically identified PVs or SOMs (Figure 3.2—Figure supplement 1, 3) demonstrate that light cast over the auditory cortex *in vitro* drives a strong suppressive current (Figure 3.2d, Figure 3.2—Figure supplement 1c, d 2c, d) and hyperpolarizes the membrane potential in these neurons (Figure 3.2—Figure supplement 1b, 2b). Assuming a 100 fold attenuation of light over 1 mm of brain tissue (Aravanis et al., 2007), the estimated irradiance in the deepest cortical layer (1.8 mW/mm^2) was strong enough to induce hyperpolarizing current in neurons *in vitro* (Figure 3.2d). *In vivo*, in both PV-Cre and SOM-Cre mice, illuminating the auditory cortex suppressed spiking activity in a small subset of recorded neurons (Figure 3.2e, f, left, putative inhibitory neurons) and increased activity in a great majority of recorded neurons (Figure 3.2e, f right, putative excitatory neurons). Shining light over A1 increased spontaneous neuronal activity in the majority of the recorded neurons in both PV-Cre mice (N = 115 neurons, 102 increased, 0 decreased, in 10 mice) (Figure 3.2g) and SOM-Cre mice (N = 104 neurons, 61 increased, 3 decreased, in 9 mice) (Figure 3.2h). These measurements demonstrate that casting light over A1 selectively and effectively suppresses the activity of either PVs or SOMs.

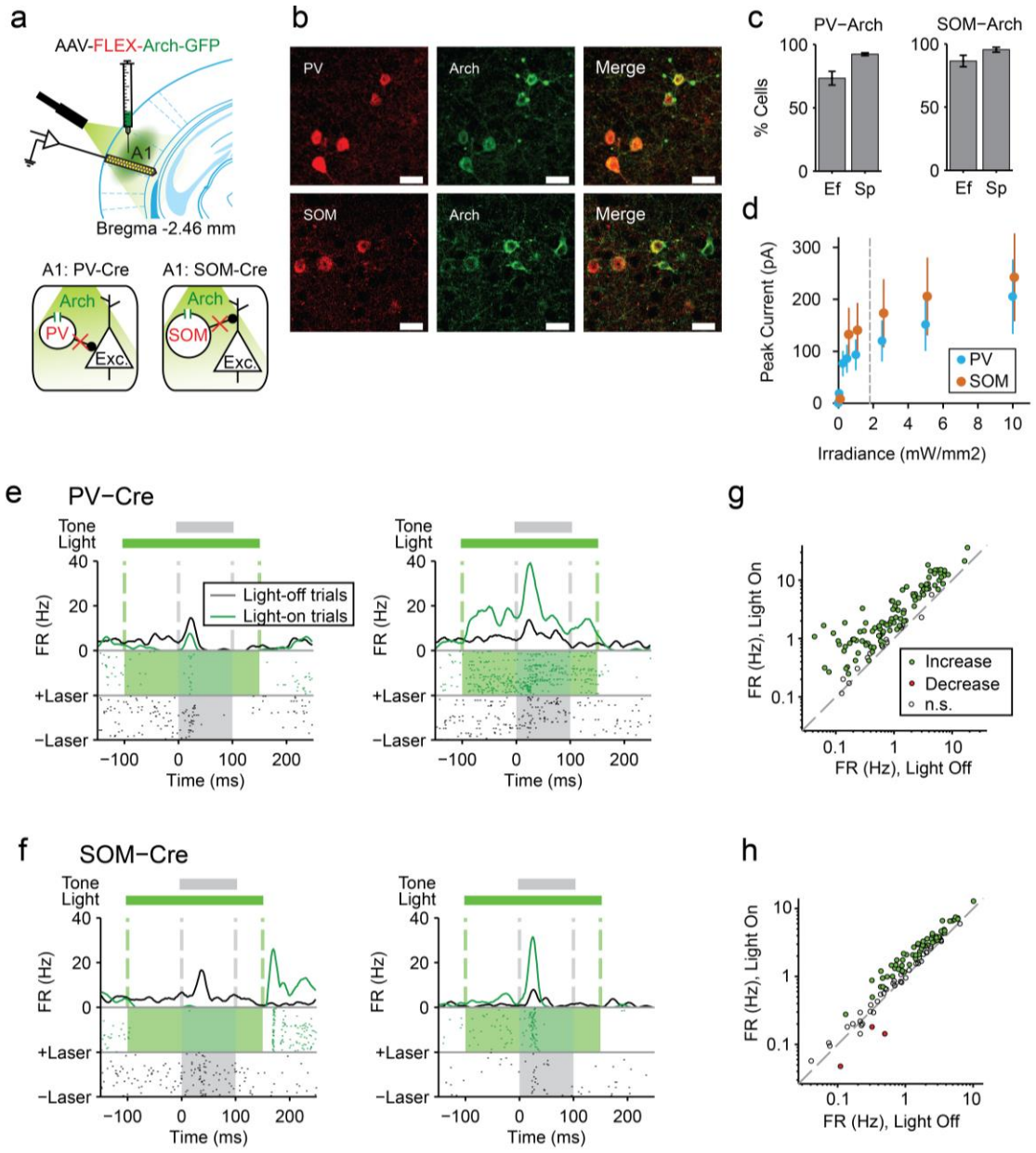

Figure 3.2. Cell type–specific optogenetic suppression of parvalbumin-positive and somatostatin-positive neurons. (**a**) Optogenetic methods diagram. Top: A1 was injected with AAV-FLEX-Arch-GFP. During experiments, an optic fiber was positioned to target A1 and neuronal activity was recorded using a multichannel silicon probe in A1. Bottom: Green light (532 nm) suppresses PVs in PV-Cre mice or SOMs in SOM-Cre mice. (**b**) Transfection of interneurons with Arch. Immunohistochemistry demonstrating co-expression of the Arch and an interneuron-type reporter in A1. Top: PV-Cre mouse A1. Red: anti-body stain for parvalbumin. Green: Arch-GFP. Merge; co-expression of Arch and parvalbumin. Bottom: SOM-Cre mouse A1. Red: anti-body stain for somatostatin. Green: Arch-GFP. Merge; co-expression of Arch and somatostatin. Scale Bar = 25 µm. (**c**) Efficiency and specificity of transfection of interneurons with Arch. Bar Plots: Efficiency (Ef) and specificity (Sp) of visual transfection of PVs (top) and SOMs (bottom) with Arch. Ef - Percent of

labelled interneurons expressing Arch. Sp -Percent of Arch-expressing cells which are also labelled interneurons. (**d**) Mean Arch mediated outward current evoked in response to increasing photostimulation power, recorded *in vitro* by whole cell patch recording in putative excitatory neurons from PV-Cre (blue, N = 5) and SOM-Cre (orange, N = 5) mice. The gray dashed line indicates the level of irradiance expected in *in vivo* experiments at the deepest recording sites, in cortical layer 6. (**e, f**) Tone responses of single representative neurons, which are suppressed (left) or activated (right) by photostimulation, from PV-Cre (**e**) and SOM-Cre (**f**) mice. Raster plot of spike times (bottom) and PSTH (top) of a single neuron response to a 100 ms long tone (gray dashed lines, shaded region) on light-on (overlapping 250-ms light pulse, green shading) and light-off trials. Light-on trials: green. Light-off trials: black. (**g, h**) Modulation of spontaneous FR by interneuron photosuppression recorded in PV-Cre (**g**) and SOM-Cre (**h**) mice. Each neuron is represented by a circle that is filled for those with significantly increased (green) or decreased (red) FR or unfilled for those without significant modulation. Gray dashed line – identity line.

To test the function of PVs and SOMs in SSA, their activity was suppressed during every 5th tone of the oddball stimulus by illuminating A1 (Figure 3.3a). To directly test the effect of interneuron suppression, we computed the SSA index separately on light-on and light-off trials for neurons responsive to both tones A and B (SSA was found in 63 out of 67 tone-responsive neurons in PV-Cre mice, 42 out of 43 tone-responsive neurons in SOM-Cre mice). Photosuppression of either PVs or SOMs affected the responses of neurons to the tones (Figure 3.3b, c), resulting in a significant reduction in SSA index across the population (Figure 3.3e, f, PV-Cre: Δ = -41%, p1 = 1e-12, t (66) = 8.6. SOM-Cre: Δ = -25%, p1 = 2e-6, t (42) = 5.4). Photo-manipulation affected responses only to the tone during which it was presented, but not to subsequent tones (Figure 3.3—Figure supplement 1). Additionally, photo-manipulation was limited to cortex since it did not affect thalamo-recipient layer CSD tone responses and SSA (Figure 3.3 – Figure supplement 2). In a control group of PV-Cre or SOM-Cre mice (6 mice), we injected a modified AAV which encoded anti-sense fluorescent reporter alone under the FLEX cassette, and computed the effect of casting light on SSA (SSA was found in 33 out of 37

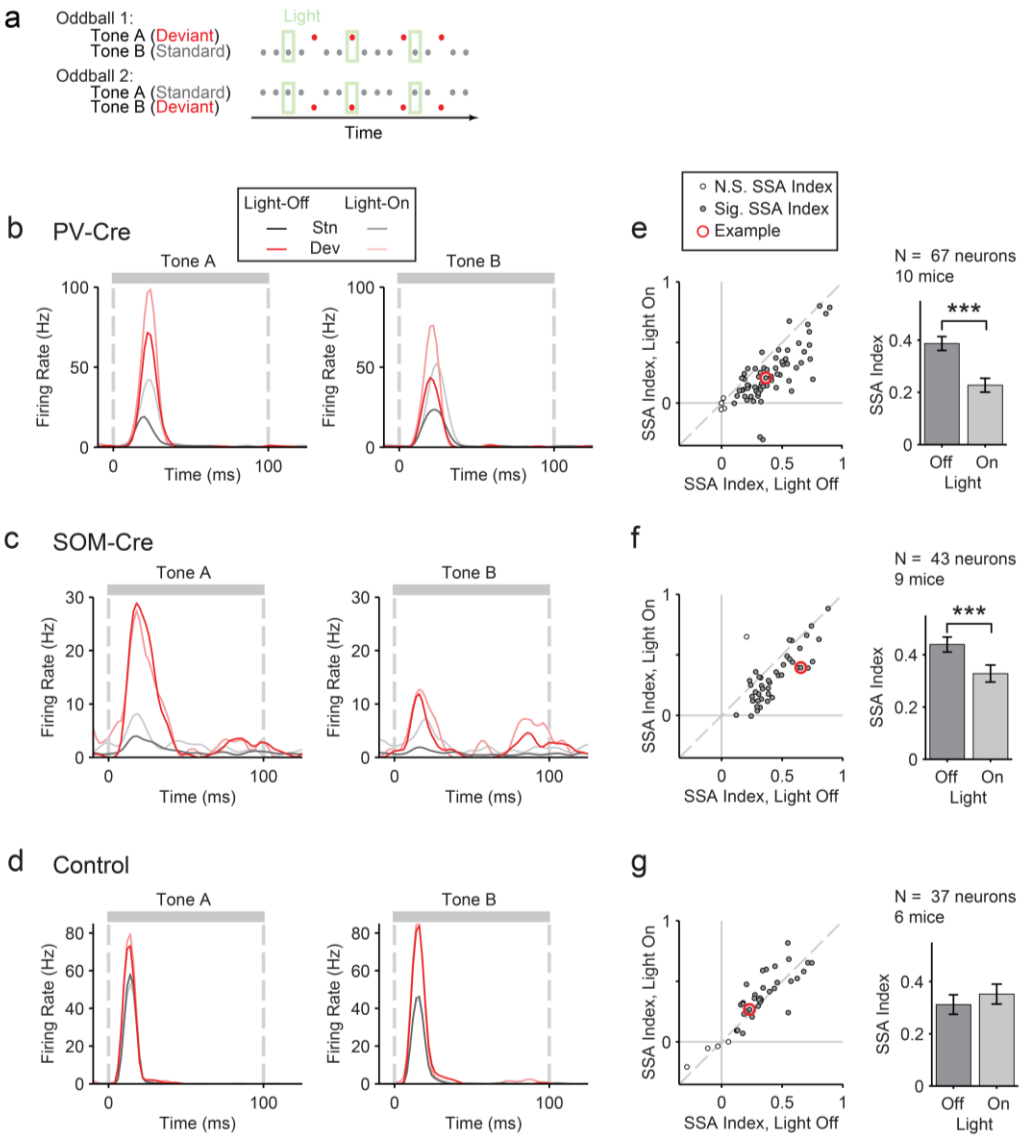

Figure 3.3 Optogenetic suppression of either PVs or SOMs reduces stimulus-specific adaptation in putative excitatory neurons in the auditory cortex. (**a**) Diagram of oddball stimuli with light; Two oddball stimuli are presented (as in Figure 3.1**a**), with 250 ms light pulses (green bars) delivered during every 5th tone, starting 100ms before tone onset. (**b-d**) Representative neuron PSTH in response to tone A (left) and B (right) as a standard (gray) or deviant (red) on light-on (light colors) and light-off trials (dark colors). Neurons recorded in PV-Cre (**b, e**), SOM-Cre (**c, f**), and control (**d, g**) mice. (**e-g**) Effect of interneuron photosuppression on SSA. Left: SSA index on light-on vs light-off trials. Each neuron is represented by a circle that is filled if the neuron exhibits significant SSA i.e. its FR in response to deviant tones is greater than that to standard tones. The respective representative neuron in **b, c,** and **d** is indicated by a red circle. Gray dashed line - identity line. Right: Mean SSA index on light-on (green) and light-off (gray) trials over neuronal population.

tone-responsive neurons in control mice). In this control group, SSA was not affected by light (Figure 3.3d, g, $p > 0.05$, $t(36) = -2.0$), confirming that Arch expression was required for the effect of the light. Therefore, the effects of interneurons are specific to intra-cortical mechanisms. These results demonstrate that both types of interneurons contribute to the reduction of the response of the neuron to the stimulus during SSA.

PVs and SOMs differentially suppress putative excitatory neuron responses to standard and deviant tones. A decrease in the SSA index may be due to several factors: (1) an increase in response to the standard only, (2) a decrease in response to the deviant, or (3) an increase in response both to the standard and the deviant, but with a relatively greater increase for the standard. Therefore, we next investigated the effect of interneuron photosuppression on FR of putative excitatory neurons evoked by the standard and deviant tones separately. The effects of PVs and SOMs diverged; in addition to increasing spontaneous activity ($\Delta = 185\%$, p-value from one-sided t-test after correction (p2) = 3e-11, $t(159) = -7.2$), suppressing PVs led to increased FR to both the standard ($\Delta = 102\%$, p2 = 3e-11, $t(159) = -7.2$) and deviant ($\Delta = 56\%$, p2 = 9e-12, $t(159) = -7.4$) tones (N = 160, Figure 3.4a, b, c, Figure 3.4—Figure supplement 1a). 83% of neurons exhibited greater FR to the standard and 46% to the deviant during PV suppression (Figure 3.4—Figure supplement 1b). The difference in FR due to suppression of PVs was not significantly different between the standard and deviant tones ($p2 > 0.05$, $t(159) = -0.1$, C = 2) but both were greater than the difference in the spontaneous firing rate (Standard: $\Delta = 25\%$, p2 = 0.001, $t(159) = -3.6$, C = 2. Deviant: $\Delta =$

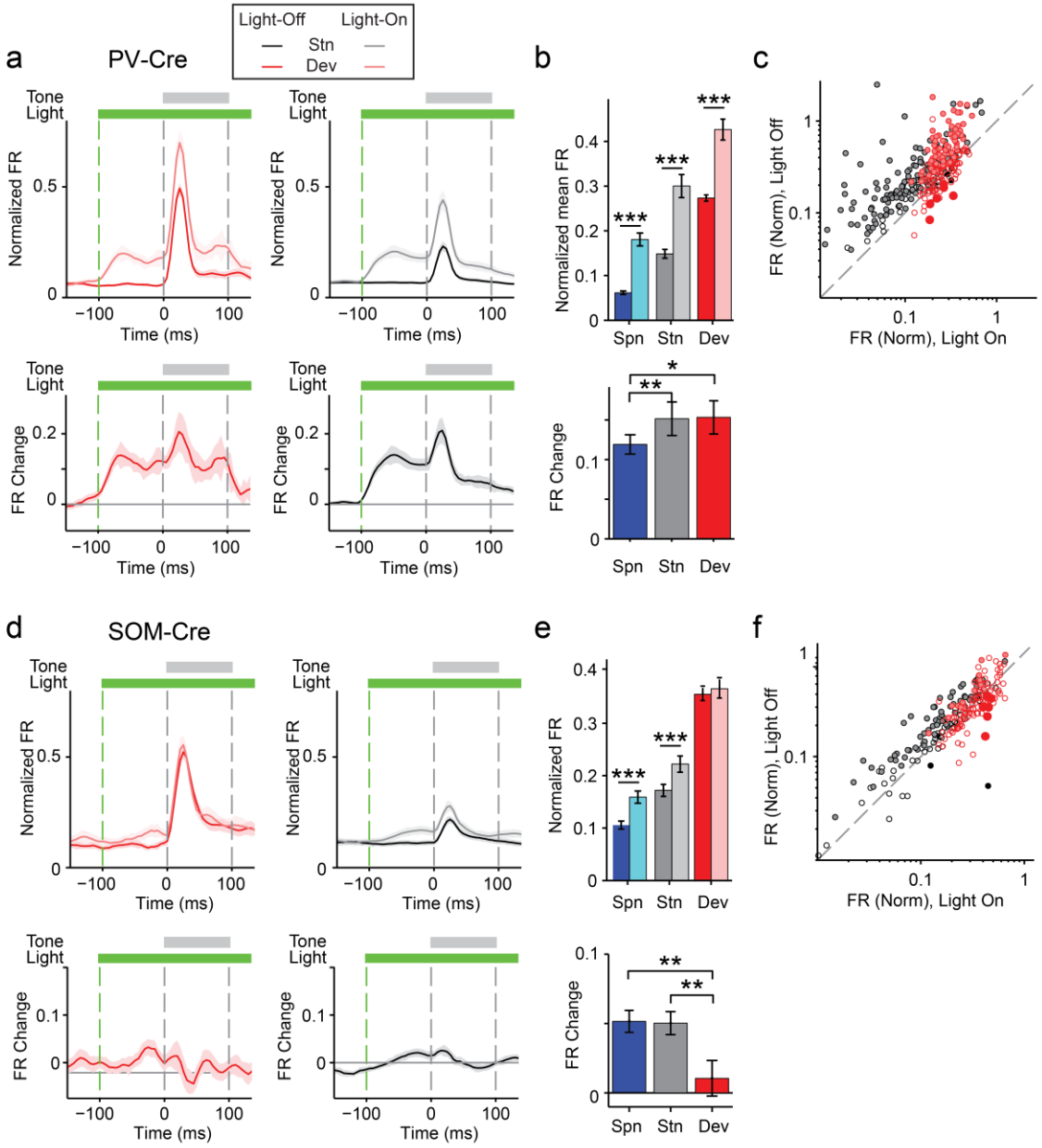

Figure 3.4. PVs and SOMs differentially affect response to standard and deviant tones. (**a, d**) Top: Mean response to deviant (left, red) and standard (right, black) tones, during light-on (light colors) and light-off trials (dark colors). Bottom: Mean of the difference between responses on light-on and light-off trials for each neuron for deviant (left, red) and standard (right, black) tone. Each trace is a population average of putative excitatory neuron PSTHs normalized to each neuron's maximum deviant tone-evoked FR on light-off trials. Shaded regions around traces indicate standard error (SE). Dashed lines indicate light onset (green) and tone onset and offset (gray). Neurons recorded in PV-Cre (**a**), SOM-Cre (**d**) mice. (**b, e**) (Top) Mean population FR on light-on and light-off trials; (Bottom) Mean population FR difference between light-on and light-off conditions for deviant (red) and standard (gray) tones and spontaneous activity (blue). Normalization as in **a**. Neurons recorded in PV-Cre (**b**), SOM-Cre (**e**) mice. (**c, f**) Modulation of PV-Cre

mouse putative excitatory neuron FR response to tones by interneuron photosuppression. Neuronal responses to each tone are represented by two circles, one for standard (black) and one for deviant (red) tone responses. Filled circles represent significantly increased (gray, pink) or decreased (black, red) response; unfilled circles: responses without significant modulation. Gray dashed line – identity line. Neurons recorded in PV-Cre (**c**)**,** SOM-Cre (**f**) mice.

26%, p2 = 0.039, t (159) = -2.4, C = 2), indicating that the change in tone-evoked FR was similar regardless of tone probability (Figure 3.4b, bottom panel). Because an equal increase in the firing rate produces a weaker *relative* effect on the response to the deviant (which is higher than to the standard), PV inactivation decreases SSA index (Figure 3.3e).

By contrast, suppressing SOMs led to an increase in FR for spontaneous activity (Δ = 46%, p2 = 2e-9, t (113) = -6.5) and during the standard (Δ = 29%, p2 = 2e-8, t (113) = -6.1) but not deviant (p2 > 0.05, t (113) = -0.8) tone (N = 114, Figure 3.4d, e, f, Figure 3.4—Figure supplement 1c). 52% of neurons exhibited greater FR to the standard and only 11% to the deviant during PV suppression (Figure 3.4—Figure supplement 1d). The increase in firing rate for spontaneous activity was not different than that during the standard tone (p2 > 0.05, t (113) = 0.2, C = 2) and the differences in FR due to suppression of SOMs were stronger for spontaneous activity and the standard tone than the deviant tone (Spontaneous: Δ = 390%, p2 = 0.004, t (113) = 3.1. Standard: Δ = 378%, p2 = 0.005, t (113) = 3.1) (Figure 3.4e, bottom panel), thereby accounting for the change in SSA with SOM inactivation (Figure 3.3f). Responses to the equal stimulus evoked consistent, yet weaker effects (Figure 3.4—Figure supplement 2).

PVs and SOMs differ in their density among different layers of the cortex and in laminar sources and targets of their inputs and outputs (Fino et al., 2013; Markram et al., 2004; Xu and Callaway, 2009). The effects of PV and SOM suppression on SSA had differential laminar distribution (Figure 3.4—Figure supplement 3). The effect of PVs on SSA was equally strong in the supra-granular and infra-granular layers, but stronger in the granular layer, i.e. the thalamo-recipient layer. This differential effect is consistent with the relative proportion of cortical interneurons that are PVs, which is higher in granular than either in infra- or supra-granular layers (Lee et al., 2010; Ouellet and de Villers-Sidani, 2014; Xu et al., 2010). In contrast, suppressing SOMs reduced SSA in the granular and infra-granular, but not supragranular layers. The relative proportion of cortical interneurons that are SOMs is greatest in the granular and infra-granular layers, but still present in supra-granular layers (Lee et al., 2010; Ouellet and de Villers-Sidani, 2014; Xu et al., 2010). As some SOMs predominantly target the distal dendrites of pyramidal neurons (Markram et al., 2004), the effect of suppressing SOMs in supra-granular layers may be evident in recordings of pyramidal neurons with cell bodies in deeper layers, supporting our results. In addition, cortical extracellular recordings may be biased toward neurons in granular and infra-granular layers, precluding adequate sampling of activity in superficial layers. In controls, we did not observe a difference in the effect of light on SSA across layers, demonstrating that the differences are not due to differential artifact of light stimulation.

Our results indicate that both PVs and SOMs affect SSA, but in different ways: (1) The increase in the firing rate of putative excitatory neurons due to PV suppression is constant, either during presentation of the standard or the deviant, and greater than changes in spontaneous activity. Thus, PVs amplify SSA in excitatory neurons by exerting a *relatively* stronger inhibitory drive for the standard than for the deviant. (2) Suppression of SOMs leads to increased putative excitatory neuron activity only during the spontaneous firing or the presentation of the standard, but not for the deviant. This suggests that the strength of SOM-mediated inhibitory drive is not significant in response to the deviant, but increases with repeated presentations of the standard.

In neurons exhibiting SSA, responses to the deviant are stronger than to the standard. This difference might lead to a 'ceiling' effect, reducing the effect of PV photosuppression on FR to the deviant, but not standard (Olsen et al., 2012). However, restricting the analysis to two subpopulations of neurons, which have matched mean and standard deviation of FR to the standard versus the deviant tones (Rust and Dicarlo, 2010; Ulanovsky et al., 2004), preserved the observed effects of photosuppression (Figure 3.4—Figure supplement 4). Suppressing PVs led to an equal increase in FR to both the standard and the deviant tone (N = 54 – Standard: Δ = 62%, p2 = 6e-8, t (53) = 6.3. Deviant: Δ = 55%, p2 = 3e-5, t (53) = 4.5. Standard vs deviant: p2 > 0.05, t (53) = 0.5). In contrast, suppressing SOMs led to a significant increase in FR to the standard, but no change in FR to the deviant (N = 44 – Standard: Δ = 30%, p2 = 7e-6, t

(43) = 5.1. Deviant: p2 > 0.19, t (43) = 1.3. Standard vs. deviant: Δ = 382%, p2 = 6e-4, t (43) = 3.7).

For neurons that responded more strongly to one of the tones ("strong" versus "weak" tone) a ceiling effect would predict that the effect of interneuron suppression would be stronger for the weak than the strong tone. However, PV and SOM suppression exhibited a similar effect on responses to the strong and the weak tones in neurons that exhibited differential responses to two tones (Figure 3.4—Figure supplement 5, 6). Suppressing PVs led to similar increases in tone-evoked FR between weak and strong tones for both deviant (N = 51, p2 > 0.05, t (50) = 1.0) and standard tones (p2 > 0.05, t (50) = -1.9). Suppressing SOMs also led to similar differential effects between strong and weak tones; standard tone-evoked FR increased equally (N = 34, p2 > 0.05, t (33) = 1.1) and deviant tone-evoked FR was equally unchanged (p2 = 0.05, t (33) = -0.1). Combined, these analyses demonstrate that the effect of PV photosuppression on SSA cannot be explained by the ceiling effect for either PVs or SOMs.

Although Arch drove strong currents in both SOM and PV neurons (Figure 3.2d, Figure 3.2—Figure supplement 1, 2), there might be a difference in expression level or efficacy of Arch between SOM-Cre and PV-Cre mice, leading to a stronger effect of photosuppression in PV-Cre than in SOM-Cre mice on tone-evoked FRs (Figure 3.4b, e). Alternatively, the difference might be attributable to the morphological or functional differences between SOMs and PVs. To address this confound, we selected tone responses that exhibited matched difference in standard tone-evoked FR between light-

on and light-off trials (N = 66, Figure 3.4—Figure supplement 7). Within these matched subpopulations, PV and SOM photosuppression exhibited differential effects similar to those of the whole population. The change in FR due to PV suppression was not significantly different between responses to the standard and deviant ($p2 > 0.05$, $t(65) = -0.3$, $C = 3$). By contrast, the change in deviant tone-evoked FR due to SOM suppression was significantly weaker than that for the standard tone ($\Delta = -78\%$, $p2 = 0.003$, $t(3.5)$, $C = 3$). By the design of the analysis, the effect of PV or SOM suppression on standard tone evoked FR was nearly identical ($p1 > 0.05$, $t(65) = -0.1$, $C = 3$). However, the change in deviant tone-evoked FR was greater for PV photosuppression than SOM photosuppression ($\Delta = 404\%$, $p1 = 0.029$, $t(65) = 2.4$, $C = 3$). Since the observed differential effects of PV and SOM suppression persisted in subsets of neurons that were matched for photosuppression-induced change in standard tone-evoked FR, these differences are unlikely due to differential expression or efficacy of Arch in the PV-Cre and SOM-Cre mice, but rather reflect functional differences between the two types of interneurons.

SOM-mediated suppression of putative excitatory neurons increases with repeated presentations of the standard tone, whereas PV-mediated suppression remains stable. Within the oddball sequence, after the presentation of the deviant, SSA takes several repeats of the standard to reach an adapted state (Ulanovsky et al., 2004). Consistent with previous findings (Ulanovsky et al., 2004), presentation of the deviant tone temporarily reduced SSA without photosuppression (Figure 3.5a; b and c, dark color

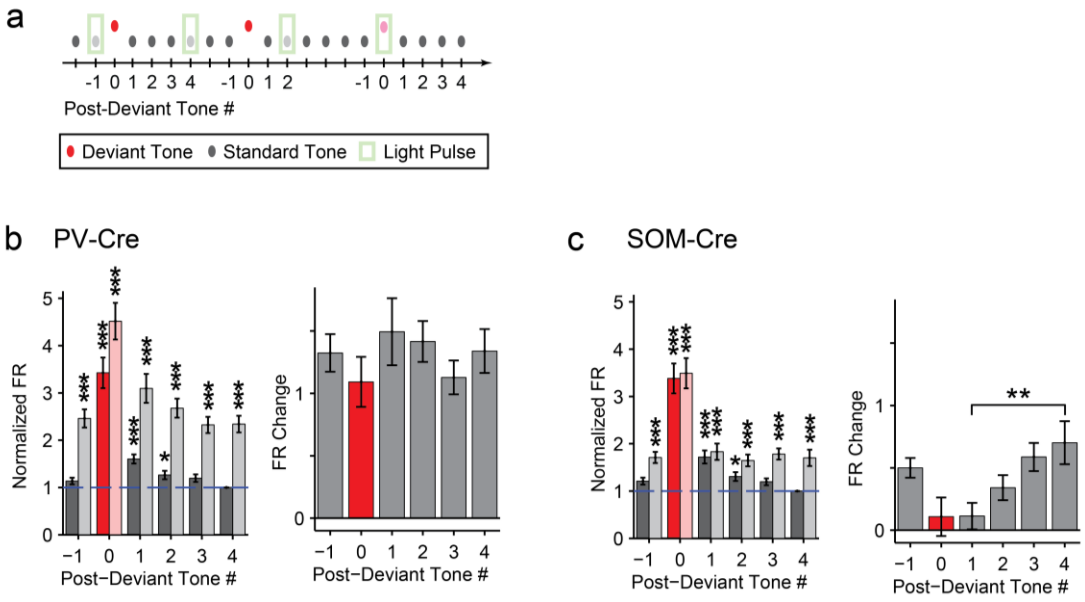

Figure 3.5. Post-deviant timecourse of interneuron-mediated effect on stimulus-specific adaptation. (**a**) Diagram of oddball stimuli illustrating post-deviant tone number used in subsequent analysis; Tones and light pulses are as indicated in Figure 3.3**a**. Numbers indicate each tone position relative to deviant tones. Responses to any standard tones following light-on standards were excluded from the analysis. ***(b, c)*** Left: Mean population FR in response to standard tones (gray) subsequent to deviant tones (red) within the oddball sequence on light-off (dark colors) and light-on (light colors) trials. All responses are normalized to the response to the fourth post-deviant standard tone on light-off trials (green dashed line). Right: Difference between FR on light-on and light-off trials in response to standard (gray) and deviant (red) tones. (**b**): PV-Cre mice. (**c**): SOM-Cre mice.

bars); Following the deviant tone (T_0) the first two standard tones (T_1 and T_2) evoked elevated FRs compared to the fourth standard tone (T_4) (PV-Cre, Figure 3.5b – N = 148, T_1: Δ = 60%, p2 = 3e-8, t (146) = 6.3, C = 11, T_2: Δ = 26%, p2 = 0.043, t (146) = 2.9, C = 11. SOM-Cre, Figure 3.5c – N = 102, T_1: Δ = 72%, p2 = 1e-5, t (101) = 5.2, C = 11, T_2: Δ = 31%, p2 = 0.013, t (101) = 3.3, C = 11). The third standard tone (T_3) and the tone prior to the deviant tone (T_{-1}) evoked responses similar to T_4 (PV-Cre, Figure 3.5b – T_{-1} and T_3: p2 > 0.05, t (146) < 2.5, C = 11. SOM-Cre, Figure 3.5c – T_{-1} and T_3: p2 > 0.05, t (101) < 2.9, C = 11). Neurons in which response to T_0 did not produce spikes were excluded. Suppressing

PVs led to a significant equal increase in FR to four consecutive presentations of the standard following the deviant (Figure 3.5b, left – for each tone, T_{-1} through T_4, with light-on compared to T_4 with light-off: $\Delta > 132\%$, $p2 < 2e\text{-}9$, $t(146) >= 6.8$, $C = 11$. Figure 3.5b, right – change in FR between light-on and light-off responses to each T_{-1} through T_3 as compared to T_4: $p > 0.05$, $t(146) < 1.8$, $C = 5$). In contrast with PVs, suppressing SOMs led to a progressively increasing effect on FR to consecutive presentations of the standard following the deviant (Figure 3.5c, left -- for each standard tone, T_{-1} through T_4, with light-on compared to T_4 with light-off: $\Delta > 64\%$, $p2 < 9e\text{-}4$, $t(101) >= 4.1$, $C = 11$. Figure 3.5c, right – difference between FR change in T_1 and T_4 with light-on: $p = 0.008$, $t(101) = -3.2$, $C = 5$. Repeated measures ANOVA with tone number (T_1 through T_4) as a factor: $F(3, 300) = 4.30$, $p = 0.0054$). These results are consistent with the interpretation that the inhibitory drive from PVs is constant throughout the stimulus regardless of tone history, whereas the effect of SOM modulation increases with repeated presentations of the standard.

The time course of the effect of interneuron photosuppression on FR of the putative excitatory neurons at the beginning of each oddball sequence exhibited similar trends for PVs and SOMs. As expected, on light-off trials, FR decreased in response to the standard tone over the first 20 repetitions of the tone (Figure 3.5—Figure supplement 1). For PV-Cre mice, the difference in FR to the standard between light-on and light-off trials did not change over this time and stayed positive for the remainder of the oddball (Figure 3.5—Figure supplement 1a). Over the first 20 trials, FR adapted with

a similar time course for both the light-on and light-off trials, so the change due to PV photosuppression in FR to standard stayed constant (Figure 3.5—Figure supplement 1a, b). In contrast, for SOM-Cre mice, FR on light-on trials increased over the first 40 trials, whereas on light-off trials, it decreased (Figure 3.5—Figure supplement 1a). As a result, the difference due to photo-manipulation in FR to the standard increased over the first 40 trials, and then stayed consistently positive throughout the stimulus presentation (Figure 3.5—Figure supplement 1c). These results demonstrate that the PV-mediated effect on putative excitatory neuronal responses did not change with repeated presentations of the standard, whereas the SOM-mediated effect increased with the repeated stimulus.

PVs and SOMs exhibit SSA. In order to understand how PVs and SOM exert the differential control of SSA in putative excitatory neurons, we used optogenetic tagging to identify the specific interneurons and to quantify whether PVs and SOMs exhibited SSA (Lima et al., 2009). Through targeted viral delivery to AC, we drove Channelrhodopsin-2 (ChR2) expression, which depolarizes neurons when stimulated by light, in either PVs or SOMs (Chow et al., 2010) (Figure 3.6a, d, Figure 3.6—Figure supplement 1a). A modified adeno-associated virus (AAV) encoding anti-sense code for ChR2 and a fluorescent reporter, under the FLEX cassette, was injected into PV-Cre or SOM-Cre mice (Boyden et al., 2005; Cardin et al., 2010; Deisseroth, 2011; Sohal et al., 2009; Zhang et al., 2010), and resulted in specific expression of ChR2, localized to PVs or SOMs (Figure 3.6—Figure supplement 1b, c PV-Cre; N = 183 neurons in 3 mice,

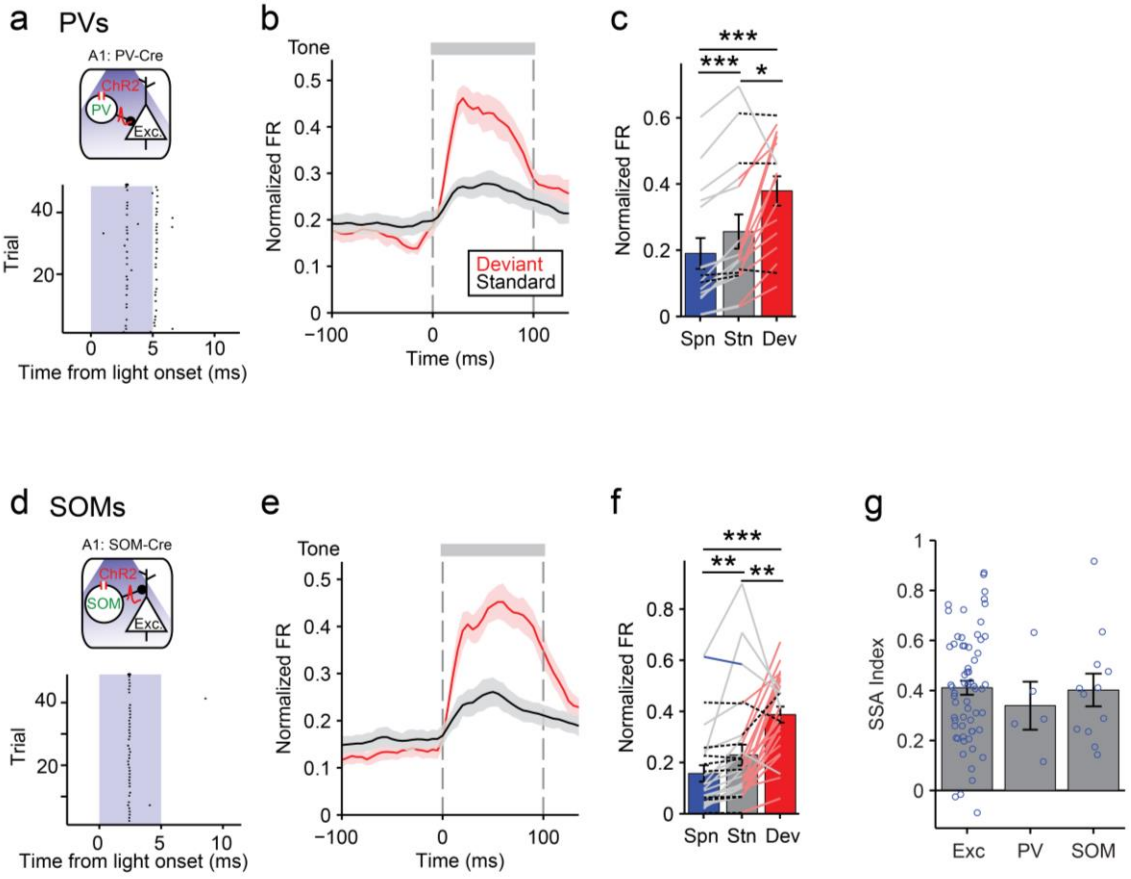

Figure 3.6. **PV and SOM interneurons exhibit stimulus-specific adaptation.** (**a, d**) Optogenetic methods. A1 was injected with AAV-FLEX-ChR2-tdTomato. During experiments, an optic fiber was positioned to target A1 and neuronal activity was recorded using a multichannel silicon probe in A1. Top diagram: Blue light (473 nm) excites PVs in PV-Cre mice or SOMs in SOM-Cre mice. Bottom. Peri-stimulus spike raster of a representative optogenetically identified PV (top) or SOM (bottom). Shaded region – blue light on. (**a**) PV-Cre. (**d**) SOM-Cre. (**b, e**) PSTH of PVs (**b**) or SOMs (**e**) FR response to deviant (red) and standard (black) tones. Normalization and dashed lines as in Figure 3.4a, b. (**c, f**) Mean PVs (**c**) or SOMs (**f**) FR response over the 100ms of deviant (Dev, red) and standard tones (Stn, gray), and 100ms of spontaneous activity prior to tone onset (Spn, blue). Each line represents a single neuron's response to each conditions, and its color indicates the magnitude of significant differences between two conditions; Pink, gray, blue and dashed black lines indicate a greater response to deviant tone, standard tone, silence and no significant change, respectively. (**g**) Mean SSA index of putative excitatory neurons (gray), PVs (cyan) and SOMs (yellow). Circles represent SSA index values of individual neurons.

specificity = 67 ± 1%, efficiency = 76 ± 5%. SOM-Cre: N = 202 neurons in 4 mice, specificity = 90 ± 3%, efficiency = 81 ± 4%). Neurons were identified as PVs or SOMs if

they responded to brief (5 ms) flashes of light with spikes within 1.5-4.5 ms of laser pulse onset Figure 3.6a, d).

Both PVs and SOMs exhibited SSA, evidenced by a significant reduction in standard tone-evoked FR compared the deviant tone response (Figure 3.6b, c, e, f, PV: N = 16, Δ = -32%, p2 = 0.023, z = -2.5, C = 2. SOM: N = 28, Δ = -41%, p2 = 0.002, z = -3.3, C = 2. Signed rank test). The SSA index was not significantly different between PVs and SOMs (Figure 3.6g, neurons responsive to both tones A and B – PV: N = 5, SOM: N = 12. PV and SOM: p2 > 0.05, C = 2. Rank sum test) and both were similar to the mean SSA index in putative excitatory neurons (Figure 3.6g – Exc: N = 67. Exc vs PV: p > 0.05 , z = 0.7, C = 2. Exc vs SOM: p > 0.05, z = 0.4, C = 2). PVs and SOMs exhibited some differences in relative response changes between the deviant, the standard and the equal tones (Figure 3.6, supplement 2b, d); PVs' response to the equal tones did not decrease significantly as compared to deviant tones (N = 16 p2 > 0.05, z = -1.7, C = 2), whereas SOMs adapted in their response to equal tones (Δ = -36%, p2 = 0.049, z = -2.3, C = 2), and then further to standard tones (N = 28, Δ = -49%, p2 = 0.022, z = -2.6, C = 2). These results suggest that SOMs may adapt at a faster time scale than PVs with repeated presentation of tones.

Adapting inhibitory interneurons facilitate SSA in exctitatory neurons in a cortical network model. Our results of recordings from PVs and SOMs present a surprising finding that PVs and SOMs adapt in response to repeated tones, countering our initial hypothesis that SOMs saturate in responses to the deviant, or facilitate with repeated

presentation of a tone. How can an adapting interneuron contribute to added adaptation in excitatory neurons? To address this question, we next developed a model of coupled excitatory-inhibitory neuronal populations. Excitatory and inhibitory neurons form tight mutually coupled networks in A1, and we hypothesized that through differential post-synaptic integration by excitatory neurons, interneurons can amplify adaptation in excitatory neurons.

As a proof-of-principle that would account for our findings that PVs and SOMs exhibit similar magnitude of SSA, yet have a differential effect on SSA in putative excitatory neurons, we constructed a simplified model of mutually coupled inhibitory-excitatory neuronal populations. We tested how responses of the model putative excitatory neurons are affected by manipulation of activity of PVs or SOMs (Figure 3.7a). Thalamocortical tone-evoked inputs were modeled including an adaptation term and resulted in reduced responses of excitatory, PV and SOM populations to repeated tones (Figure 3.7—Figure supplement 1a, b). The model replicated the differential effects of manipulation of PV and SOM activity on responses to standard and deviant tones in putative excitatory neurons (Figure 3.7b-e): When PVs were suppressed optogenetically, the responses to both the standard and the deviant tones increased (Figure 3.7b, c). By contrast, when SOMs were suppressed, although the spontaneous FR and standard tone-evoked FR were elevated, the responses to the deviant tone remained constant, whereas the responses to the standard tone increased (Figure 3.7d, e). SOMs have been

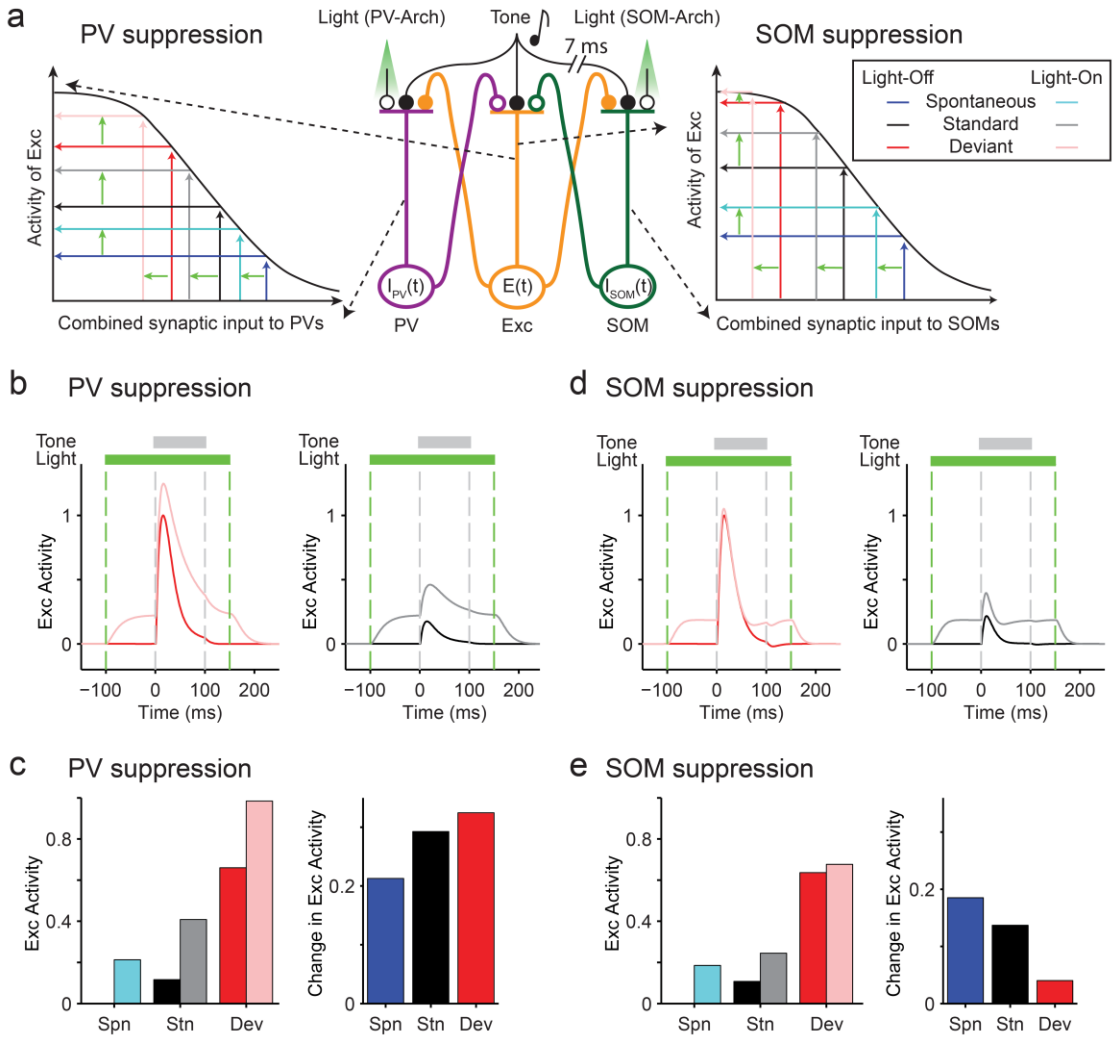

Figure 3.7. Mutually coupled excitatory-PV-SOM neuronal model accounts for differential effects of PVs and SOMs on SSA in putative excitatory neurons. (**a**) Center: Diagram of coupled network model. Excitatory (Exc) and two types of inhibitory interneurons (PV and SOM), receive tone-evoked inputs. They make reciprocal connections on each other; Exc makes excitatory synapses on PV or SOM; PV and SOM inhibit Exc. Closed circles: excitatory synapses. Open circles: inhibitory synapses. Orange outlines: excitatory input-output pathway. Purple outlines: PV input-output pathway. Green outlines: SOM input-output pathway. The effect of optogenetic modulation was modeled as an additional input current delivered to inhibitory neuronal populations. Adaptation was modeled as decaying synaptic coefficient with slow adaptation. Left and right inset plots: Combined input-output transfer function that represents the transformation between synaptic inputs and the activity of excitatory neurons. The values of inputs are depicted by arrows for the spontaneous and tone-evoked activity in response to deviant and standard tones under light–off (dark color) and light-on (light color) conditions, with change due to light highlighted by light green arrows. (**b, d**) Tone-evoked responses of model neuronal excitatory population to deviant (red) and standard tones (gray), i.e. the first and fourth consecutive

tone presented, under light-off (dark colors) and light-on (light colors) conditions. Dashed lines indicate light onset and offset (green) and tone onset and offset (gray). (**b**) Light suppresses PVs. (**d**) Light suppresses SOMs. (**c, e**) Left: Spontaneous FR (blue) and standard (black) and deviant (red) tone-evoked FRs on light-off (dark colors) and light-on (light colors) conditions. Right: Mean difference between responses on light-on and light-off conditions. (**c**) Light suppresses PVs. (**e**) Light suppresses SOMs.

shown to inhibit PVs (Cottam et al., 2013a; Pfeffer et al., 2013; Sturgill and Isaacson, 2015). Including inhibition between SOMs and PVs did not affect the model outcome, with suppression of PVs resulting in suppression of excitatory responses to both the standard and the deviant, and suppression of SOMs driving specific suppression of excitatory responses to the standard, but not the deviant (Figure 3.7 – Figure supplement 2).

An explanation for the difference of the effects of PVs and SOMs can be provided by examining the combined transfer function between pre-synaptic inputs and post-synaptic activity of excitatory neurons separately for PVs and SOM suppression (Figure 3.7a, insets): Light-driven modulation of PV activity has the same effect on excitatory neuron responses at spontaneous, standard-tone evoked and deviant-tone evoked activity (Figure 3.7a, left inset). Spontaneous, standard and deviant input levels all fall within the linear portion of the transfer function between inputs and change in the excitatory neuron activity. On the other hand, for SOMs, modulation of their activity in the deviant tone-evoked regime drives small to no changes in excitatory neuronal activity, whereas modulation of SOM activity in the spontaneous and standard tone-evoked regime drives significant changes in excitatory neuronal activity (Figure 3.7a right inset). The deviant-tone evoked activity falls on the saturating part of the input-

output transfer function, whereas the standard-tone evoked and spontaneous inputs fall on the linear part of the transfer function. Then, shifts in SOM inputs due to photosuppression evoke small changes during deviant tone responses, but larger changes during either standard or spontaneous activity. Either PV or SOM manipulation would result in reduction of combined SSA of excitatory neurons.

Discussion

The majority of neurons in the auditory cortex selectively reduce their responses to frequent, but not rare sounds, exhibiting stimulus-specific adaptation. However, the cortical mechanisms involved in the production and stimulus-specificity of SSA within the auditory cortex are not well understood. Here we found that, in addition to adaptation at the level of thalamocortical inputs, two distinct types of interneurons, PVs and SOMs, differentially contributed to SSA in the primary auditory cortex. Optogenetic suppression of either PVs or SOMs led to a reduction in SSA in putative excitatory neurons (Figure 3.3). Suppression of PVs led to an equal increase in the firing rate of the putative excitatory neurons in response to the standard and the deviant (Figure 3.4). By contrast, suppression of SOMs significantly increased the response to the standard, but lacked a significant effect on the response to the deviant (Figure 3.4). This series of findings expands on the “adaptation in narrowly tuned units” model, which proposes that repeated presentation of the standard stimulus drives adaptation within more narrowly tuned inputs, such as thalamocortical inputs (Mill et al., 2011; Nelken, 2014;

Taaseh et al., 2011). Our data indicate dual effects of cortical inhibition on SSA: (1) PVs contribute to SSA by providing constant amount of inhibition, resulting in a *relatively* higher inhibitory drive during the presentation of the standard, as compared to the deviant. Taking into account the non-linear synaptic input to FR output function of a typical pyramidal neuron, the constant inhibition amplifies the effect of thalamocortical depression in suppressing the response of the neuron to repeated stimulus (Figure 3.7 a). (2) The selective increase of the inhibitory drive from SOMs for standard stimulus as compared to the deviant stimulus responses might be explained by a shift in the non-linear transfer function between inputs to SOMs and their outputs to excitatory neurons, possibly due to facilitation of SOM-to-excitatory neuron synapses (Silberberg and Markram, 2007; Tan et al., 2008) (Beierlein et al., 2003; Reyes et al., 1998) (Figure 3.7 a).

Surprisingly, we found that, despite the differential effect of PV and SOM suppression on tone-evoked responses in putative excitatory neurons, both PVs and SOMs exhibit stimulus-specific adaptation. This finding is consistent with previous results that found that thalamocortical synapses onto inhibitory neurons and synapses from inhibitory neurons to excitatory cells can be depressing (Ma et al., 2012; Tan et al., 2008). How does suppression of these interneurons result in differential reduction in SSA in excitatory neurons? Our model provides an intuition for this effect: The mutually coupled excitatory-inhibitory network model demonstrates that the observed differential effects of PV and SOM suppression may be due to their differential action on

excitatory neuronal responses in the unadapted and adapted state (Figure 3.7). Tone-evoked responses of PVs would fall on the linear portion of the transfer function between PV activity and excitatory neuron depolarization, while the same tones maximally affect inputs from SOMs onto excitatory neurons, with stimulus-specific adaptation shifting the inputs to the linear, more sensitive range of inputs from SOMs. SSA may serve thus an additional function: to adjust the responses of neurons in a range that is more sensitive to small changes in the inputs from both excitatory and inhibitory neuronal populations. More generally, the simulation demonstrates that a circuit element, such as PVs or SOMs, that itself adapts may further amplify adaptation in the excitatory neurons.

To estimate the differential contribution of PVs or SOMs inputs to the excitatory neurons, we measured the difference in the firing rate of neurons due to optogenetic partial suppression of their firing. This measurement provides an estimate of the change in the firing rate of the putative excitatory neurons with the change in combined inputs to the inhibitory neurons, thereby allowing estimation of the synaptic transfer function (Figure 3.7a, insets). A simple biologically plausible network incorporating these transfer functions can reproduce the observed responses (Figure 3.7). There are several caveats to this interpretation. First, the firing rate may not linearly translate onto synaptic input strength because of the spiking non-linear rectification between the inputs and outputs of the putative excitatory neuron: a small change in FR in the low-FR regime might correspond to a greater change in the synaptic drive than a similar-sized change in FR in

the high-FR regime. However, our findings would still hold were this the case: In examining the effect of SOM suppression on response to the deviant, the actual difference in the synaptic drive between the deviant and the standard would then be even greater than observed. At the other end of the non-linearity, the analysis of neuronal responses sorted based on their firing rate to the standard and the deviant revealed that the "ceiling effect" would not contribute to a decreased effect of photostimulation on the response to the deviant in SOM-Cre mice (Figure 3.4—Figure supplement 4, 5, 6, 7). Second, PVs and SOMs may inhibit not only the excitatory neurons, but also each other. SOMs make synapses onto PVs (Cottam et al., 2013a; Isaacson and Scanziani, 2011; Ma et al., 2012), thereby potentially suppressing them with repeated presentation of the standard. Therefore, when SOMs are suppressed, some PVs may be disinhibited, and therefore provide a stronger suppression of excitatory neurons. The null effect on responses to the deviant during SOM suppression could result from a combination of increase in inhibition from dis-inhibited PVs in addition to reduced inhibition of SOMs onto excitatory neurons. Including inhibition from SOMs to PVs in the proof-of-principle model supported experimental findings (Figure 3.8 – Supportive Figure 3.2). Third, other interneuron types, such as vasopressin-positive interneuron (VIPs) may be involved in the circuit (Pi et al., 2013), and the changes that we observe may reflect several inhibitory stages of processing.

One must be cautious in translating the data from our experiments as a strict description of neuronal activity in awake animals, as our results were based on

recordings from mice under light isoflurane anesthesia. Other forms of anesthesia, such as pentobarbital-based (Cheung et al., 2001; Gaese and Ostwald, 2001), ketamine (Otazu et al., 2009) and high concentrations of isoflurane (Cheung et al., 2001; Ter-Mikaelian et al., 2007), can affect multiple aspects of sound-evoked responses in the auditory cortex. Nonetheless, our results are likely to extend for awake mice, since isoflurane anesthesia-induced effects on neuronal activity decrease as the concentration of isoflurane is reduced to the levels used in our recordings (Land et al., 2012). In addition, all recordings and manipulations were performed under identical anesthetic conditions, and our conclusions are based on the relative comparison of the effects of suppressing PVs and SOMs, which are expected to hold under awake conditions (Centanni et al., 2013).

While not demonstrated directly, SSA has been linked to detection of deviant sounds (Ulanovsky et al., 2003), which may be facilitated by a relatively enhanced neuronal response to a change in the ongoing sound (Grimm and Escera, 2012; Nelken et al., 2003; Winkler et al., 2009). By suppressing the responses to a frequently presented tone, the responses of neurons to a rare stimulus become relatively enhanced. However, whether and how modulating SSA in the auditory cortex affects auditory behavior has not yet been tested. Inhibitory interneurons may prove to have a complementary role in shaping auditory perception in addition to receptive field reorganization driven by synaptic plasticity (Froemke et al., 2013). The use of optogenetic methods to test the function of inhibitory interneurons in SSA overcomes

the limitations of lesion or pharmacological studies (Duque et al., 2014; Elliott and Trahiotis, 1972), which only allow for prolonged, non-selective inactivation (Moore et al., 2001). By combining optogenetic manipulation of interneuron activity with behavioral measurements, future experiments will explore whether interneuron-mediated SSA indeed affects the auditory behavior of the subject, such as enhanced ability to detect unexpected events.

Materials and Methods

Animals. All experiments were performed in adult male mice (supplier - Jackson Laboratories; age, 12-15 weeks; weight, 22-32 g; PV-Cre mice, strain: *B6;129P2-Pvalbtm1 (cre)Arbr/J*; SOM-Cre: *Ssttm2.1 (cre)Zjh/J*) housed at 28° C on a 12 h light-dark cycle with water and food provided *ad libitum*. In PV-Cre mice, Cre recombinase (Cre) is expressed in parvalbumin-positive interneurons; in SOM-Cre mice, Cre is expressed in somatostatin-positive interneurons (Taniguchi et al., 2011). This study was performed in strict accordance with the recommendations in the Guide for the Care and Use of Laboratory Animals of the National Institutes of Health. All of the animals were handled according to a protocol approved by the Institutional Animal Care and Use Committee of the University of Pennsylvania (Protocol Number: 803266). All surgery was performed under isoflurane anesthesia, and every effort was made to minimize suffering.

Viral vectors. Modified AAVs were obtained from Penn VectorCore. Modified AAV encoding Archaerhodopsin (Arch) under FLEX promoter was used for selective

suppression of PVs or SOMs (catalog number AV-9-PV2432, AAV9.CBA.Flex.Arch-GFP.WPRE.SV40, Addgene22222, serotype 2/9) (Chow et al., 2010). Modified AAV encoding GFP alone under FLEX promoter was used as a control for the specific action of Arch on the neuronal populations (catalog number AV-9-ALL854, AAV9.CAG.Flex.eGFP.WPRE.bGH, AllenInstitute854, serotype 2/9). Modified AAV encoding Channelrhodopsin (ChR2) under FLEX promoter was used for selective excitation of PVs or SOMs (catalog number AV-9-18917P, AAV9.CAGGS.Flex.ChR2-tdTomato.WPRE.SV40, Addgene18917, serotype 2/9).

Virus injection. 2-3 weeks prior to the start of experimental recordings, a 0.5 mm diameter craniotomy was drilled over primary auditory cortex (2.6 mm caudal and 4.1 mm lateral from bregma) under aseptic conditions while the mouse was anesthetized with isoflurane. A 750 nl bolus of AAV in water was injected into A1 (1 mm ventral from pia mater) using a stereotaxic syringe pump (Pump 11 Elite Nanomite, Harvard Apparatus). The craniotomy was covered with bone wax and a small custom head-post was secured to the skull with dental acrylic.

Electrophysiological recordings. All recordings were carried out inside a double-walled acoustic isolation booth (Industrial Acoustics). Electrodes were targeted to A1 on the basis of stereotaxic coordinates and in relation to blood vessels. In electrophysiological recordings, the location was confirmed by examining the click and tone pip responses of the recorded units for characteristic responses of neurons in core auditory areas, as described previously by our group in the rat (Carruthers et al., 2013) and by other

groups in the mouse (Guo et al., 2012; Linden and Schreiner, 2003; Marlin et al., 2015). While the electrodes were targeted to A1, some recordings may include data from the anterior auditory field (AAF), adjacent to A1 (Linden et al., 2003). Mice were placed in the recording chamber, anesthetized with isoflurane, and the head-post secured to a custom base, immobilizing the head. After drilling a craniotomy and creating a durotomy exposing auditory cortex, a silicon multi-channel probe (A1x32-Poly2-5mm-50s-177[Poly-2] or A1x32-tri-5mm-91-121-A32 [Triode], Neuronexus) was slowly lowered to between 750 µm and 1 mm into the cortex, perpendicular to the cortical surface and used to record electrical activity. Raw signals from 32 channels were bandpass filtered at 600-6000 Hz and thresholded for spike analysis, or at 10-300 Hz for local field potential (LFP) and current-source density (CSD) analysis (Poly-2 probe only), digitized at 32 kHz and stored for offline analysis (Neuralynx). Common-mode noise was removed by referencing a probe inserted in the brain outside the auditory cortex. On the Poly-2 probe, two rows of 16 electrodes each on a single shank were arranged such that each electrode site was 50 µm away from all three closest neighbors. This arrangement allowed us to record densely across depth, i.e. one electrode for every 25 µm in depth. On the triode, electrodes were arranged in groups of 3 equidistant sites, forming an equilateral triangle (25 µm separation). The triodes were separated vertically by 91 µm center-to-center distance, spanning 1 mm, with single sites on each end.

Unit identification. Spike sorting was performed using commercial software (Offline Sorter, Plexon) (Carruthers et al., 2013). In order to improve isolation of single units

from recordings using low-impedance probes, spiking activity was sorted across three (Triode, 25 μm separation) or four (Poly-2, 50 μm separation) adjacent electrode sites (Niell and Stryker, 2008; Olsen et al., 2012). We used a stringent set of criteria to isolate single units from multiunit clusters (Bizley et al., 2010; Brasselet et al., 2012; Carruthers et al., 2015; Carruthers et al., 2013; Durand et al., 2012; Otazu et al., 2009; Picard et al., 2014). Single-unit clusters contained <1% of spikes within a 1.0-ms interspike interval, and the spike waveforms across 3 or 4 channels had to form a visually identifiable distinct cluster in a projection onto a three-dimensional subspace. Putative excitatory neurons were identified based on their expected response patterns to sounds and the lack of significant suppression of the spontaneous FR due to light (Lima et al., 2009; Moore and Wehr, 2013). While this subpopulation may still contain inhibitory neurons, only 2% of all recorded neurons were significantly photo-suppressed at baseline (one-sided paired t-test, significance taken at $p<0.05$). The low impedance of the extracellular probes precluded us from conducting a more detailed analysis of cortical subpopulations based on the spike waveform (Bartho et al., 2004; Moore and Wehr, 2013).

Acoustic stimulus. Stimuli were delivered via a magnetic speaker (Tucker-David Technologies), directed toward the mouse's head. Speakers were calibrated prior to the experiments to +- 3 dB over frequencies between 1 and 40 kHz, by placing a microphone (Brüel and Kjaer) in the location of the ear contralateral to the recorded A1 hemisphere, recording speaker output and filtering stimuli to compensate for acoustic aberrations

(Carruthers et al., 2013). First, to measure tuning, a train of 50 pure tones of frequencies spaced logarithmically between 1 and 80 kHz, at 65 dB sound pressure level relative to 20 µPa (SPL), in pseudo-random order, was presented 20 times. Each tone was 100 ms long, with an inter-stimulus interval (ISI) of 300 ms. Frequency response functions were calculated online for several multiunits, and two frequencies (separated by 0.39 octaves), which elicited spiking responses of similar strength, were selected as tone A and B. Next, a series of stimuli composed of tones A and B were presented in interleaved blocks, repeated 4 times. Each oddball stimulus consisted of a train of 653 A and B tones (100 ms long, 300 ms ISI, 65 dB SPL). In oddball stimulus 1, 90% of the tones were A (standard), while 10% of the tones were B (deviant). We used a frozen sequence of standard and deviant tones in pseudorandom order and counterbalanced with respect to the number of standard tones preceding each deviant. In oddball 2, the probabilities of tones A and B were reversed so that tone B was the standard and A the deviant. In the equal probability stimulus, A and B each comprised 50% of tones.

Light presentation. An optic fiber was use to direct 532 nm laser light (Shanghai Laser & Optics Century). After positioning the silicon probe, an optic fiber was placed over the surface of auditory cortex. To limit Becquerel effect artifacts due to light striking electrodes, we positioned the optical fiber parallel to the silicon probe (Han et al., 2009; Kvitsiani et al., 2013). During every 5th tone of the oddball and equal probability stimuli, light was cast over A1 to suppress interneurons. The light onset was 100 ms prior to tone onset, and lasted for 250 ms. At 180 mW/mm^2, light pulses were intense enough to

significantly modulate multiunit activity throughout all cortical layers. The effect of optical stimulation was not significant for responses to subsequent tones (Figure 3.3—Figure supplement 1).

Immunohistochemistry. Brains were post-fixed in paraformaldehyde (4%, PFA) and cryoprotected in 30% sucrose. Coronal sections (40μm) were cut using a cryostat (Leica CM1860), washed in PBS containing 0.1% Triton X-100 (PBST; 3 washes, 5 min), incubated at room temperature in blocking solution (for PV 10% normal goat serum and 5% bovine serum albumin in PBST; for SOM 10% normal goat serum with 0.1% sodium azide and 2% cold water fish gelatin in PBS; 3h), and then incubated in primary antibody diluted in blocking solution overnight at 4°C. The following primary antibodies were used: anti-PV (PV 25 rabbit polyclonal, 1:500, Swant) or anti-SOM (AB5494 rabbit polyclonal, 1:200, Millopore). After incubation, sections were washed in blocking solution (3 washes, 5 min), incubated for 2hr at room temperature with secondary antibodies (Alexa 594 goat anti-rabbit IgG; for PV 1:1000 and SOM 1:400), and then washed in PBS (3 washes, 5min each). Sections were mounted using fluoromount-G (Southern Biotech) and confocal images were acquired (Leica SP5). Cells were identified in independent fluorescent channels and subsequently scored for colocalization by hand using ImageJ's cell counter plug-in. Transfection efficiency is the percent of antibody labelled neurons which are co-labelled with GFP. Transfection specificity is the percent of GFP expressing neurons which are co-labeled with the antibody.

In vitro slice preparation. Acute brain slices were prepared from mice using standard techniques essentially as previously described (Goldberg et al., 2011). Mice were anesthetized via inhaled isoflurane and then trans-cardially perfused with 10 mL of oxygenated, ice-cold artificial cerebrospinal fluid (ACSF) at a rate of 5 mL/minute, that contained, in mM: 87 NaCl, 75 sucrose, 2.5 KCl, 1.25 NaH_2PO_4, 26 $NaHCO_3$, 10 glucose, 0.5 $CaCl_2$, 4 $MgSO_4$. Slices (300 µm thick) were cut on a Leica VT1200S and incubated in cutting solution in a holding chamber at 32° C for approximately 30 minutes followed by continued incubation at room temperature prior to electrophysiological recording, at which point slices were transferred to a submersion type recording chamber attached to the microscope stage. ACSF used for recording contained, in mM: 125 NaCl, 2.5 KCl, 1.25 NaH_2PO_4, 26 $NaHCO_3$, 10 glucose, 2 $CaCl_2$, and 1 $MgSO_4$. The solution was continuously bubbled with 95% O_2 and 5% CO_2 throughout cutting, slice incubation, and recording, so as to maintain a pH of approximately 7.4.

In vitro electrophysiology. Cells were identified via GFP expression under epifluorescence microscopy, and subsequently visualized using a 40X, 0.8 NA water-immersion objective (Olympus) on an Olympus BX-61 upright microscope equipped with infrared differential interference contrast optics. Recordings were performed using the whole-cell patch clamp technique. Access resistance (Ra) was < 25 MΩ upon break-in; data obtained from a given cell was rejected if Ra changed by > 20% during the course of the experiment. Internal solution contained, in mM: potassium gluconate, 130; potassium chloride, 6.3; EGTA, 0.5; $MgCl_2$, 1.0; HEPES, 10; Mg-ATP, 4; Na-GTP, 0.3;

biocytin, 0.1%. Osmolarity was adjusted to 285-290 mOsm using 30% sucrose. Voltage was recorded using a MultiClamp 700B amplifier (Molecular Devices, Union City, CA), lowpass filtered at 10 kHz, digitized at 16-bit resolution (Digidata 1550) and sampled at 20 kHz. pCLAMP 10 software (Axon Instuments) was used for data acquisition, and analysis was performed using the Clampfit module of pCLAMP.

In vitro optogenetics. Cells were illuminated with a 561nm solid state laser (Coherent) routed to the standard X-Y galvanometer of a two-photon microscope (Bruker Corporation, Billerica, MA) via a single mode fiber. Illuminance at the specimen was estimated using a 10µm pinhole aperture (Edmund Optics) and a photodiode power sensor (Thorlabs).

In vivo tone response firing rate. For each putative excitatory neuron, the spontaneous FR and tone-evoked FRs were measured as the mean FR over 50 ms pre and post tone onset, respectively. For each identified interneuron, FRs were measured 100 ms pre and post tone onset. FR was measured separately for each tone, A and B, as standard, deviant and equal probabilities, and for light-off and light-on trials. FR normalization was carried out separately for each tone, A and B, for each neuron by dividing the response under all conditions by the maximum FR (across 5ms bins) of the deviant tone, light-off condition. Performing this normalization by dividing response in all conditions by the mean, rather than maximum FR of the deviant tone, light-off condition did not alter significant results (Figure 3.4 – Figure supplement 8). For all FR analyses, each neuron's responses to tones A and B were treated separately, and each was only included if the

light-off deviant tone-evoked FR was significantly greater than the spontaneous FR (Wilcoxon signed rank test $p < 0.05$). Further, tone responses were only included in analysis if the neuronal FR during each oddball stimulus exceeded 0.02 Hz, and the neuron was significantly tuned to the tone. Tuning was considered significant if the spike count in response to a tone (A or B) was significantly higher than the pool of spike counts across all tones outside one octave band centered on tones A and B ($N = 42$, t-test, $p1 < 0.05$). Population responses in each condition were measured as the mean and standard error of FRs across tone responses in each experimental group.

Stimulus-specific adaptation index. For each neuron, SSA index is a measure of the strength of SSA based on its mean FR with respect to tone probability. FRs to tones A and B were summed according to their standard or deviant probability within each oddball stimulus (Ulanovsky et al., 2003). Thus, SSA index was computed as:

$$SSA\ Index = \frac{(D_A + D_B) - (S_A + S_B)}{D_A + D_B + S_A + S_B}$$

Where S and D indicate the mean firing rate for standard and deviant trials, respectively, and their subscripts indicate the tone frequency condition. SSA index was computed separately for light-off and light-on conditions. Population SSA indices were measured as the mean and standard error of SSA indices across all neurons of each population. Criteria for inclusion in the analysis was the same as in *tone response FR* analysis described above, with the added criterion that the deviant tone-evoked FR must be

greater than spontaneous FR for each of tones A and B (Wilcoxon signed rank test $p < 0.05$).

Localization of cortical layers and CSD. To calculate the CSD, the net current density moving through cortical tissue at 32 positions along the cortical axis was calculated based on LFPs of responses to tones recorded on each electrode, by using the second order central finite difference to calculate the second spatial derivative across the LFPs over the vertically arranged electrodes (Szymanski et al., 2009). Across the CSD profile, the deepest current sink corresponds to the thalamo-recipient granular layer (Kaur et al., 2005; Szymanski et al., 2009) allowing us to reconstruct the laminar location of recorded neurons. Neurons recorded on electrodes falling within the deepest sink were assigned to the granular layer, while those superior and inferior were assigned to the supra-granular and infra-granular layers (Figure 3.1e, f, Figure 3.4—Figure supplement 3). The tone-evoked amplitude of the CSD was measured by first calculating root mean square of each channel during the first 50ms post tone onset, and then calculating the mean across all electrodes determined to fall within either the deepest short latency sink (granular layer) or pooled across all electrodes either above (supra-granular layer) or below (infra-granular layer). For each session, the granular layer CSD amplitude for all tone conditions was normalized across conditions by the deviant tone, light-off condition, and the mean across sessions was statistically analyzed. The SSA index was calculated as described in *Stimulus-specific adaptation index* on the basis of the amplitude.

Statistical tests. For all statistical tests in which N>=30, we applied the student's t-test (Matlab) unless specified otherwise, and reported the p-value, degrees of freedom and t-statistic. For all tests with N < 30, sample variance was tested for normality using the Komogorov-Smirnov test. If any group's variance was non-normal, we applied a non-parametric test, e.g. Wilcoxon sign rank or rank sum test (Matlab), and provided the z-statistic for any group with a normal distribution. For all tests, Bonferroni correction was applied for multiple comparisons, and reported as "C=X" where X is the factor by which the p-value was adjusted. Statistical tests were single-tailed if there was a reasonable prior expectation about the direction of the difference between samples. p1 refers to one-sided, and p2 refers to two-sided statistics set. In all Figure s, single, double and triple stars indicate p < 0.05, 0.01 and 0.001 respectively. Error bars in all Figure s represent the standard error of the mean, unless otherwise noted.

Excitatory-inhibitory network model. We constructed models of the excitatory-inhibitory neuronal circuit to understand the coupling of excitatory interneurons with PV and SOM interneurons. We constructed firing-rate models based on Wilson-Cowan dynamics [28-30]. The parameters were chosen in order to achieve a match to experimental data. The mean activity level of each population was modeled as:

$$\frac{dE}{dt} = \frac{1}{\tau_E}[-E(t) + (k - r)S(j_{ETone}(t) + S_{inh}(j_{IE}I(t))]$$

$$\frac{dI}{dt} = \frac{1}{\tau_I}[-I(t) + (k - r)S(j_{inh}(t) + j_{ITone}(t) + j_{EI}E(t))]$$

where $E(t)$ is the activity of the excitatory population; $I(t)$ is the activity of the inhibitory population; $S(x)$ is the transfer function between the combined "synaptic" input and the neuronal FR. S (x) is linear with respect to intermediate inputs, but imposes a minimum and maximum activation limits. $S_{inh}(x)$ is the transfer function between the inhibitory firing rate and excitatory post-synaptic current; j_{EI} and j_{IE} are excitatory-inhibitory and inhibitory-excitatory synaptic weights (.2 and -1.0 for PVs, .05 and -.39 for SOMs, respectively); $j_{ETone}(t)$ and $j_{ITone}(t)$ are tone-evoked input currents to excitatory and inhibitory neurons, respectively, modeled as 50 ms long exponentially decaying inputs of maximum amplitude 3 (delayed by 7ms for SOMs, which do not receive direct thalamic inputs, relative to PVs, which receive direct thalamic inputs); τ_E (10 ms) and τ_I (10 ms) are synaptic time constants for excitatory and inhibitory neurons; k and r represent the maximum and minimum FR of neurons respectively ($k = 15, r = 1$); $j_{inh}(t)$ is the negative input to inhibitory neurons due to Arch. The optogenetic modulation was modeled as a unitary 250 ms pulse. To capture the differences in inputs due to repeated tone exposures, we modeled thalamic inputs reflecting the tone inputs with synaptic depression. We modeled the conductance of the thalamic projections, g_{Inp}, as changing according to the equation:

$$\frac{dg_{Inp}}{dt} = (g_0 - g_{Inp})/T_g - (g_{Inp} r)/T_r$$

Where g_0 is the maximum conductance $(g_0 = 1)$, r is the gating coefficient representing tone-evoked thalamic input, T_g is the timescale for replenishment ($T_g = 3\ s$), T_r is the timescale for depletion ($T_r = 80\ ms$). We took r to be a step function with an

exponential decay (with 40 ms time constant and amplitude of 3). The full input to auditory cortical neural populations is then equal to $g_{Inp}r$. In train of four tones, the first tone-evoked response was taken as the deviant tone, and the fourth tone as the standard tone.

For the inhibitory-to-excitatory inputs, we used a sigmoidal transfer function and showed the existence of parameter regimes consistent with our results. For PVs, we used a sigmoid of the form:

$$S_{PV}(r_{PV}) = \frac{1}{1 + \exp[-p(r_{PV} - \theta)]}$$

where p = 0.3 and θ= 9. This gives a facilitating response at low input levels and a linear response at high input levels. For SOMs, we used a hyperbolic tangent that provided a saturating non-linearity:

$$S_{SOM}(r_{SOM}) = \frac{1 - \exp[-2r_{SOM}/s]}{1 + \exp[-2r_{SOM}/s]}$$

where s = 3. For visualization, the baseline firing rate of neurons was removed and the peak tone response to a “deviant” without optogenetic manipulation normalized to 1.

We also constructed a model coupling excitatory neurons and SOM and PV interneurons using a generalization of the above dynamics, which may be written:

$$\frac{dN_i}{dt} = \frac{1}{T_i}\left(-N_i + (k - r)S\left(j_{tone,i}(t) + j_{ext,i}(t) + \sum_k j_{ki} * S_k(N_k) \right) \right)$$

where N_i is the firing rate of the ith population (EXC, PV, SOM), $T_i = 10\ ms$ is the time constant for each population, $k = 15$, $r = 1$, S has different maximum and minimum values for each population ($x_{min,E} = -1$, $x_{max,E} = 1.75$, $x_{min,PV} = -.5$, $x_{max,PV} = 4$, $x_{min,SOM} = 0$, $x_{max,SOM} = 3$). $S_E(x) = x$, and S_{SOM} and S_{PV} use the definitions above. $j_{E,E} = j_{SOM,SOM} = j_{PV,PV} = j_{PV,SOM} = 0$, $j_{E,SOM} = .25$, $j_{SOM,E} = -.25$, $j_{E,PV} = .4$, $j_{PV,E} = -1$, and $j_{SOM,PV} = -.1$. $j_{ext,PV} = 1.5, j_{ext,SOM} = 1$. Tone inputs are the same as described above.

Bibliography

Anderson, L.A., Christianson, G.B., Linden, J.F., 2009. Stimulus-specific adaptation occurs in the auditory thalamus. J Neurosci 29, 7359-7363.

Antunes, F.M., Nelken, I., Covey, E., Malmierca, M.S., 2010. Stimulus-specific adaptation in the auditory thalamus of the anesthetized rat. PLoS One 5, e14071.

Aravanis, A.M., Wang, L.P., Zhang, F., Meltzer, L.A., Mogri, M.Z., Schneider, M.B., Deisseroth, K., 2007. An optical neural interface: in vivo control of rodent motor cortex with integrated fiberoptic and optogenetic technology. J Neural Eng 4, S143-156.

Asari, H., Zador, A., 2009. Long-lasting context dependence constrains neural encoding models in rodent auditory cortex. J Neurophysiol 102, 2638-2656.

Barlow, H.B., 1961. Possible principles underlying the transformation of sensory messages, in: Rosenblith, W. (Ed.), Sensory Communication. MIT Press, Cambridge, MA, pp. 217-234.

Bartho, P., Hirase, H., Monconduit, L., Zugaro, M., Harris, K.D., Buzsaki, G., 2004. Characterization of neocortical principal cells and interneurons by network interactions and extracellular features. J Neurophysiol 92, 600-608.

Bauerle, P., von der Behrens, W., Kossl, M., Gaese, B.H., 2011. Stimulus-specific adaptation in the gerbil primary auditory thalamus is the result of a fast frequency-specific habituation and is regulated by the corticofugal system. J Neurosci 31, 9708-9722.

Beierlein, M., Gibson, J.R., Connors, B.W., 2003. Two dynamically distinct inhibitory networks in layer 4 of the neocortex. J Neurophysiol 90, 2987-3000.

Bizley, J.K., Walker, K.M., King, A.J., Schnupp, J.W., 2010. Neural ensemble codes for stimulus periodicity in auditory cortex. J Neurosci 30, 5078-5091.

Boyden, E.S., Zhang, F., Bamberg, E., Nagel, G., Deisseroth, K., 2005. Millisecond-timescale, genetically targeted optical control of neural activity. Nat Neurosci 8, 1263-1268.

Brasselet, R., Panzeri, S., Logothetis, N.K., Kayser, C., 2012. Neurons with stereotyped and rapid responses provide a reference frame for relative temporal coding in primate auditory cortex. J Neurosci 32, 2998-3008.

Cardin, J., Carlen, M., Meletis, K., Knoblich, U., Zhang, F., Deisseroth, K., Tsai, L.-H., Moore, C., 2010. Targeted optogenetic stimulation and recording of neurons in vivo using cell-type-specific expression of Channelrhodopsin-2. Nature protocols 5, 247-254.

Carruthers, I.M., Laplagne, D.A., Jaegle, A., Briguglio, J., Mwilambwe-Tshilobo, L., Natan, R.G., Geffen, M.N., 2015. Emergence of invariant representation of vocalizations in the auditory cortex. J Neurophysiol, jn 00095 02015.

Carruthers, I.M., Natan, R.G., Geffen, M.N., 2013. Encoding of ultrasonic vocalizations in the auditory cortex. J Neurophysiol 109, 1912-1927.

Centanni, T.M., Engineer, C.T., Kilgard, M.P., 2013. Cortical speech-evoked response patterns in multiple auditory fields are correlated with behavioral discrimination ability. J Neurophysiol 110, 177-189.

Cheung, S.W., Nagarajan, S.S., Bedenbaugh, P.H., Schreiner, C.E., Wang, X., Wong, A., 2001. Auditory cortical neuron response differences under isoflurane versus pentobarbital anesthesia. Hear Res 156, 115-127.

Chow, B.Y., Han, X., Dobry, A.S., Qian, X., Chuong, A.S., Li, M., Henninger, M.A., Belfort, G.M., Lin, Y., Monahan, P.E., Boyden, E.S., 2010. High-performance genetically targetable optical neural silencing by light-driven proton pumps. Nature 463, 98-102.

Cottam, J.C., Smith, S.L., Hausser, M., 2013a. Target-specific effects of somatostatin-expressing interneurons on neocortical visual processing. J Neurosci 33, 19567-19578.

Cottam, J.C., Smith, S.L., Hausser, M., 2013b. Target-specific effects of somatostatin-expressing interneurons on neocortical visual processing. J Neurosci 33, 19567-19578.

Das, A., Gilbert, C.D., 1999. Topography of contextual modulations mediated by short-range interactions in primary visual cortex. Nature 399, 655-661.

DeFelipe, J., 2002. Cortical interneurons: from Cajal to 2001. Prog Brain Res 136, 215-238.

Deisseroth, K., 2011. Optogenetics. Nat Methods 8, 26-29.

Douglas, R.J., Martin, K.A., 2004. Neuronal circuits of the neocortex. Annu Rev Neurosci 27, 419-451.

Duque, D., Malmierca, M.S., Caspary, D.M., 2014. Modulation of stimulus-specific adaptation by GABA (A) receptor activation or blockade in the medial geniculate body of the anaesthetized rat. J Physiol 592, 729-743.

Duque, D., Perez-Gonzalez, D., Ayala, Y.A., Palmer, A.R., Malmierca, M.S., 2012. Topographic distribution, frequency, and intensity dependence of stimulus-specific adaptation in the inferior colliculus of the rat. J Neurosci 32, 17762-17774.

Durand, S., Patrizi, A., Quast, K.B., Hachigian, L., Pavlyuk, R., Saxena, A., Carninci, P., Hensch, T.K., Fagiolini, M., 2012. NMDA receptor regulation prevents regression of visual cortical function in the absence of Mecp2. Neuron 76, 1078-1090.

Elliott, D.N., Trahiotis, C., 1972. Cortical lesions and auditory discrimination. Psychol Bull 77, 198-222.

Escera, C., Malmierca, M.S., 2014. The auditory novelty system: an attempt to integrate human and animal research. Psychophysiology 51, 111-123.

Farley, B.J., Quirk, M.C., Doherty, J.J., Christian, E.P., 2010. Stimulus-specific adaptation in auditory cortex is an NMDA-independent process distinct from the sensory novelty encoded by the mismatch negativity. J Neurosci 30, 16475-16484.

Fino, E., Packer, A.M., Yuste, R., 2013. The logic of inhibitory connectivity in the neocortex. Neuroscientist 19, 228-237.

Fishman, Y.I., Steinschneider, M., 2012. Searching for the mismatch negativity in primary auditory cortex of the awake monkey: deviance detection or stimulus specific adaptation? J Neurosci 32, 15747-15758.

Froemke, R.C., Carcea, I., Barker, A.J., Yuan, K., Seybold, B.A., Martins, A.R., Zaika, N., Bernstein, H., Wachs, M., Levis, P.A., Polley, D.B., Merzenich, M.M., Schreiner, C.E., 2013. Long-term modification of cortical synapses improves sensory perception. Nat Neurosci 16, 79-88.

Gaese, B.H., Ostwald, J., 2001. Anesthesia changes frequency tuning of neurons in the rat primary auditory cortex. J Neurophysiol 86, 1062-1066.

Garcia-Lazaro, J.A., Ho, S.S., Nair, A., Schnupp, J.W., 2007. Shifting and scaling adaptation to dynamic stimuli in somatosensory cortex. Eur J Neurosci 26, 2359-2368.

Gentet, L.J., Kremer, Y., Taniguchi, H., Huang, Z.J., Staiger, J.F., Petersen, C.C., 2012. Unique functional properties of somatostatin-expressing GABAergic neurons in mouse barrel cortex. Nat Neurosci 15, 607-612.

Goldberg, E.M., Jeong, H.Y., Kruglikov, I., Tremblay, R., Lazarenko, R.M., Rudy, B., 2011. Rapid developmental maturation of neocortical FS cell intrinsic excitability. Cereb Cortex 21, 666-682.

Grimm, S., Escera, C., 2012. Auditory deviance detection revisited: evidence for a hierarchical novelty system. Int J Psychophysiol 85, 88-92.

Guo, W., Chambers, A.R., Darrow, K.N., Hancock, K.E., Shinn-Cunningham, B.G., Polley, D.B., 2012. Robustness of cortical topography across fields, laminae, anesthetic states, and neurophysiological signal types. J Neurosci 32, 9159-9172.

Hackett, T., Barkat, T., O'Brien, B., Hensch, T., Polley, D., 2011. Linking topography to tonotopy in the mouse auditory thalamocortical circuit. J Neurosci 31, 2983-2995.

Hamilton, L.S., Sohl-Dickstein, J., Huth, A.G., Carels, V.M., Deisseroth, K., Bao, S., 2013. Optogenetic activation of an inhibitory network enhances feedforward functional connectivity in auditory cortex. Neuron 80, 1066-1076.

Han, X., Qian, X., Bernstein, J.G., Zhou, H.H., Franzesi, G.T., Stern, P., Bronson, R.T., Graybiel, A.M., Desimone, R., Boyden, E.S., 2009. Millisecond-timescale optical control of neural dynamics in the nonhuman primate brain. Neuron 62, 191-198.

Happel, M.F., Deliano, M., Handschuh, J., Ohl, F.W., 2014. Dopamine-modulated recurrent corticoefferent feedback in primary sensory cortex promotes detection of behaviorally relevant stimuli. J Neurosci 34, 1234-1247.

Isaacson, J.S., Scanziani, M., 2011. How inhibition shapes cortical activity. Neuron 72, 231-243.

Kanold, P.O., Nelken, I., Polley, D.B., 2014. Local versus global scales of organization in auditory cortex. Trends Neurosci 37, 502-510.

Kaur, S., Rose, H.J., Lazar, R., Liang, K., Metherate, R., 2005. Spectral integration in primary auditory cortex: laminar processing of afferent input, in vivo and in vitro. Neuroscience 134, 1033-1045.

Kepecs, A., Fishell, G., 2014. Interneuron cell types are fit to function. Nature 505, 318-326.

Khatri, V., Bruno, R.M., Simons, D.J., 2009. Stimulus-specific and stimulus-nonspecific firing synchrony and its modulation by sensory adaptation in the whisker-to-barrel pathway. J Neurophysiol 101, 2328-2338.

Kraus, N., McGee, T., Littman, T., Nicol, T., King, C., 1994. Nonprimary auditory thalamic representation of acoustic change. J Neurophysiol 72, 1270-1277.

Kvitsiani, D., Ranade, S., Hangya, B., Taniguchi, H., Huang, J.Z., Kepecs, A., 2013. Distinct behavioural and network correlates of two interneuron types in prefrontal cortex. Nature 498, 363-366.

Land, R., Engler, G., Kral, A., Engel, A.K., 2012. Auditory evoked bursts in mouse visual cortex during isoflurane anesthesia. PLoS One 7, e49855.

Lee, S., Hjerling-Leffler, J., Zagha, E., Fishell, G., Rudy, B., 2010. The largest group of superficial neocortical GABAergic interneurons expresses ionotropic serotonin receptors. J Neurosci 30, 16796-16808.

Lee, S.H., Kwan, A.C., Zhang, S., Phoumthipphavong, V., Flannery, J.G., Masmanidis, S.C., Taniguchi, H., Huang, Z.J., Zhang, F., Boyden, E.S., Deisseroth, K., Dan, Y., 2012. Activation of specific interneurons improves V1 feature selectivity and visual perception. Nature 488, 379-383.

Lima, S., Hromadka, T., Znamenskiy, P., Zador, A., 2009. PINP: a new method of tagging neuronal populations for identification during in vivo electrophysiological recording. PLoS One 4, e6099.

Linden, J.F., Liu, R.C., Sahani, M., Schreiner, C.E., Merzenich, M.M., 2003. Spectrotemporal structure of receptive fields in areas AI and AAF of mouse auditory cortex. J Neurophysiol 90, 2660-2675.

Linden, J.F., Schreiner, C.E., 2003. Columnar transformations in auditory cortex? A comparison to visual and somatosensory cortices. Cereb Cortex 13, 83-89.

Ma, Y., Hu, H., Agmon, A., 2012. Short-term plasticity of unitary inhibitory-to-inhibitory synapses depends on the presynaptic interneuron subtype. J Neurosci 32, 983-988.

Malmierca, M.S., Cristaudo, S., Perez-Gonzalez, D., Covey, E., 2009. Stimulus-specific adaptation in the inferior colliculus of the anesthetized rat. J Neurosci 29, 5483-5493.

Markram, H., Toledo-Rodriguez, M., Wang, Y., Gupta, A., Silberberg, G., Wu, C., 2004. Interneurons of the neocortical inhibitory system. Nat Rev Neurosci 5, 793-807.

Marlin, B.J., Mitre, M., D'Amour J, A., Chao, M.V., Froemke, R.C., 2015. Oxytocin enables maternal behaviour by balancing cortical inhibition. Nature 520, 499-504.

McGarry, L.M., Packer, A.M., Fino, E., Nikolenko, V., Sippy, T., Yuste, R., 2010. Quantitative classification of somatostatin-positive neocortical interneurons identifies three interneuron subtypes. Front Neural Circuits 4, 12.

Metherate, R., Cruikshank, S.J., 1999. Thalamocortical inputs trigger a propagating envelope of gamma-band activity in auditory cortex in vitro. Experimental brain research 126, 160-174.

Mill, R., Coath, M., Wennekers, T., Denham, S.L., 2011. A neurocomputational model of stimulus-specific adaptation to oddball and Markov sequences. PLoS Comput Biol 7, e1002117.

Moore, A.K., Wehr, M., 2013. Parvalbumin-expressing inhibitory interneurons in auditory cortex are well-tuned for frequency. J Neurosci 33, 13713-13723.

Moore, D.R., Rothholtz, V., King, A.J., 2001. Hearing: cortical activation does matter. Curr Biol 11, R782-784.

Nelken, I., 2014. Stimulus-specific adaptation and deviance detection in the auditory system: experiments and models. Biol Cybern.

Nelken, I., Fishbach, A., Las, L., Ulanovsky, N., Farkas, D., 2003. Primary auditory cortex of cats: feature detection or something else? Biol Cybern 89, 397-406.

Niell, C.M., Stryker, M.P., 2008. Highly selective receptive fields in mouse visual cortex. J Neurosci 28, 7520-7536.

Olsen, S.R., Bortone, D.S., Adesnik, H., Scanziani, M., 2012. Gain control by layer six in cortical circuits of vision. Nature 483, 47-52.

Otazu, G.H., Tai, L.H., Yang, Y., Zador, A.M., 2009. Engaging in an auditory task suppresses responses in auditory cortex. Nat Neurosci 12, 646-654.

Ouellet, L., de Villers-Sidani, E., 2014. Trajectory of the main GABAergic interneuron populations from early development to old age in the rat primary auditory cortex. Front Neuroanat 8, 40.

Perez-Gonzalez, D., Malmierca, M.S., Covey, E., 2005. Novelty detector neurons in the mammalian auditory midbrain. Eur J Neurosci 22, 2879-2885.

Pfeffer, C.K., Xue, M., He, M., Huang, Z.J., Scanziani, M., 2013. Inhibition of inhibition in visual cortex: the logic of connections between molecularly distinct interneurons. Nat Neurosci 16, 1068-1076.

Pi, H.J., Hangya, B., Kvitsiani, D., Sanders, J.I., Huang, Z.J., Kepecs, A., 2013. Cortical interneurons that specialize in disinhibitory control. Nature 503, 521-524.

Picard, N., Leslie, J.H., Trowbridge, S.K., Subramanian, J., Nedivi, E., Fagiolini, M., 2014. Aberrant development and plasticity of excitatory visual cortical networks in the absence of cpg15. J Neurosci 34, 3517-3522.

Reyes, A., Lujan, R., Rozov, A., Burnashev, N., Somogyi, P., Sakmann, B., 1998. Target-cell-specific facilitation and depression in neocortical circuits. Nat Neurosci 1, 279-285.

Rudy, B., Fishell, G., Lee, S., Hjerling-Leffler, J., 2011. Three groups of interneurons account for nearly 100% of neocortical GABAergic neurons. Dev Neurobiol 71, 45-61.

Rust, N.C., Dicarlo, J.J., 2010. Selectivity and tolerance ("invariance") both increase as visual information propagates from cortical area V4 to IT. J Neurosci 30, 12978-12995.

Silberberg, G., Markram, H., 2007. Disynaptic inhibition between neocortical pyramidal cells mediated by Martinotti cells. Neuron 53, 735-746.

Sohal, V.S., Zhang, F., Yizhar, O., Deisseroth, K., 2009. Parvalbumin neurons and gamma rhythms enhance cortical circuit performance. Nature 459, 698-702.

Staiger, J.F., Zilles, K., Freund, T.F., 1996. Recurrent axon collaterals of corticothalamic projection neurons in rat primary somatosensory cortex contribute to excitatory and inhibitory feedback-loops. Anat Embryol (Berl) 194, 533-543.

Sturgill, J.F., Isaacson, J.S., 2015. Somatostatin cells regulate sensory response fidelity via subtractive inhibition in olfactory cortex. Nat Neurosci 18, 531-535.

Szymanski, F.D., Garcia-Lazaro, J.A., Schnupp, J.W., 2009. Current source density profiles of stimulus-specific adaptation in rat auditory cortex. J Neurophysiol 102, 1483-1490.

Taaseh, N., Yaron, A., Nelken, I., 2011. Stimulus-specific adaptation and deviance detection in the rat auditory cortex. PLoS One 6, e23369.

Tan, Z., Hu, H., Huang, Z.J., Agmon, A., 2008. Robust but delayed thalamocortical activation of dendritic-targeting inhibitory interneurons. Proc Natl Acad Sci U S A 105, 2187-2192.

Taniguchi, H., He, M., Wu, P., Kim, S., Paik, R., Sugino, K., Kvitsiani, D., Fu, Y., Lu, J., Lin, Y., Miyoshi, G., Shima, Y., Fishell, G., Nelson, S.B., Huang, Z.J., 2011. A resource of Cre driver lines for genetic targeting of GABAergic neurons in cerebral cortex. Neuron 71, 995-1013.

Ter-Mikaelian, M., Sanes, D.H., Semple, M.N., 2007. Transformation of temporal properties between auditory midbrain and cortex in the awake Mongolian gerbil. J Neurosci 27, 6091-6102.

Thomas, J.M., Morse, C., Kishline, L., O'Brien-Lambert, A., Simonton, A., Miller, K.E., Covey, E., 2012. Stimulus-specific adaptation in specialized neurons in the inferior colliculus of the big brown bat, Eptesicus fuscus. Hear Res 291, 34-40.

Ulanovsky, N., Las, L., Farkas, D., Nelken, I., 2004. Multiple time scales of adaptation in auditory cortex neurons. J Neurosci 24, 10440-10453.

Ulanovsky, N., Las, L., Nelken, I., 2003. Processing of low-probability sounds by cortical neurons. Nat Neurosci 6, 391-398.

Weible, A.P., Moore, A.K., Liu, C., DeBlander, L., Wu, H., Kentros, C., Wehr, M., 2014. Perceptual gap detection is mediated by gap termination responses in auditory cortex. Curr Biol 24, 1447-1455.

Wilson, N.R., Runyan, C.A., Wang, F.L., Sur, M., 2012. Division and subtraction by distinct cortical inhibitory networks in vivo. Nature 488, 343-348.

Winkler, I., Denham, S.L., Nelken, I., 2009. Modeling the auditory scene: predictive regularity representations and perceptual objects. Trends Cogn Sci 13, 532-540.

Xu, X., Callaway, E.M., 2009. Laminar specificity of functional input to distinct types of inhibitory cortical neurons. J Neurosci 29, 70-85.

Xu, X., Roby, K.D., Callaway, E.M., 2010. Immunochemical characterization of inhibitory mouse cortical neurons: three chemically distinct classes of inhibitory cells. J Comp Neurol 518, 389-404.

Zhang, F., Gradinaru, V., Adamantidis, A.R., Durand, R., Airan, R.D., de Lecea, L., Deisseroth, K., 2010. Optogenetic interrogation of neural circuits: technology for probing mammalian brain structures. Nature protocols 5, 439-456.

Zhao, L., Liu, Y., Shen, L., Feng, L., Hong, B., 2011. Stimulus-specific adaptation and its dynamics in the inferior colliculus of rat. Neuroscience 181, 163-174.

Supplementary Figures

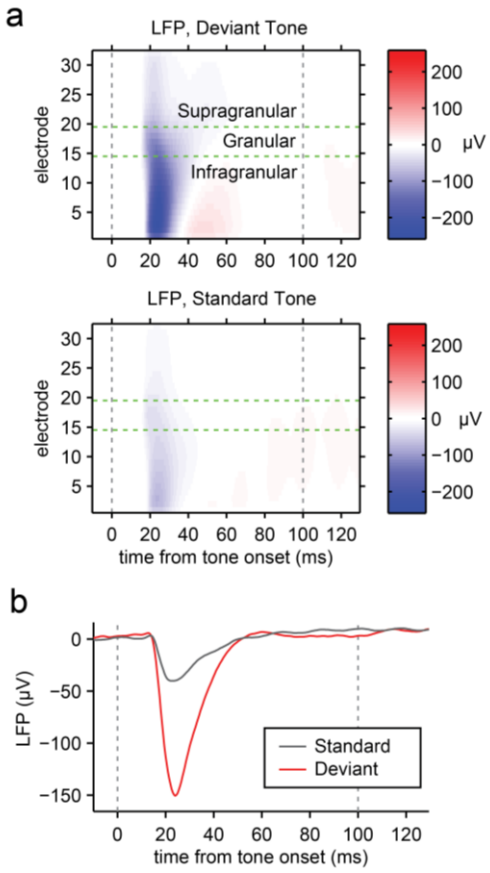

Figure 3.1—Figure supplement 1. Local field potentials recorded in A1 exhibit stimulus-specific adaptation. (**a**) Representative peri-stimulus LFPs across cortical layers. Top: Mean response to deviant tones. Bottom: Mean response to standard tones. Gray dashed lines indicate tone onset and offset. Green dashed lines indicate the margins between cortical layers. (**b**) Mean LFP collected from the thalamo-recipient granular layer, in response to standard (gray) and deviant (red) tones. Gray dashed lines indicate tone onset and offset.

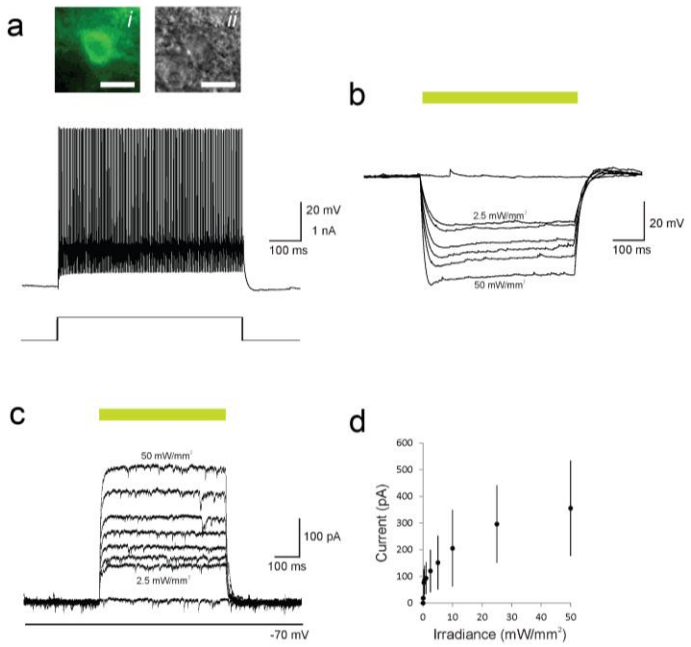

Figure 3.2—Figure supplement 1. Optogenetic control of PVs in mouse primary auditory cortex via photostimulation of Arch in acute slices. (**a**) Sustained high-frequency firing pattern typical of a PV-positive FS cell (top) in response to rectangular current injection (bottom; 600pA) recorded *in vitro* via whole cell patch clamp. Inset, epifluorescence (i) and corresponding IR-DIC image (ii) of the depicted cell. Scale bar – 20 µm. (**b**) Membrane hyperpolarization mediated by 532nm light. (**c**) Outward current mediated by photoactivation of Arch. (**d**) Plot of light-induced outward current vs. illuminance (mW/mm2). Error bars – standard deviation.

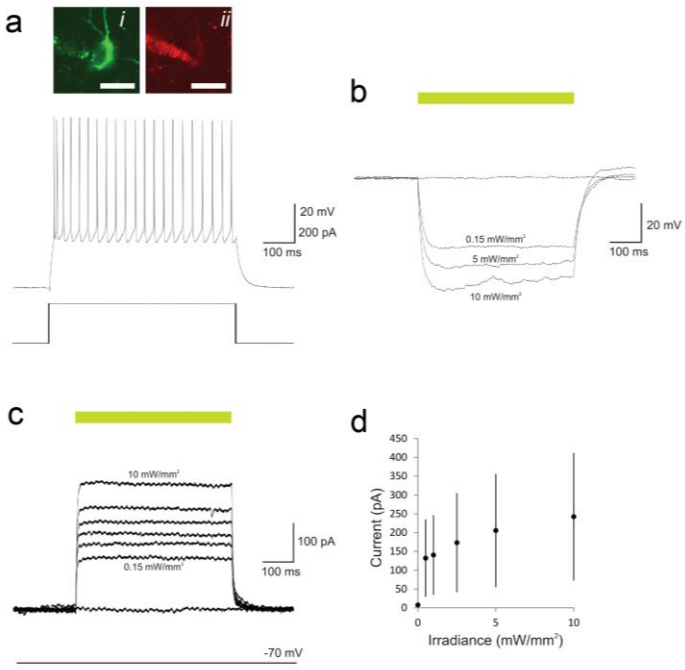

Figure 3.2—Figure supplement 2. Optogenetic control of SOMs in mouse primary auditory cortex via photostimulation of Arch in acute slices. (**a**) Adapting discharge pattern typical of a somatostatin-positive cell (top) in response to rectangular current injection (bottom; 200pA) recorded *in vitro* via whole cell patch clamp. Inset, endogenous GFP fluorescence of the recorded cell illustrating AAV9.Arch.GFP expression (i) filled with Alexa 594 (ii) and imaged using a two-photon microscope. Scale bar – 20 µm. (**b**) Membrane hyperpolarization mediated by 532nm light. (**c**) Outward current mediated by photoactivation of Arch. (**d**) Plot of light-induced outward current vs. illuminance (mW/mm2). Errorbars – standard deviation.

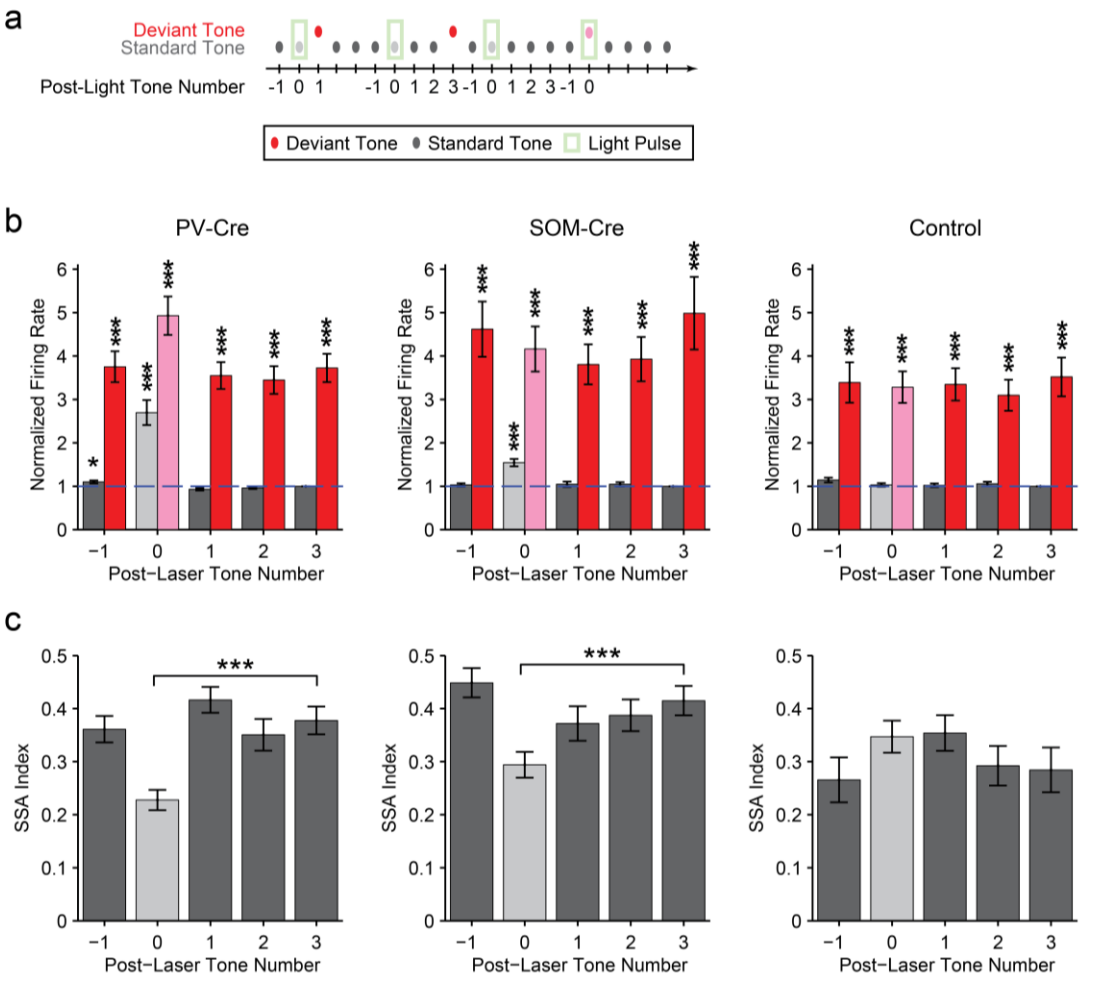

Figure 3.3—Figure supplement 1. Photostimulation during standard tone does not affect SSA during subsequent tones on light-off trials. (**a**) Diagram of oddball stimuli illustrating post-photostimulation tone number: Tones and light pulses indicated as in Figure 3.3**a**. Numbers indicate each tone position relative to light pulses as included in the analysis below. Any tones following deviant tones were excluded from the analysis. (**b**) The mean population FR in response to standard (gray) and deviant (red) tones subsequent to light-on trials are not affected by light presentation (dark bars: light-off. light bars: light-on). For each neuron, responses are normalized by the response to the third post-laser standard tone (T_3, indicated by blue dashed line). In PV-Cre mice, the standard tone-evoked FR with light-on (T_0) and the tone preceding it (T_{-1}) were significantly higher than that of standard T_3 (N = 159, T_{-1}: Δ = 10%, p2 = 0.037, t(158) = 2.9, C = 9. T_0: Δ = 170%, p2 = 2e-7, t(158) = 5.9, C = 9), while the two post-light tones (T_1 and T_2) were not significantly different (N = 159, T_1 and T_2: p2 > 0.05, t(158) < 2.6, C = 9). In SOM-Cre mice, the standard T_0-evoked FR was greater than that of T_3 (N = 114, Δ = 54%, p2 = 4e-8, t(113) = 6.4, C = 9) while all light-off tones were not significantly different (T_{-1}, T_1, and T_2: p2 > 0.05, t(113) < 0.9, C = 9). In control mice, no standard tones evoked greater FR than T_3, (N = 107, T_{-1} through T_2: p2 < 0.05, t(106) < 2.7). In all three groups, deviant tones in all positions evoked greater FRs than standard T_3, (Δ > 209%, p2 < 5e-5, t(106)

> 4.7, C = 9). (**c**) Mean SSA index for each sequential tone position (for $T_{-1,0,1,2,3}$), calculated based on the pair of standard and deviant tones at each respective position. Each tone response, tone A or B, was used to calculate a separate SSA index:

$$SSA\ Index = \frac{D_A - S_A}{D_A + S_A}\ or\ \frac{D_B - S_B}{D_B + S_B}$$

Where S and D indicate mean FR evoked by standard and deviant tone probabilities, respectively, and their subscripts indicate the tone frequency condition. Compared to T_3, SSA index was significantly reduced only for T_0, the only light-on trial, in both PV-Cre and SOM-Cre mice (PV-Cre: Δ = -40%, p2 = 4e-10, t(158) = -6.9, C = 4. SOM: Δ = -29%, p2 = 2e-7, t(158) = -5.8, C = 4), as expected from Figure 3.3**e**, **f**, **g**. In both PV-Cre and SOM-Cre mice, the SSA index at all of the other sequential tone positions, T_{-1} through T_2 was not significantly different than that of T_3 (p2 > 0.05, t(113) < 1.9, C = 4), indicating that the effects of photosuppression were not detectable beyond T_0. In control mice, the SSA index was not different compared to T_3 for any tone position, even T_0 (p2 > 0.05, t(106) < 1.8, C = 4). Together, this analysis demonstrates that the optogenetic effects are acute to illumination periods, and unlikely to confound interpretation of effects observed during light-off trials.

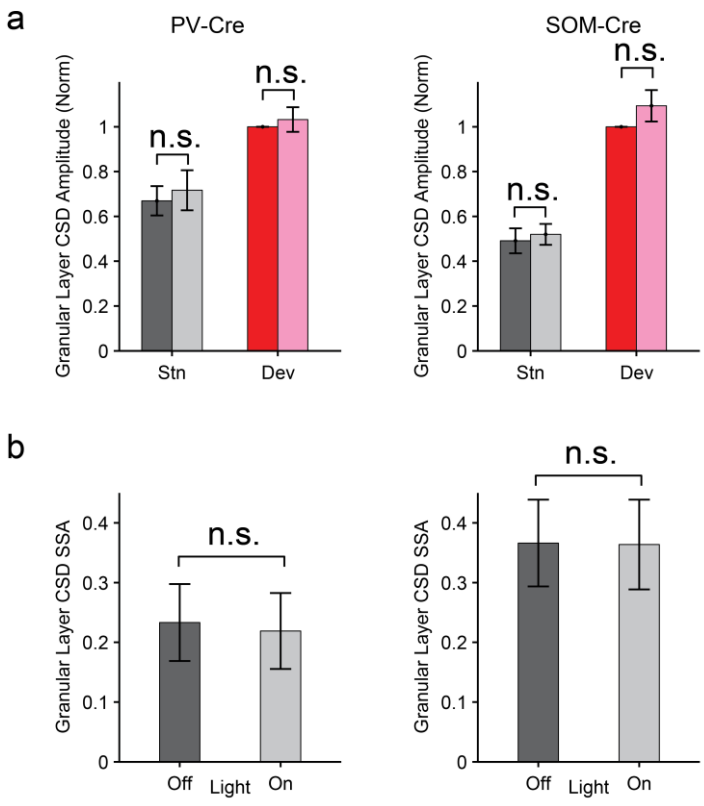

Figure 3.3—Figure supplement 2. Interneuron photosuppression does not affect thalamocortical responses to standard or deviant. (**a**) In PV-Cre and SOM-Cre mice, the mean granular layer CSD SSA index was not significantly different between the light-off and light-on conditions for standard or deviant tones ($p2 > 0.05$, for each condition; left, PV-Cre: N = 16. Center, SOM-Cre: N = 12). (**b**) In both experimental groups, the mean granular layer CSD amplitude was not significantly different between the light-off and light-on conditions for standard or deviant tones ($p2 > 0.05$, for each condition; left, PV-Cre: N = 8. Center, SOM-Cre: N = 6).

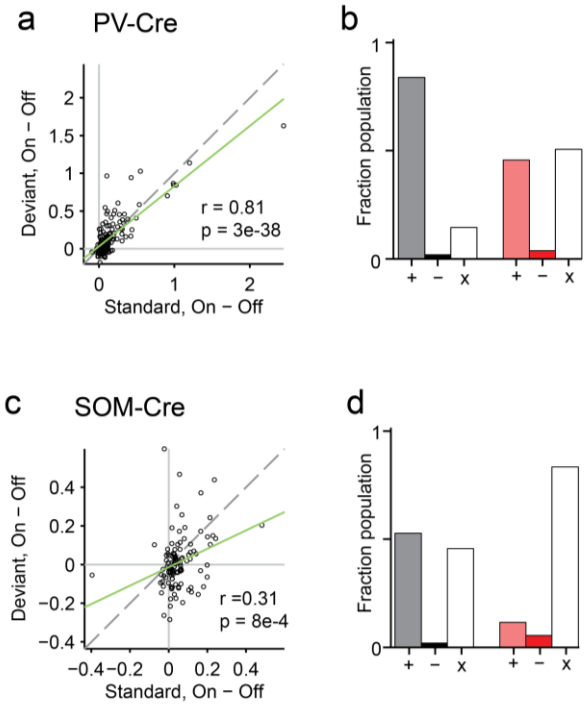

Figure 3.4—Figure supplement 1. PVs and SOMs differentially affect response to standard and deviant tones. (**a, c**) Correlation between standard and deviant tone response change by photostimulation. Each neuron's response to each tone, A and B, is represented by one circle. Gray dashed line – identity line. Green dashed line – regression line. Neurons recorded in PV-Cre (**a**) and SOM-Cre (**c**) mice. (**b, d**) Proportion of putative excitatory population exhibiting significantly increased (gray, pink), decreased (black, red), or unchanged (unfilled) FR to standard and deviant tones due to photosuppression. Neurons recorded in PV-Cre (**a**)**,** SOM-Cre (**c**) mice.

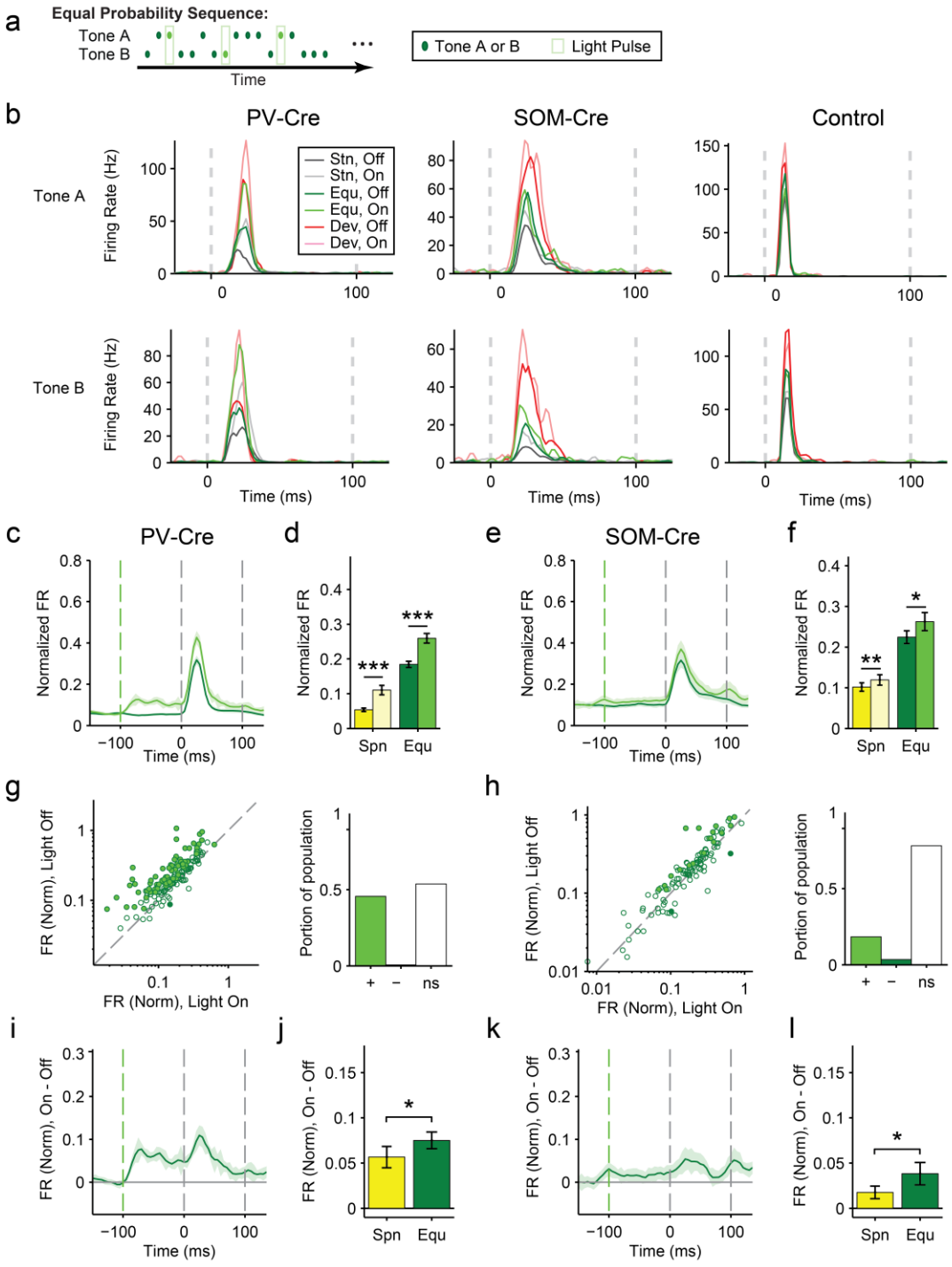

Figure 3.4—Figure supplement 2. Consistent effects of PV and SOM suppression in response to equal probability tones. (**a**) Diagram of equal probability tone stimulus; an equal number of pseudorandom tones A and B are presented with 250 ms light pulses (green bars) delivered during every 5th tone, starting 100ms before tone onset. (**b**) Effect of interneuron photosuppression on putative excitatory neuron responses to standard and deviant and equal probability tones. Mean FR of single neuron responses

to standard (gray), equal (green) and deviant (red) tones on laser-off (dark colors) vs laser-on (light colors) trials. Top: responses to tone A. Bottom: Responses to tone B. Left: neuron from PV-Cre mouse. Center: neuron from SOM-Cre mice Right: neuron from control mouse. (**c, e**) PSTH of FR to equal probability tones, during light-on (light green) and light-off trials (dark green). Each trace is a population average of putative excitatory neuron PSTHs normalized to each neuron's maximum deviant tone-evoked FR on light-off trials. Shaded regions around traces indicate standard error (SE). Dashed lines indicate light onset (green) and tone onset and offset (gray). Neurons recorded in PV-Cre (**c**, N = 160) and SOM-Cre (**e**, N = 114) mice. (**d, f**) Population mean spontaneous FR (50ms prior to tone onset, yellow) and equal-tone evoked FR (50 ms from tone onset, green) for light-off (dark colors) and light-on (light colors) trials. Normalized as in **c**. Neurons display an increase in spontaneous FR and equal tone-evoked FR with light-on for both PV-Cre (**d** – Spn: Δ105%, p2 = 3e-6, t(159) = -8.1. Equ: Δ = 41%, p2 = 1e-13, t(159) = 4.8) and SOM-Cre (**f**, Spn: Δ = 17%, p2 = 0.002, t(113) = -3.1. Equ: Δ = 17%, p2 = 0.012, t(113) = -2.54) mice. (**g, h**) Modulation of PV-Cre mouse putative excitatory neuron FR response to tones by interneuron photosuppression. Left: Circle: Response of each neuron to tone A and/or B. Filled: significantly increased (light green) or decreased (dark green) response; Unfilled: non-significant modulation. Gray dashed line – identity line. Right: Fraction of neuronal tone responses in the population that increased (light green), decreased (dark green) or did not significantly change with light. Neurons recorded in PV-Cre (**g**), SOM-Cre (**h**) mice. (**i, k**) Mean of the difference between light-on and light-off trials for each neuron for equal probability tones FR response PSTHs. Normalization and dashed lines as in **c**. Neurons recorded in PV-Cre (**i**), SOM-Cre (**k**) mice. (**j, l**) Mean population FR difference between light-on and light-off conditions for spontaneous activity (yellow) and equal probability tones (green). Measured and normalized as in **d** and **f**. Neurons display a larger increase in equal-tone evoked FR than spontaneous FR with light-on for those recorded in both PV-Cre (**j**, Δ = 32%, p2 = 0.029, t(159) = 2.2), SOM-Cre (**l**, Δ = 118%, p2 = 0.047, t(113) = 2.0) mice.

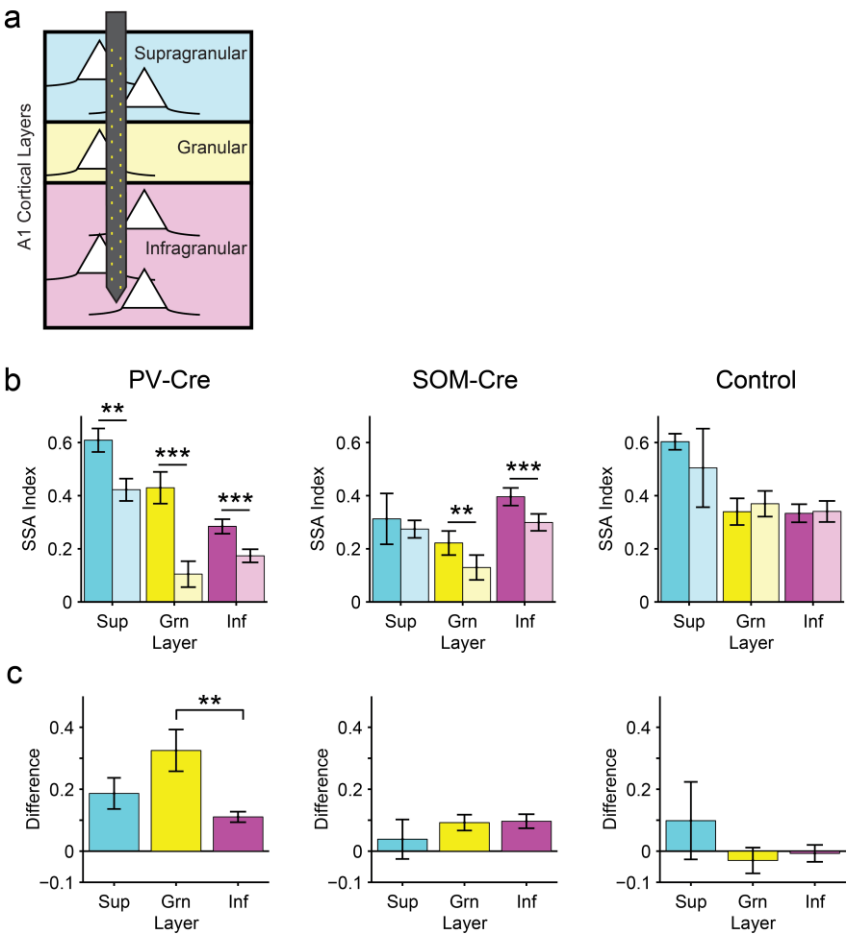

Figure 3.4—Figure supplement 3. PVs and SOMs have differential effects on SSA across different layers of cortex. (**a**) Diagram of multi-electrode recording across the supra-granular, granular and infra-granular layers of A1. (**b**) SSA index for cortical supra-granular (Sup, cyan), granular (Grn, yellow) and infra-granular (Inf, magenta) layers on light-off (dark colors) and light-on (light colors) trials. (**c**) Difference in SSA index between responses on light-on and light-off trials for each layer as shown in **b**. Suppressing PVs reduced SSA throughout all cortical layers (**b** left – Sup: N = 15, Δ = -31, p2 = 0.002. Grn: N = 27, p2 = 2e-4, z = 3.8. Inf: N = 79, Δ = -39%, p2 = 1e-8, z = 5.7). Notably, the effect of PVs was significantly stronger in the granular than in the infragranular layers (**c** left – Δ = 194%, p = 0.014, C = 2), but was not different between the supragranular and the granular or infragranular layers (p > 0.05, z < 1.8, C = 2). In the controls, SSA index was not significantly reduced between light-on and light-off trials in any layer (**b** right – Sup: N = 3. Grn: N = 21. Inf: N = 75. For each layer: p2 > 0.05, z <1.4), demonstrating that the light-induced effects required Arch. In contrast, suppressing SOMs reduced SSA in the granular (N = 7, Δ = -42%, p2 = 0.031) and infragranular (N = 63, Δ = -24%, p2 = 6e-7, z = 5.0) layers, but did not have a significant effect on SSA in the supragranular layers (N = 3, p2 > 0.05) (**b**, center). In SOM-Cre mice and controls, there was no difference between effects of photosuppression on SSA index in different layers (**c**, center and right – p > 0.05, z < 1.1). Signed rank test for b and ranked sum test used for c

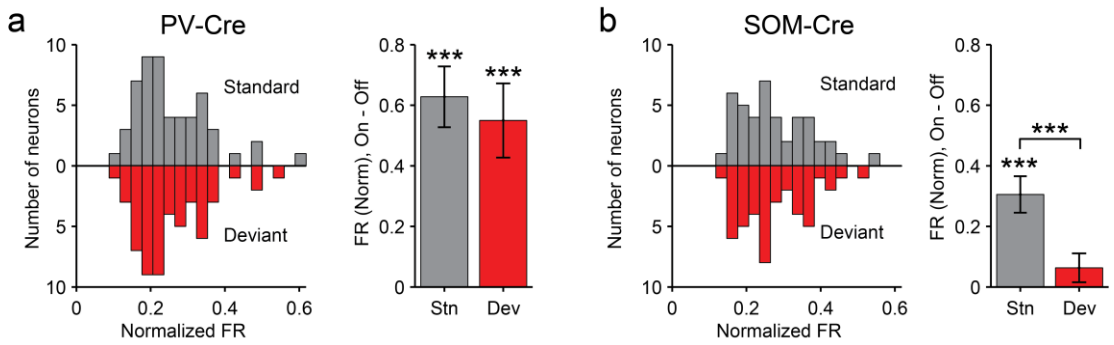

Figure 3.4—Figure supplement 4. Differences between PV and SOM effects on standard and deviant tones are preserved for subsets of neurons matched for FR. (**a**) Left: Two subsets of neurons recorded in PV-Cre mice with matched FR response magnitude to standard (gray, above x-axis) and deviant (red, below x-axis) tones on light-off trials. Right: Difference between light-on and light-off FR in response to standard (gray) and deviant (red) tones for the respective subsets of neurons. (**b**) Same as **a** for neurons recorded in SOM-Cre mice.

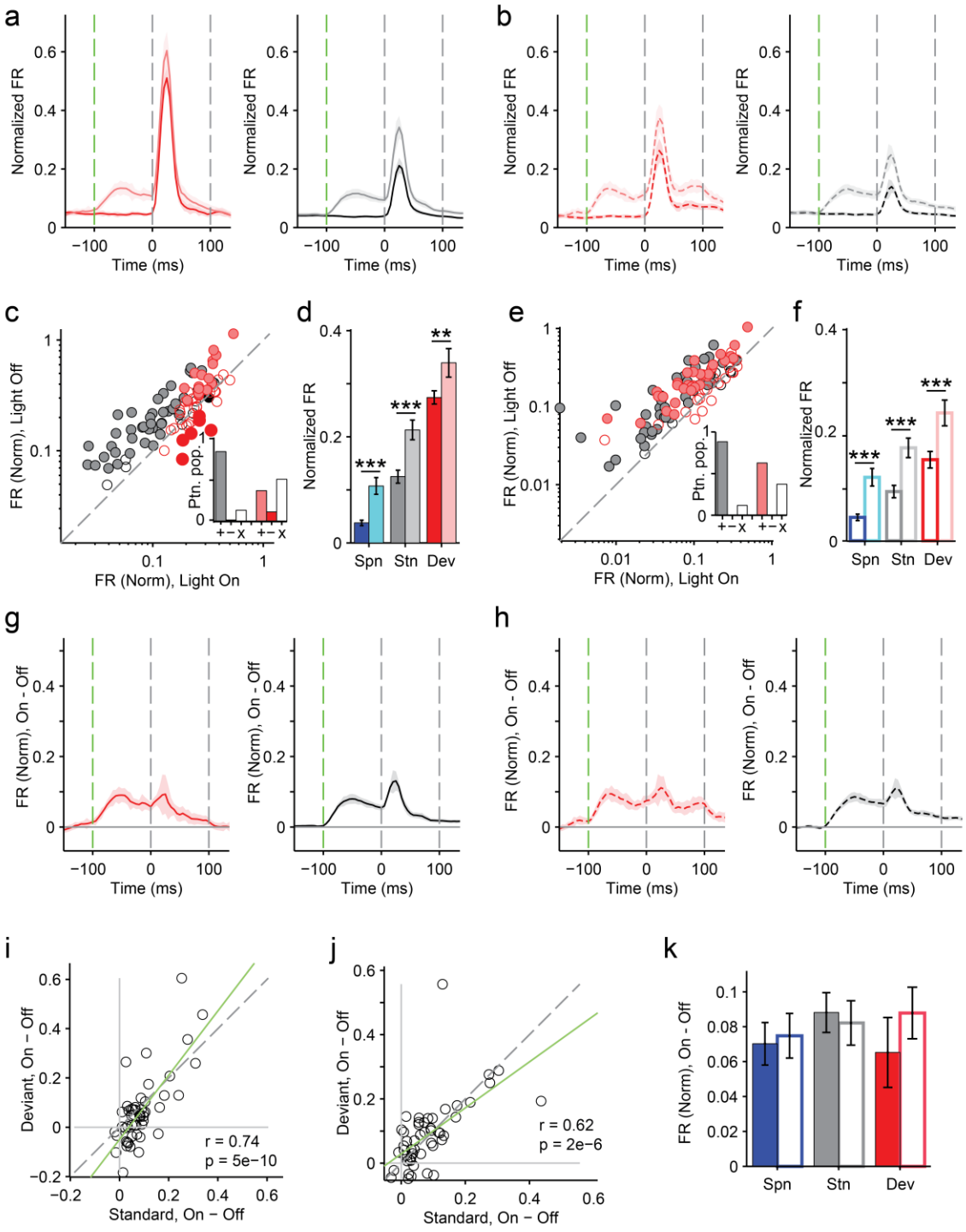

Figure 3.4—Figure supplement 5. Effects of PV suppression are identical for tones that evoke strong or weak responses in putative excitatory neurons. Each neuron's response to oddball tones A and B are pooled according to their response strength. The tone which evokes a higher peak FR as a deviant is pooled across neurons as the 'strong tone' response, while the tone which evoked a lower peak FR is pooled as the 'weak tone' response. (**a-j**) Data are presented as in Figure 3.4. Strong tone response data are

presented on the left (**a, c, d, g, i**) with solid lines and filled bars, and weak tone response data are presented on the right (**b, e, f, h, j**) with dashed lines and unfilled bars. All data are from PV-Cre mice. (**k**) Mean population FR difference between light-on and light-off conditions for deviant (red) and standard (gray) tones and spontaneous activity (blue) for strong (filled) and weak (unfilled) tones. Measured and normalized as in D and F. Photosuppression of PVs led to increased spontaneous FR (Spn) and standard (Stn) and deviant (Dev) tone-evoked FR for both strong (**d** – Spn: Δ = 187%, p2 = 4e-7, t(50) = -5.8. Stn: Δ = 71%, p2 = 3e-10, t(50) = -7.8. Dev: Δ = 24%, p2 = 0.002, t(50) = -3.3) and weak tones (**f** – Spn: Δ = 171%, p2 = 3e-7, t(50) = -5.9. Stn: Δ = 89%, p2 = 2e-8, t(50) = -6.5. Dev: Δ = 58%, p2 = 2e-7, t(50) = -6.0) (N = 51). There were no significant differences between strong and weak tones for the change in spontaneous FR and standard and deviant tone-evoked FR (**k**, Spn, Stn and Dev: $p > 0.05$, $t(50) < 2.0$).

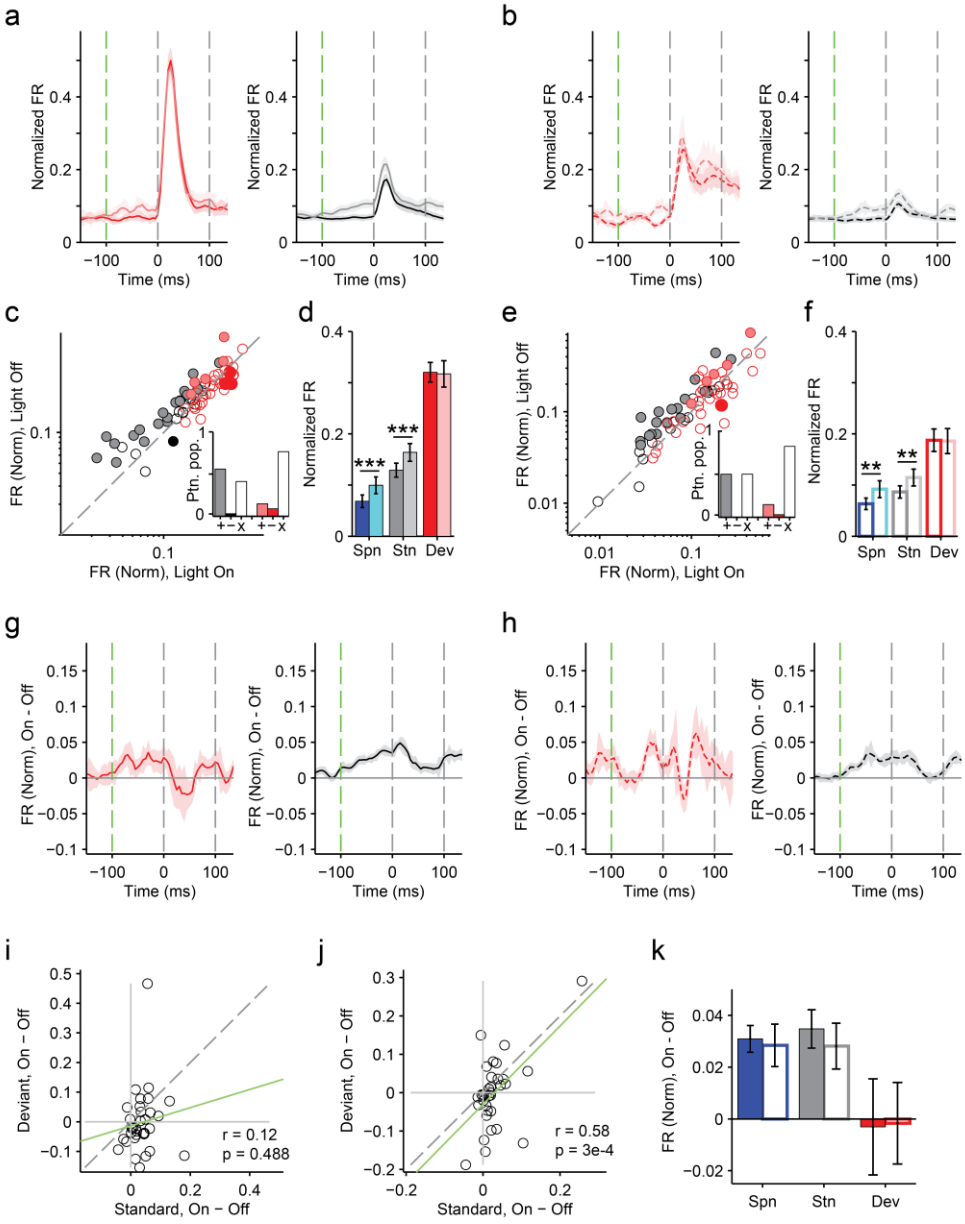

Figure 3.4—Figure supplement 6. Effects of SOM suppression are identical for tones that evoke strong or weak responses in putative excitatory neurons. (**a-k**) Data are presented as in Figure 3.4—Figure supplement 5. All data are from SOM-Cre mice. Photosuppression of SOMs lead to increased spontaneous FR and standard tone-evoked FR, and did not change deviant tone-evoked FR for both strong (**d** – Spn: Δ = 45%, p2 = 7e-7, t(33) = -6.1. Stn: Δ = 27%, p2 = 4e-5, t(33) = -4.7. Dev: p2 > 0.05, t(33) = -0.2) and weak tones (**f** – Spn: Δ = 45%, p2 = 0.001, t(33) = -3.5. Stn: Δ = 32%, p2 = 0.003, t(33) = -3.2. Dev: p2 > 0.05, t(33) = -0.1) (N = 34). There were no significant differences between strong and weak tones for the change in spontaneous FR and standard and deviant tone-evoked FR (Spn, Stn, and Dev: p > 0.05, 0.28 and 0.95, t(33) < 1.2).

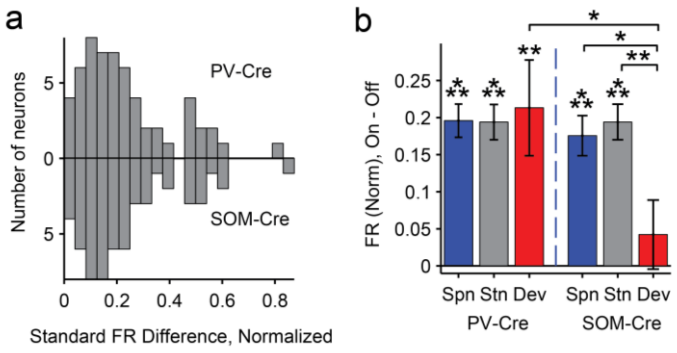

Figure 3.4—Figure supplement 7. Differences between PV and SOM effects on standard and deviant tones are preserved for subsets of neurons matched for strength of laser effects on standard tones. (**a**) Two subsets of tone responses (N = 66) matched across PV-Cre (above x-axis) and SOM-Cre (below x-axis) mice for standard tone-evoked FR difference between light-on and light-off conditions. (**b**) Difference between light-on and light-off FR for spontaneous FR (blue) and standard (gray) and deviant (red) tone-evoked FR and for the PV-Cre (left) and SOM-Cre (right) subsets. With PV photosuppression, spontaneous FR, standard and deviant tone-evoked FR increased (Spn: 20%, p2 =1e-12, t(65) = 8.8, Stn: 19%, p2 = 1e-11, t(65) = 8.2, Dev: 21%, p2 = 0.001, t(65) = 3.3), and there were no significant differences between spontaneous and tone-evoked FR changes (Spn v Stn: p2 > 0.05, t(65) = 0.1, C = 3, Spn v Dev: p2 > 0.05, t(65) = -0.3, C = 3, Stn v Dev: p2 > 0.05, t(65) = -0.3, C = 3). With SOM photosuppression, spontaneous FR and standard tone-evoked FR increased (Spn: 17%, p2 = 1e-8, t(56) = 6.6, Stn: 19%, p2 = 2e-11, t(65) = 8.1), while deviant tone-evoked FR did not change (p > 0.05, t(65) = 0.9). These changes were not significantly different between spontaneous FR and standard tone-evoked FR (Spn v Stn: p > 0.05, t(65) = -1.2), but both were greater than the change in deviant tone-evoked FR (Spn v Dev: 309%, p2 = 0.022, t(65) = 2.8, C = 3, Stn v Dev: 360%, p2 = 0.003, t(3.5), C = 3). By design, the change in standard tone-evoked FR was nearly identical between PV-Cre and SOM-Cre mice (p1 > 0.05, t(65) = -0.1, C = 3). Spontaneous FR was also similarly modulated by PV and SOM photosuppression (p1 > 0.05, t(65) = 0.8, C = 3). However, deviant tone-evoked FR was more strongly modulated by PV photosuppression than by SOM photosuppression (405%, p1 = 0.029, t(65) = 2.4, C = 3).

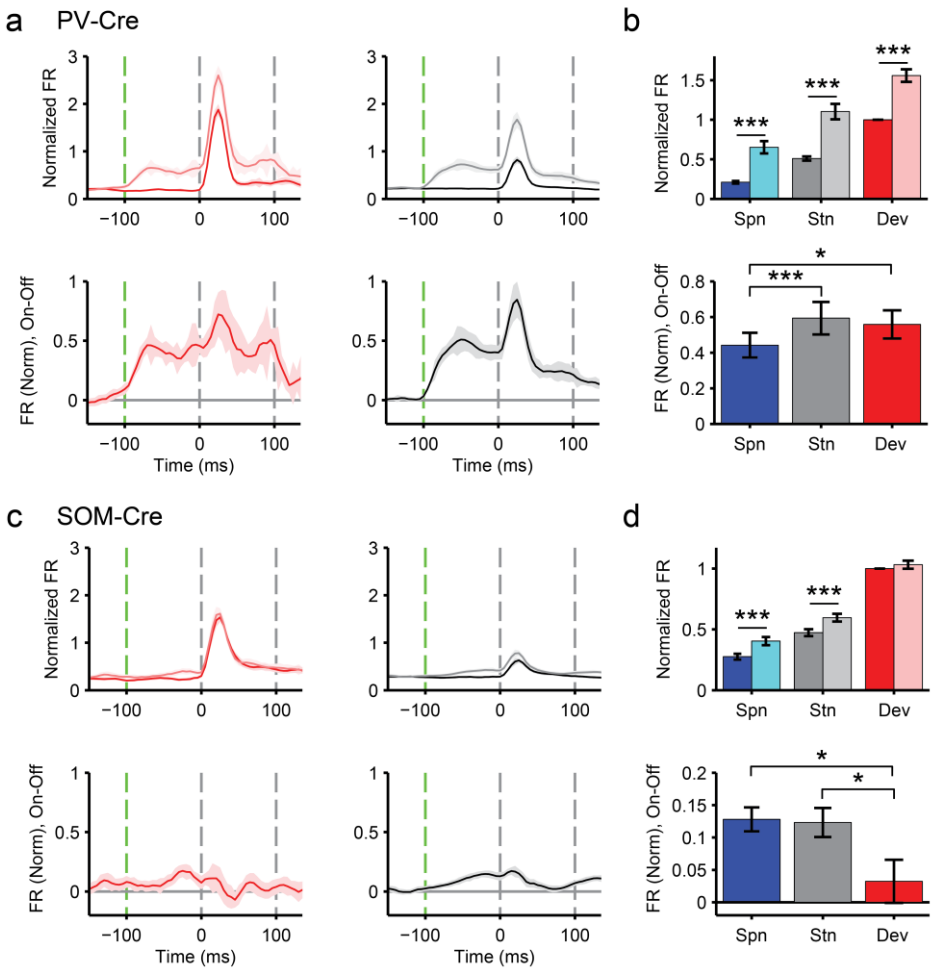

Figure 3.4—Figure supplement 8. Differences between PV and SOM effects on standard and deviant tone responses are preserved when FRs are normalized by the mean onset response. **a**, **b**, **c** and **d** as in Figure 3.4 **a**, **b**, **d** and **e**, respectively. (**a**, **b**) In PV-Cre mice, spontaneous FR and standard and deviant-tone evoked FR increased with light (**b** top – Spn: Δ = 210%, p2 = 2e-9, t(159) = -6.4. Stn: Δ = 116%, p2 = 9e-10, t(159) = -6.5. Dev: Δ = 56%, p2 = 5e-11, t(159) = -7.1). For FR changes between light-on and light-off conditions, there was no difference significant difference between standard and deviant-tone evoked FRs (**b**, bottom – Stn vs Dev: p2 >0.05, t(159) = 0.7, C = 2), but both were great than the difference in spontaneous FR (Spn vs Stn: Δ = 34%, p2 = 1e-4, t(159) = -4.1, C = 2. Spn vs Dev: Δ = 26%, p2 = 0.029, t(159) = -2.5). (**c**, **d**) In PV-Cre mice, spontaneous and standard-tone evoked FRs increased with light (**d** top – Spn: Δ = 46%, p2 = 2e-10, t(113) = -7.0. Stn: Δ = 26%, p2 = 2e-7, t(113) = -5.5), but deviant tone-evoked FRs did not (Dev: p2 > 0.05, t(113) = -1.0). For FR changes between light-on and light-off conditions, there was no difference between spontaneous and standard-tone evoked FR (**d**, bottom – Spn vs Stn: p2 > 0.05, t(113) = -0.3, C = 2), but both were significantly great than deviant-tone evoked FR differences (Spn vs Dev: Δ = 298%, p2 = 0.011, t(113) = 2.8 Stn vs Dev: Δ = 282%, p2 = 0.016, t(113) = 2.7, C = 2).

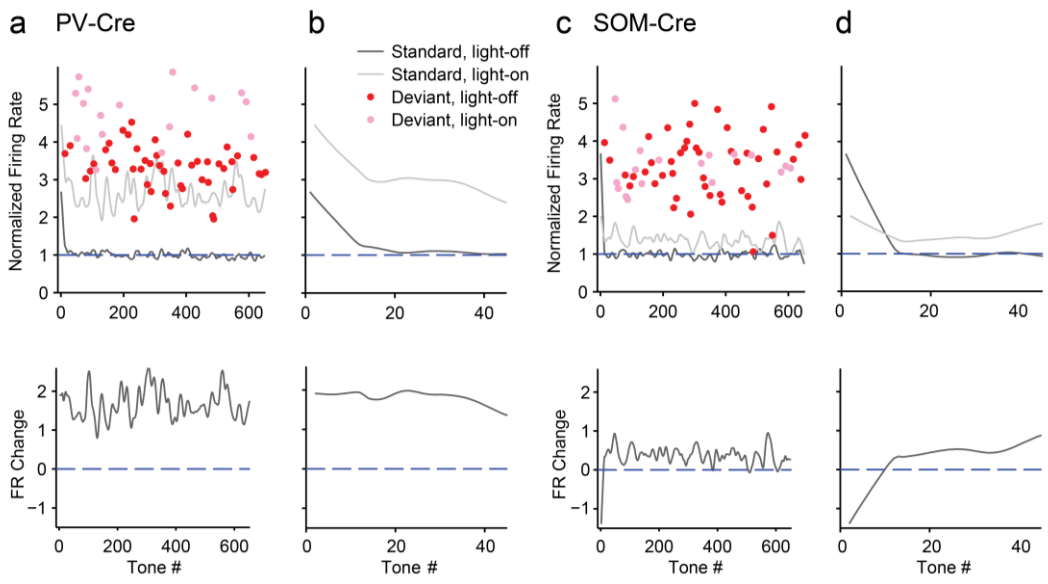

Figure 3.5—Figure supplement 1. Initial timecourse of interneuron-mediated effect on stimulus-specific adaptation. The inhibitory influence of PV+ interneurons is persistent while that of SOM+ interneurons builds up over the first 40 tones. (**a, b, c, d**) Top: Mean population FR in response to consecutive tones of the oddball sequence. Lines represent FR to standard tones on light-off (dark gray) and light-on (light gray) trials, interpolated to continuous lines. Dots represent FR to deviant tones on light-off (red) and light-on (pink) trials. Bottom: Difference between FR on light-on and light-off trials to standard tones of the oddball sequence. Left: Whole oddball sequence. Right: First 50 tones of each sequence. a, b: PV-Cre mice. c, d: SOM-Cre mice.

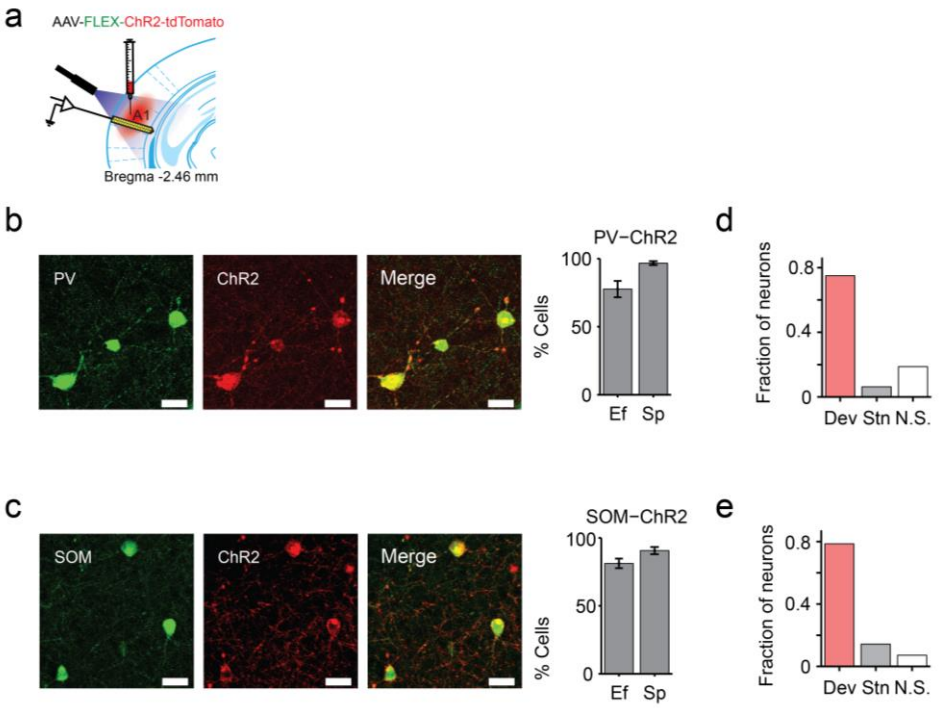

Figure 3.6—Figure supplement 1. Optical tagging of PVs and SOMs. (**a**) Diagram of optogenetic methods. A1 was injected with AAV-FLEX-ChR2-tdTomato. During experiments, an optic fiber was positioned to target A1 and neuronal activity was recorded using a multichannel silicon probe in A1. (**b, c**) Transfection of interneurons with ChR2. Images: Immunohistochemistry demonstrating co-expression of ChR2 and an interneuron-type reporter in A1. Bar Plots: Efficiency (Ef) and specificity (Sp) of visual transfection of PVs (top) and SOMs (bottom) with ChR2. Ef - Percent of labelled interneurons expressing ChR2. Sp -Percent of ChR2 expressing cells which are also labeled interneurons. (**b**) PV-Cre mouse A1. Green; anti-body stain for parvalbumin. Red; ChR2-tdTomato. Merge; co-expression of ChR2 and PVs. (**c**) SOM-Cre mouse A1. Green; anti-body stain for somatostatin. Red; ChR2-tdTomato. Merge; co-expression of ChR2 and SOMs. Scale Bar = 25 µm. (**d, e**) Fraction of PVs (**d**) or SOMs (**e**) exhibiting a greater response to deviants than standards (pink), the reverse (gray), or neither (white).

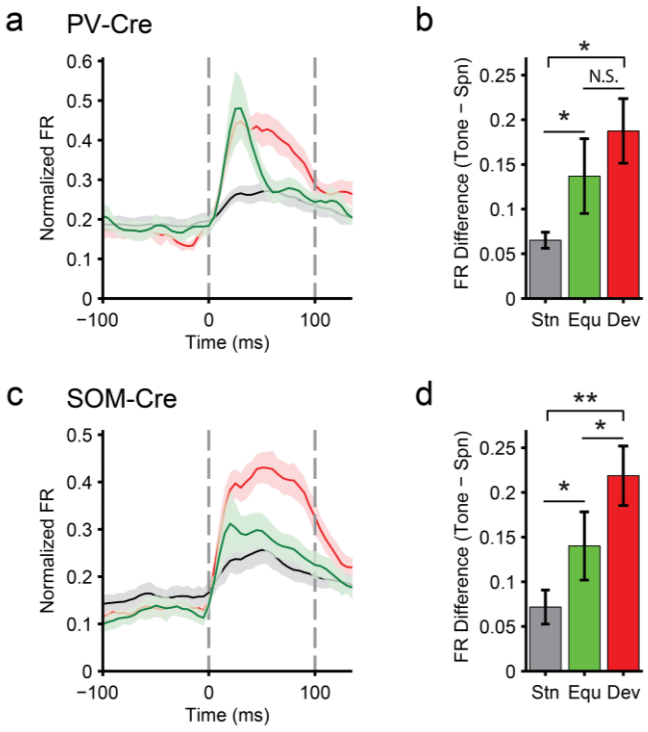

Figure 3.6—Figure supplement 2. PVs and SOMs have different adaptation profiles for equal probability tones. (**a, c**) PSTH of PVs (**a**) or SOMs (**c**) FR response to standard (black), equal probability (green) and deviant (red) tones. Normalization and dashed lines as in Figure 3.4a, b.(**b, d**) Mean PV (**b**) or SOM (**d**) population FR response to standard (gray), equal probability (green) or deviant (red) tones over 100ms tone duration. The mean spontaneous FR (during the 100ms prior to all tones) of oddball and equal probability stimuli was subtracted from respective tone-evoked mean FRs. In PVs, equal probability tones evoked FRs greater than standard tones (**b** – N = 16, Δ = 110%, p2 = 0.030, z = -2.4, C = 2), and not significantly different that deviant tones (p2 > 0.05, z = -1.7, C = 2). In SOMs, equal tones evoked higher FRs than standard tones (**c** – N = 28, Δ = 95%, p2 = 0.022, z = -2.6, C = 2), and lower FRs than deviant tones (Δ = -36%, p2 = 0.049, z = -2.3, C = 2). In both types of interneuron, deviant tones evoked higher FRs than standard tones (**b**, PV - Δ = 188%, p2 = 0.010, z = -2.8, C = 2. **c**, SOM – Δ = 205%, p2 = 0.002, z = -3.3, C = 2).

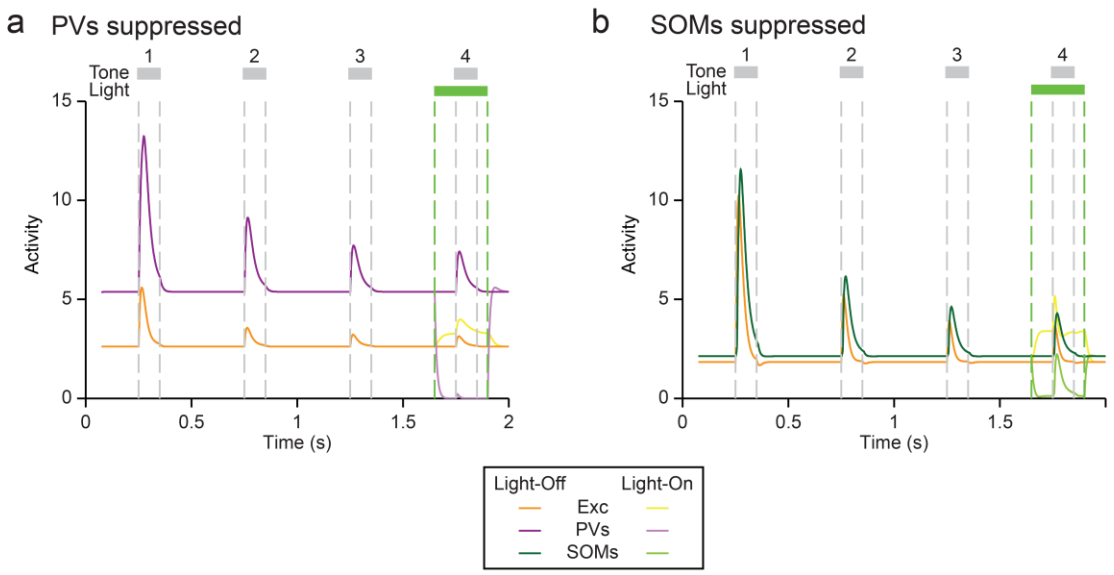

Figure 3.7—Figure supplement 1. Adaptation to repeated tones in model excitatory and inhibitory neurons. Responses evoked by four consecutive tones Exc (purple), PVs (orange, **a**) and SOMs (green, **b**). Note adaptation in the responses of both excitatory and inhibitory neurons. During 4th tone, there is light-evoked suppression of interneuron activity. Light-On: solid; Light-Off: dashed lines. (**a**) Light suppresses PVs. (**b**) Light suppresses SOMs.

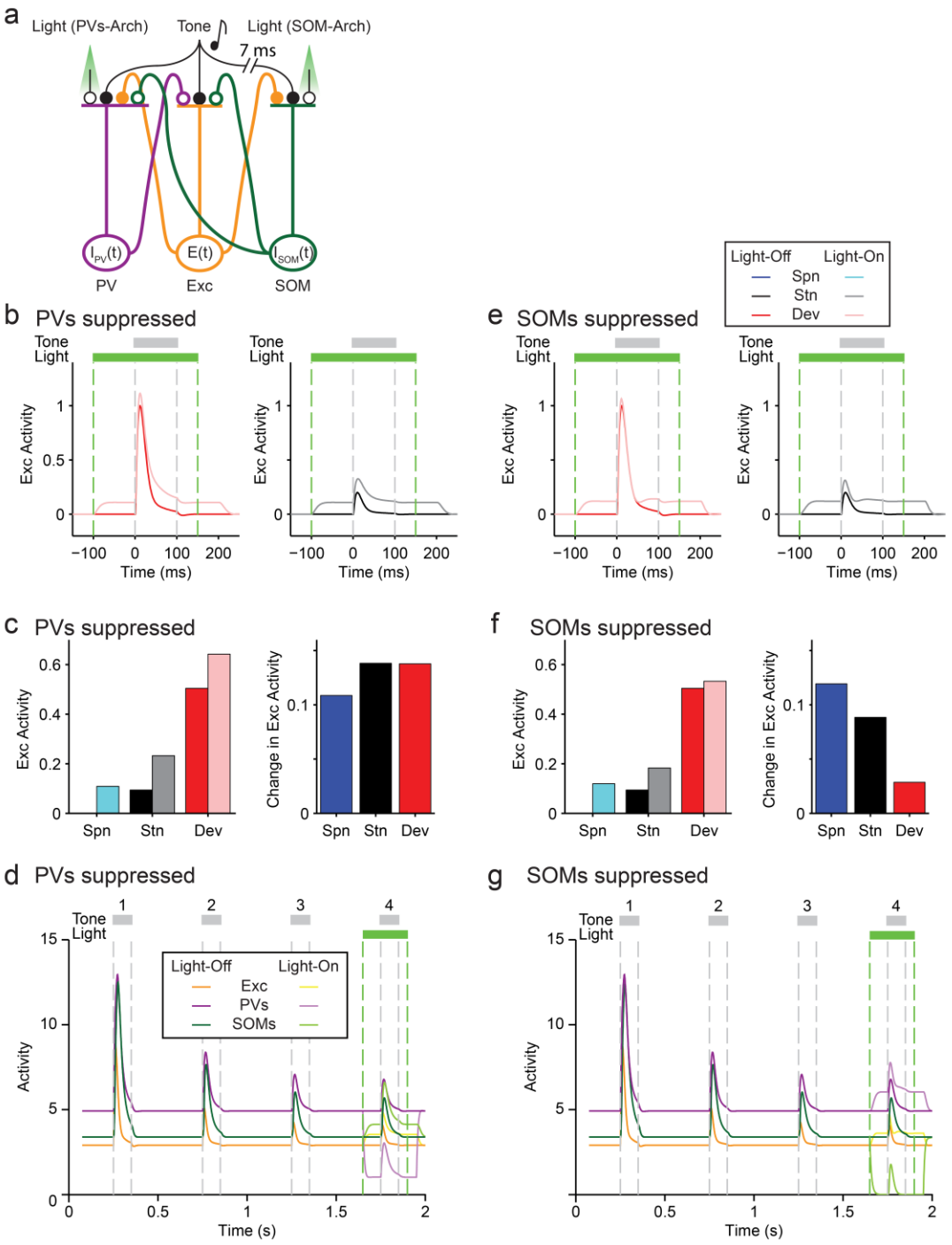

Figure 3.7—Figure supplement 2. Excitatory-inhibitory model with inhibitory inputs from SOM to PV population accounts for differential effects of PVs and SOMs on SSA in putative excitatory neurons. (**a**) Center: Diagram of coupled network model. Model is as in Figure 3.7, with additional inhibitory inputs from SOM to Exc population. (**b, e**) Tone-evoked responses of model neuronal excitatory population to deviant (red) and standard tones (gray), i.e. the first and fourth consecutive tone presented, under light-off

(dark colors) and light-on (light colors) conditions. Dashed lines indicate light onset and offset (green) and tone onset and offset (gray). (**b**) Light suppresses PVs. (**e**) Light suppresses SOMs. (**c, f**) Left: Spontaneous FR (blue) and standard (black) and deviant (red) tone-evoked FRs on light-off (dark colors) and light-on (light colors) conditions. Right: Mean difference between responses on light-on and light-off conditions. (**c**) Light suppresses PVs. (**f**) Light suppresses SOMs. (**d, g**) Responses evoked by four consecutive tones Exc (purple), PVs (orange) and SOMs (green). Note adaptation in the responses of both excitatory and inhibitory neurons. During the 4th tone, there is light-evoked suppression of interneuron activity. Dark traces: Light-off. Light traces: Light-on. (**d**) Light suppresses PVs. (**g**) Light suppresses SOMs.

4. Cortical interneurons control temporal adaptation.

Introduction

Adaptation is a ubiquitous property of cortical neurons, and is of fundamental importance for such diverse aspects of auditory processing as spectral and temporal information processing. There are different forms of adaptation: Adaptation to first order stimulus statistics such as temporal, frequency and amplitude modulation, spectral density, as well as adaptation to second order statistics and meta-adaptation. Adaptation is a crucially important function of neuronal networks. First, adaptation serves to maximize information transmission and increase computational efficiency with limited resources. Second adaptation sharpens sensitivity of neuronal responses to changes in the stimulus. Most stimuli encountered in the natural world should lead to some form of adaptation due to the temporally dynamic structure natural sounds (Wark et al., 2007). Thus, in order to understand how the brain encodes most sounds, it is crucial that we understand the mechanisms of adaptation.

Cortical inhibitory interneurons play a crucial role in information processing and shape how information is represented. There are multiple classes of interneurons, with parvalbumin-positive and somatostatin-positive interneurons being most prominent. Whereas in the visual cortex, evidence is accumulating for a divisive function of SOMs, and a subtractive function of either PVs or SOMs (Atallah et al., 2012; Lee et al., 2012;

Wilson et al., 2012), in the auditory cortex, mixed effects have been observed (Aizenberg et al., 2015; Phillips and Hasenstaub, 2016; Seybold et al., 2015). Surprisingly, very little is known about inhibitory neurons function in adaptation, especially considering how adaptation shapes responses to most stimuli. In the retina, which is one of the most extensively studied neuronal circuits, adaptation to the statistics of visual scenes has been linked to differential recruitment of specific inhibitory neuronal subtypes (Baccus and Meister, 2002). Also in visual cortex, responses to unexpected visual stimuli has been linked to SOM-mediated inhibition (Hamm and Yuste, 2016). As described in the previous chapter, we found that these PVs and SOMs contributed differentially to adaptation in the auditory cortex, which was consistent with the differences in their morphology (Natan et al., 2015). How cortical neurons contribute to adaptation is only beginning to be understood.

A particularly important aspect of adaptation is suppression of responses to repeated sounds. We recently investigated the role of inhibitory interneurons in cortical adaptation (Natan et al., 2015). By measuring the changes in stimulus-specific adaptation of putative excitatory neurons due to optogenetic selective suppression of either PVs or SOMs, we found that both interneurons contributed to adaptation. However, they exerted a differential effect: SOMs provided inhibition that increased with repeated tones, thus potentially directly contributing to adaptation. By contrast, PVs provided constant inhibition, which results in a relatively stronger suppression of the excitatory response in the adapted state. A limitation of the study was that the

function of the two types of interneurons was tested using a two-tone oddball stimulus, which was selected to span one quarter octave of the best frequency of the excitatory neuron, which did not allow us to map out the effects across the frequency tuning spectrum. Here, we investigated whether and how the adapting effects differed as a function of frequency preference for neurons.

To test the frequency distributed structure of inhibition of excitatory neuronal responses, we presented repeated tones to an awake, head-fixed mouse, and recorded neuronal activity, while optogenetically inactivating either PVs or SOMs on a subset of trials. We hypothesized that PVs would provide uniform suppression in both adapted and non-adapted states, whereas SOM suppression would be selective for the adapted state, and be greater for frequencies in the receptive field center (close to center frequency) and weaker for receptive field sidebands (Figure 4.1).

Results

Cortical neurons exhibit adaptation to the stimulus. To understand whether and how frequency tuning of a neuron influenced its adaptation to a repeated tone, we measured the frequency response function of the neuron, and presented repeated tones, chosen across the frequency response function (Figure 4.2A, B). Tones were repeated 8 times at 2.5 Hz, followed by 2.4 s of silence to allow adaptation to reverse.

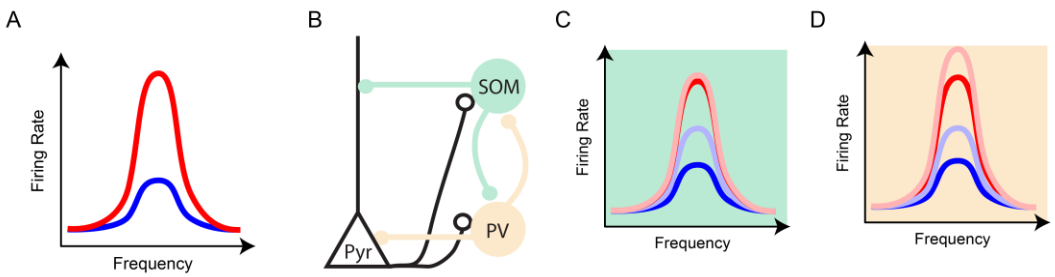

Figure 4.1. Predicted modulatory effects of adaptation and cortical inhibition across tuning. A) Model of an auditory cortex neuron tuning curve before adaptation (Red line) and predicted modulation after adaptation (Blue line). B) Cortical inhibitory circuitry. Excitatory-inhibitory circuits exhibit dense reverse connectivity. Somatostatin-positive interneurons (SOMs) form inhibitory synapses onto the distal dendrites of pyramidal neurons (Pyr) and onto parvalbumin-positive interneurons (PVs). PVs form inhibitory synapses onto proximal dendrites and somas of Pyrs and onto SOMs. Pyrs form excitatory synapses onto local SOMs and parvalbumin-positive PVs interneurons. C) Model of predicted modulatory effects of SOMs on Pyr tuning curve. Before adaptation, suppressing SOMs does not change responses across the tuning curve (pink line). After adaptation, suppressing SOMs increases responses across the tuning curve (light blue line). D) Model of predicted modulatory effects of PVs on Pyr tuning curve before and after adaptation. Before and after adaptation, suppressing PVs increases responses across the tuning curve.

Whereas cortical neurons adapt across a range of tone repeat rates (Ulanovsky et al., 2004), the relatively long (300 ms) inter-tone interval was chosen to incorporate the timecourse of optogenetic stimulation as well as enable comparison of results to prior studies (Natan et al., 2015). This time course furthermore targets long-term adaptation, which is likely affected by intra-cortical feedback mechanisms which take place over hundreds of milliseconds. Neurons responded to repeated tones with initially strong response, which gradually reduced over tone pip repeats (Figure 4.2C).

Optogenetic manipulation of PV and SOM activity. To better understand the function of inhibitory interneurons in cortical adaptation, we use viral transfection to drive selective expression of Archaerhodopsin in SOMs or PVs in the auditory cortex of SOM-

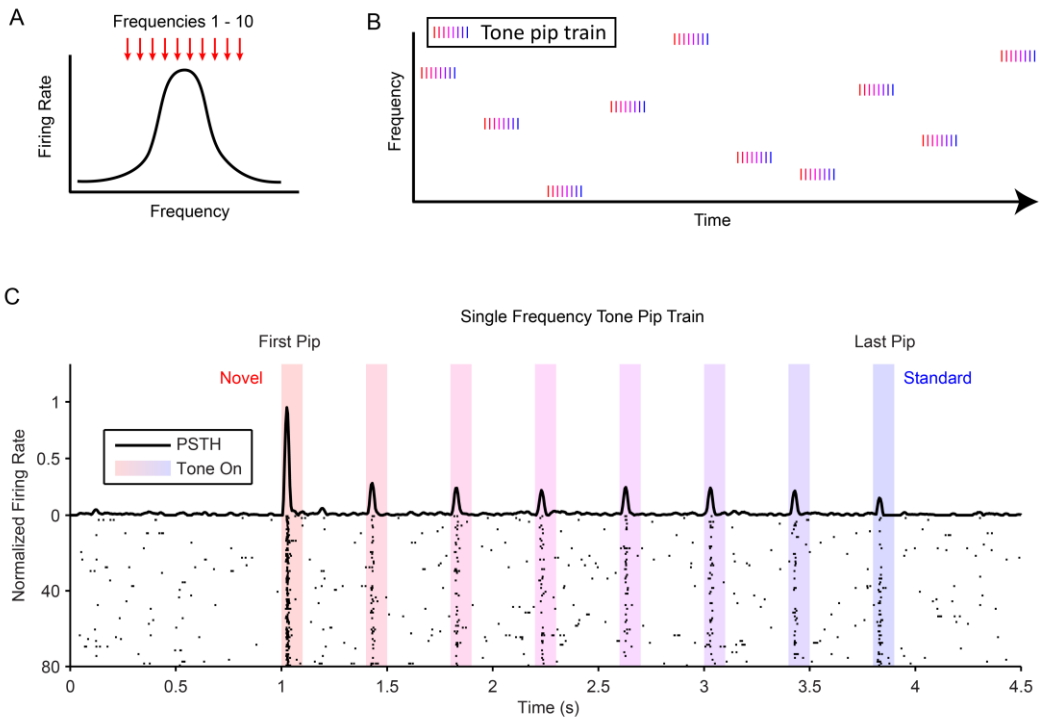

Figure 4.2. Tone pip train stimulus for testing adaptation across tuning. A) 10 evenly spaced frequencies (red arrows) spanning a portion of the neuron's tuning curve (black line) are selected to construct the tone train stimulus set. B) Each tone train is composed of 8 tone pips of a single frequency. Each train is separated by a 1.6 second inter-trial interval, and tone frequency is selected in pseudorandom counterbalanced sequence. Tone mark color (red to blue) illustrates the evolution of the train's selected frequency from novel (red) to standard (blue). C) Raster plot and PSTH depicting a single neuron's strongly adapting spiking responses to several repeats of a tone train of a single frequency. Shaded areas indicate tone pips, and color corresponds as in B. D) Overlay of tuning curves vs span of tone train frequencies

Cre or PV-Cre mice, respectively (Figure 4.3A, B). Viral expression was confirmed post-mortem via immunohistochemistry (Figure 4.3C) as previously published. Illuminating the auditory cortex increased neuronal activity in many recorded neurons, as expected for suppression of inhibitory activity in either SOM-Arch or PV-Arch mice (Figure 4.3D, E). In SOM-Cre mice, 42% if neurons exhibited increased, and 5% of neurons decreased

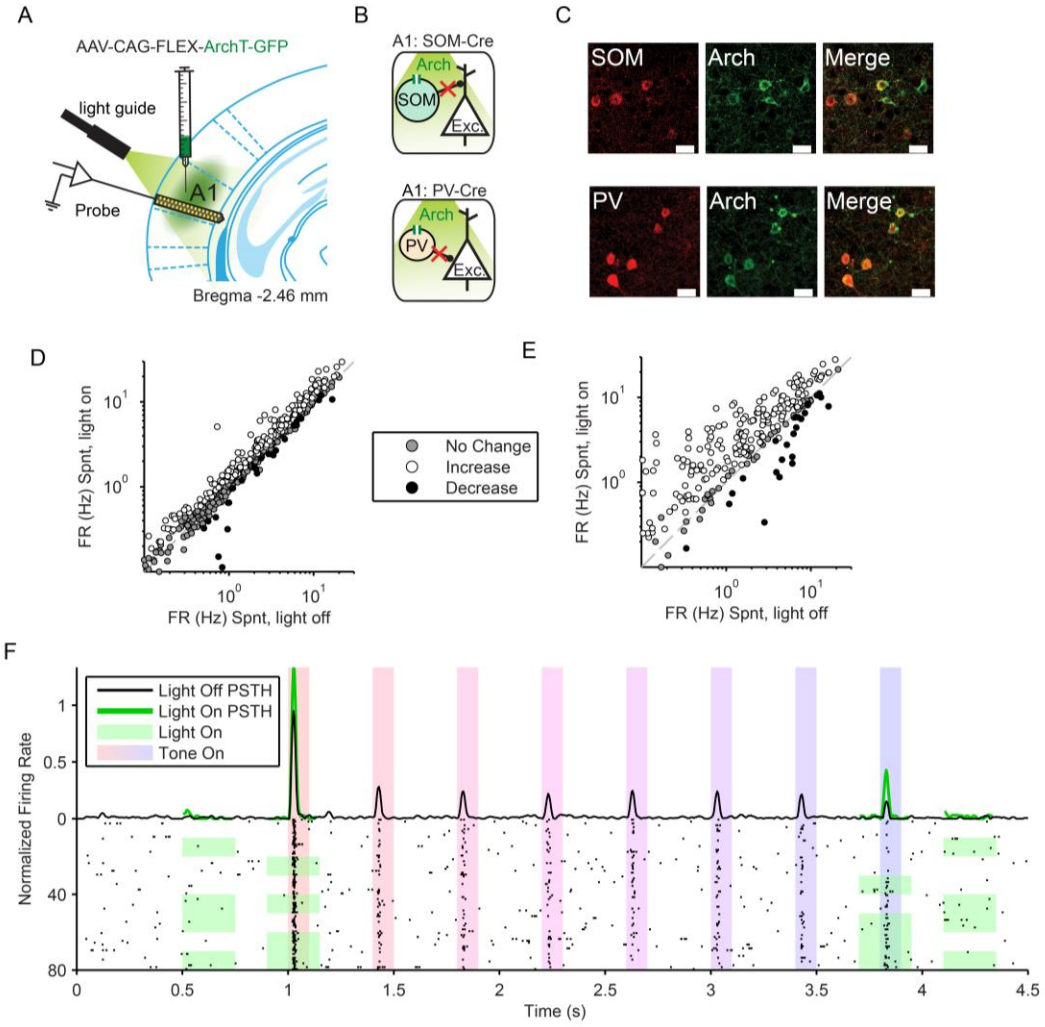

Figure 4.3. Optogenetic methods. A) Optogenetic methods diagram. A1 was injected with AAV-CAG-FLEX-ArchT-GFP. During experiments, an optic fiber was positioned to target A1 and neuronal activity was recorded using a multichannel silicon probe in A1. Bottom: Green light (532 nm) suppresses PVs in PV-Cre mice or SOMs in SOM-Cre mice. B) Green light (532 nm) suppresses SOMs in SOM-Cre mice (top) or PVs in PV-Cre mice (bottom). C) Transfection of interneurons with ArchT. Immunohistochemistry demonstrating co-expression of the Arch and an interneuron-type reporter in A1. Bottom: SOM-Cre mouse A1. Red: anti-body stain for somatostatin. Green: Arch-GFP. Merge; co-expression of ArchT and somatostatin. Top: PV-Cre mouse A1. Red: anti-body stain for parvalbumin. Green: Arch-GFP. Merge; co-expression of ArchT and parvalbumin. Scale Bar = 25 µm. D and E) Spontaneous firing rate with versus without optogenetic suppression of SOMs (D) or PVs (E). Each dot represents a single neuron and indicates that optogenetic suppression significantly increased (white), decreased (black) or had no effect on spontaneous firing. F) Raster plot and PSTH depicting of a single neuron's spiking responses with (green) and without optogenetic modulation (black). Green shading in raster plot indicates light pulse times and trials.

spontaneous activity, whereas 53% were not significantly affected by the optogenetic manipulation. In PV-Cre mice, 74% of neurons exhibited increased, and 9% of neurons decreased spontaneous activity, whereas 17% were not significantly affected by the optogenetic manipulation.

The laser was presented on half of the trials either during the first or last tones, and either preceding the first tone, or following the last tone in a block-randomized fashion (Figure 4.3F). Laser presentation affected neuronal responses. For a representative neuron, the spontaneous firing rate was only slightly increased (Figure 4.3F) either before or after the tone train, whereas the responses to the first and the last tone were significantly increased.

Temporal adaptation provides a divisive effect on neuronal responses across the tuning curve. To better understand the dynamics of adaptation, we examined the structure of adaptation for tones distributed across the frequency response function of each neuron (Figure 4.4). We measured the mean spiking response to the first and last tone pip at each of 10 frequencies (Figure 4.4A). We sorted the tone frequency for each unit from preferred to non-preferred frequency based on the mean firing rate, and compared the responses to tones at different frequencies before and after adaptation (for eighth versus first tone) in adapted neurons (Figure 4.4B). A representative neuron demonstrated divisive scaling of adaptive effects: a linear fit to the tone-evoked responses for eighth versus first tone provided a non-significant y-intercept, and a significant slope <1. We interpret these changes as a gain-like modulation in frequency

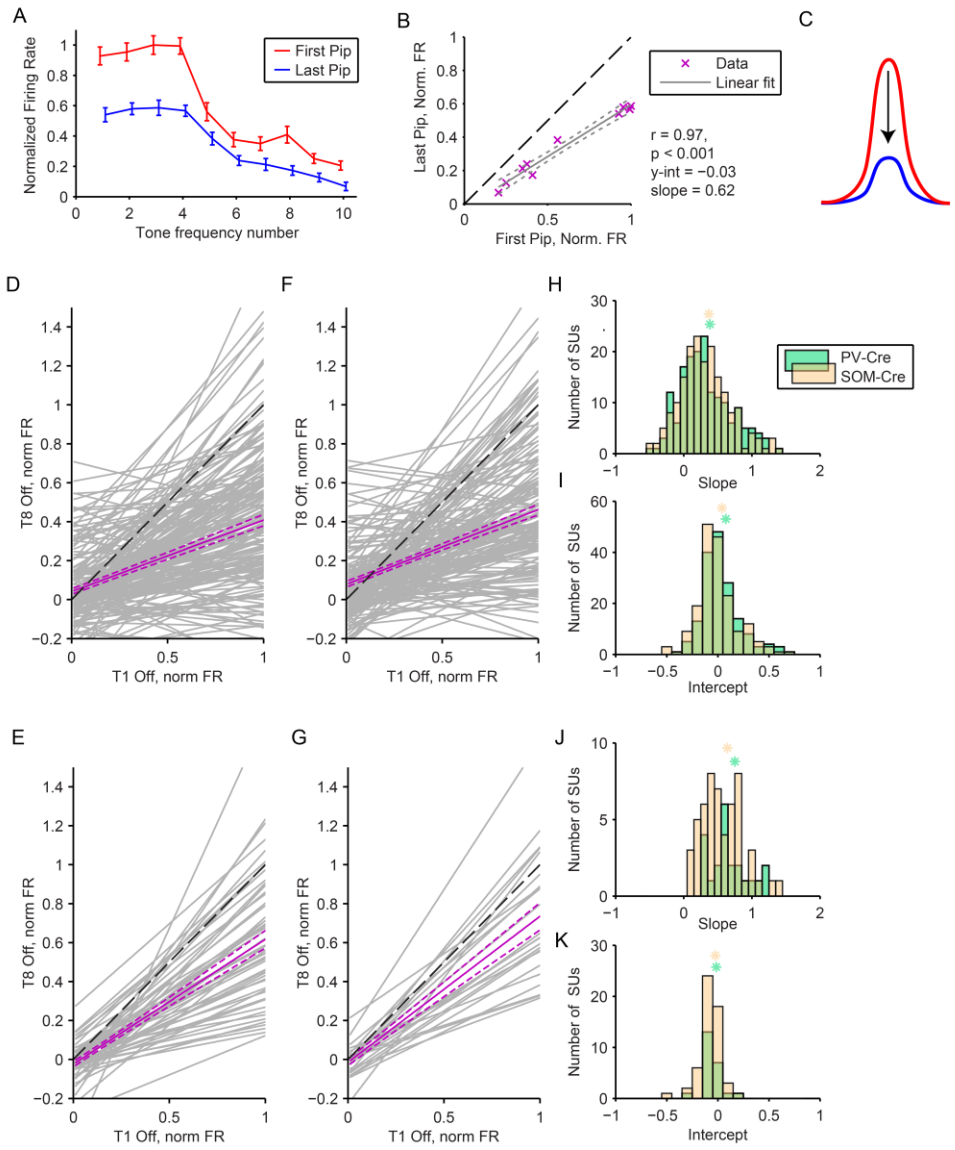

Figure 4.4. Adaptation scales responses across tuning curve. A) Single unit normalized mean firing rate in response to first (red) and last (blue) tone pip of each train across ten frequencies. B) Same single unit as is A, normalized mean firing rate response to the first versus last tone pip across each of ten frequencies (purple 'x's). Grey lines - linear fit (solid) and fit error (dashed). Dashed black line – unity line. C) Model of tuning before (red) and after (blue) adaptation depicting gain-like attenuation. D-G) Linear fits to first versus last pip normalized firing rate responses for each single unit (grey) and population average (purple). D and F) Population including all neurons recorded in SOM-Cre animals (D) and PV-Cre animals (F). E and G) Population including only neurons for which the slope of the linear fit is significant with and without optogenetic suppression, ensuring each neuron is frequency sensitive. SOM-Cre animals (E). PV-Cre animals (G). H-K) Slope (H and J) and intercept (I and K) of the linear fit for all neurons (H and I) and selected neurons (J and K). Asterisks – mean of each population. Green - SOM-Cre. Yellow - PV-Cre.

response scaling over the tuning curve (Figure 4.4C). Over all neurons that exhibited any optogenetic modulation during tone-evoked activity, in either SOM-Arch (n = 184) or PV-Arch (n = 169) groups, the average responses exhibited a divisive adaptation effect (slope < 1, and intercept not significantly different from 0) (Figure 4.4D, F). Over individual neurons, however, there was a mix of divisive and subtractive effects. Some units had a y-intercept significantly different than 0 pointing to a linear shift, and many units had either a positive or a negative slope, which was mostly less than 1 (Figure 4.4H, I), matching previously described heterogeneous effects of optogenetic modulation (Seybold et al., 2015; Phillips and Hasenstaub, 2016). There were no significant differences between the PV-Cre and SOM-Cre populations (slope – $p = 0.70$, intercept – $p = 0.07$).

Because we were interested in testing how adaptation and inhibition affects responses across tuning in further analysis, we selected a subpopulation of neurons that exhibited a significant frequency preference both for the first and last tone pip. Thus, inclusion in this subpopulation required that the linear fit to the set of first vs last tone pip responses was significant. For this subset of neurons in both SOM-Cre (n = 55) and PV-Cre (n = 23) mice, the slope was positive, with no significant shift in the intercept whereas the offset was not significant different from 0, further supporting a divisive adaptation model (Figure 4.4E, G, J, K). There were no significant differences between the PV-Cre and SOM-Cre populations (slope – $p = 0.211$, intercept – $p = 0.71$).

The effects of PV and SOM suppression differ in the adapted and non-adapted regimes. The effects of suppressing SOM and PV activity differed across the population of tuned neurons selected as above (Figure 4.5). SOM-Cre and PV-Cre population mean neuronal response to tone trains exhibit adaptation (Figure 4.5A, B), responding to first tone pips more strongly than to last tone pips. Typically, population neuronal firing rates were disinhibited when either PVs or SOMs were suppressed with light before or after the tone train.

As a population, suppressing SOM neurons had no overall effect on responses to the first tone pip ($p > 0.05$) and significantly disinhibited response to the last tone ($p = 0.001$). SOM inhibition significantly increased from the first to last tone pip ($p = 0.007$) (Figure 4.5 C, D). The time course of the difference in the tone-evoked responses on light-on and light-off conditions differed significantly between responses to the first and last tone pips (Figure 4.5 C), further illustrating that adaptation shifted the effect of SOM inhibition toward disinhibition of excitatory neurons. These findings suggest the SOMs provide tone-evoked inhibition, which increases in the adapted regime.

By contrast, whereas suppressing PVs drove a significant increase in the spontaneous activity, PV suppression resulted in no significant change in the tone-evoked response over the neuronal population for either the first ($p = 0.70$) or last tones ($p = 0.70$) (Figure 4.5E, F). PVs drove a similar amount of suppression and activation, resulting in a non-significant difference in effect across the population and no significant difference between the adapted and non-adapted responses ($p = 0.14$). These results

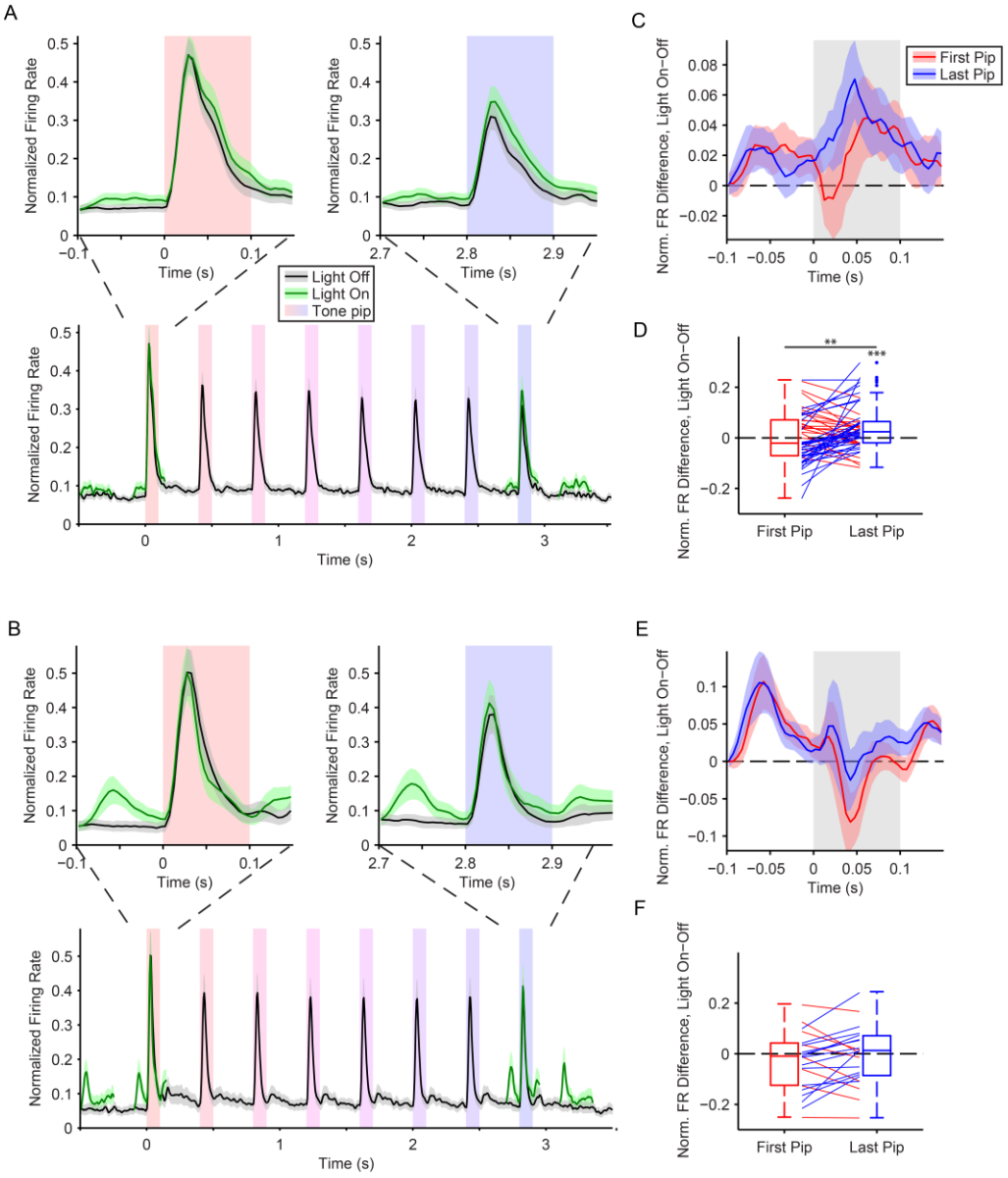

Figure 4.5. SOM inhibition increases with stimulus repetition. A and B) Selected neuron population average firing rate in response to tone trains with (green) and without (black) optogenetic suppression of SOMs (A) and PVs (B). Top: PSTH during first (left) and last (right) pip. Bottom: PSTH over whole tone train. C and E) Overlay of PSTHs of the mean of the per-neuron difference in firing rate between trials with and without optogenetic suppression of SOMs (C) and PVs (E) for the first (red) and last (blue) pip.

D and F) Summary of per-neuron differences in firing rate between trials with and without optogenetic suppression in the first and last tone onset response (0-50ms from tone onset) for SOMs (D) and PVs (F). Line color indicates that the effect of suppression increased (blue) or decreased (red) from the first to last pip.

suggest that PVs provide as much excitation and inhibition to the excitatory neurons in either adapted or non-adapted regime.

SOM inhibition contributes to multiplicative scaling after adaptation. We next tested whether the effects of PVs or SOMs differed for tones in the center and on the sidebands of the frequency tuning curve of excitatory neurons (Figure 4.6). We compared the response change due to PV or SOM suppression on excitatory responses to tones across the entire tuning curve, for either the first (Figure 4.6A, C) or last tone (Figure 4.6B, D). Suppressing SOMs slightly disinhibited responses to the first tone only for non-preferred frequencies. By contrast, in the adapted regime, suppressing SOMs preferentially disinhibited responses to tones at preferred frequencies. Indeed, there was a significant positive shift in the firing rate for preferred frequencies in the suppression-versus-tone frequency curve (slope > 1, $p = 0.031$) and no change in the intercept ($p = 0.16$), suggesting that SOMs increasingly contributed to adaptation of responses across frequency tuning in a gain like manner (Figure 4.6E, F).

By contrast, suppressing PVs had a stronger disinhibitory effect on neuronal responses at non-preferred tone frequencies than at preferred frequencies during both the first and last tone pips. Over the population, neither the slope ($p = 0.10$) or intercept ($p = 0.89$) significantly changed from the first to last tone (Figure 4.6G, H). This suggests

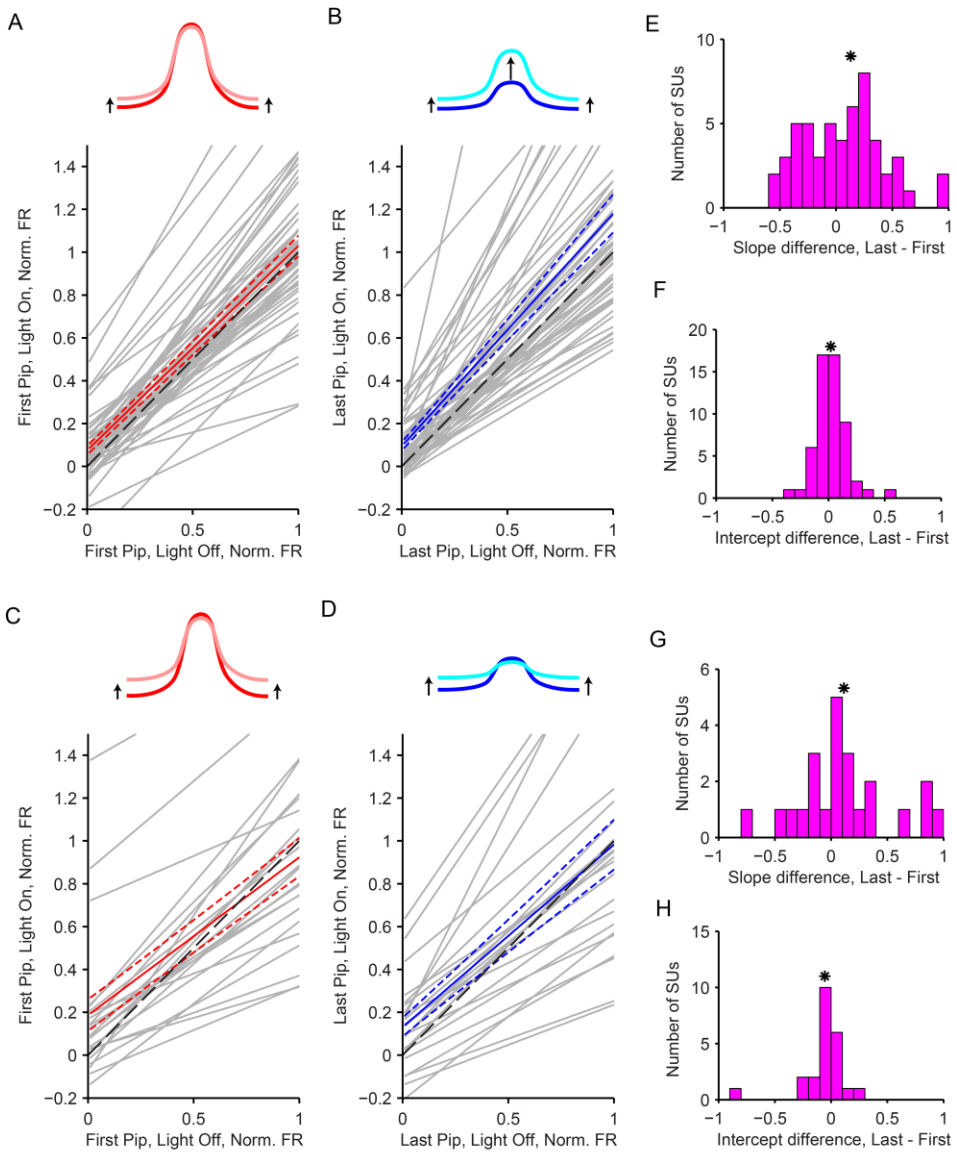

Figure 4.6. SOM inhibition contributes to scaling after adaptation. A-D) Top: Model depiction of tuning curve in response to the first (red) and last (blue) tone pip with (light) and without (dark) optogenetic suppression of SOMs (A and B) or PVs (C and D). Arrows emphasize regions of significant modulation. Bottom: Linear fits to the first (A and C) or last (B and D) tone pip firing rate responses in selected neurons, with versus without optogenetic suppression of SOMs (A and B) or PVs (C and D) for each neuron (grey) and population average (red or blue). E-H) Slope (E and G) and intercept (F and H) of the linear fit for selected neurons in SOM-Cre animals (E and F) or PV-Cre animals (G and H), respectively. Red - first pip. Blue - last pip. Asterisks – mean value.

that suppressing PVs preferentially disinhibited neuronal responses in the side-bands of frequency curves, and was insensitive to tone repetition.

Effects of SOMs, but not PVs, on excitatory neuronal activity become stronger with adaptation. To examine how the effects of optogenetic manipulation of PV or SOM activity changed with adaptation for individual neurons, we compared the change in the tone-evoked responses of excitatory neurons for the first and last tone for the adapting and non-adapting neurons separately (Figure 4.7, 8). In this analysis, each neuron-frequency pair was considered as separate samples. For the adapting response population, neuron-frequency pairs for which the first tone pip evoked significantly stronger spiking than the last pip were included (Figure 4.7 and 8 A-H). For the non-adapting response population, only neuron-frequency pairs from neurons in which the first and last tone pip-evoked spiking was not significantly different at any frequency were included (Figure 4.7 and 8 I-P).

SOM inhibition affected first and last tone pip-evoked responses differentially between adaptive and non-adaptive responses. Among adapting responses, SOM suppression led to heterogeneous first tone pip-evoked modulation; 30% increased and 34% decreased (Figure 4.7C). By contrast, more last tone pip-evoked responses increased (54%) and few decreased (2%) (Figure 4.7D). On average, SOM suppression leads to significant inhibition of first tone pip-evoked responses ($p = 0.027$) and significant disinhibition of last tone pip-evoked responses ($p < 0.001$), showing that the strength of SOM inhibition increased from the first to the last tone pip ($p < 0.001$)

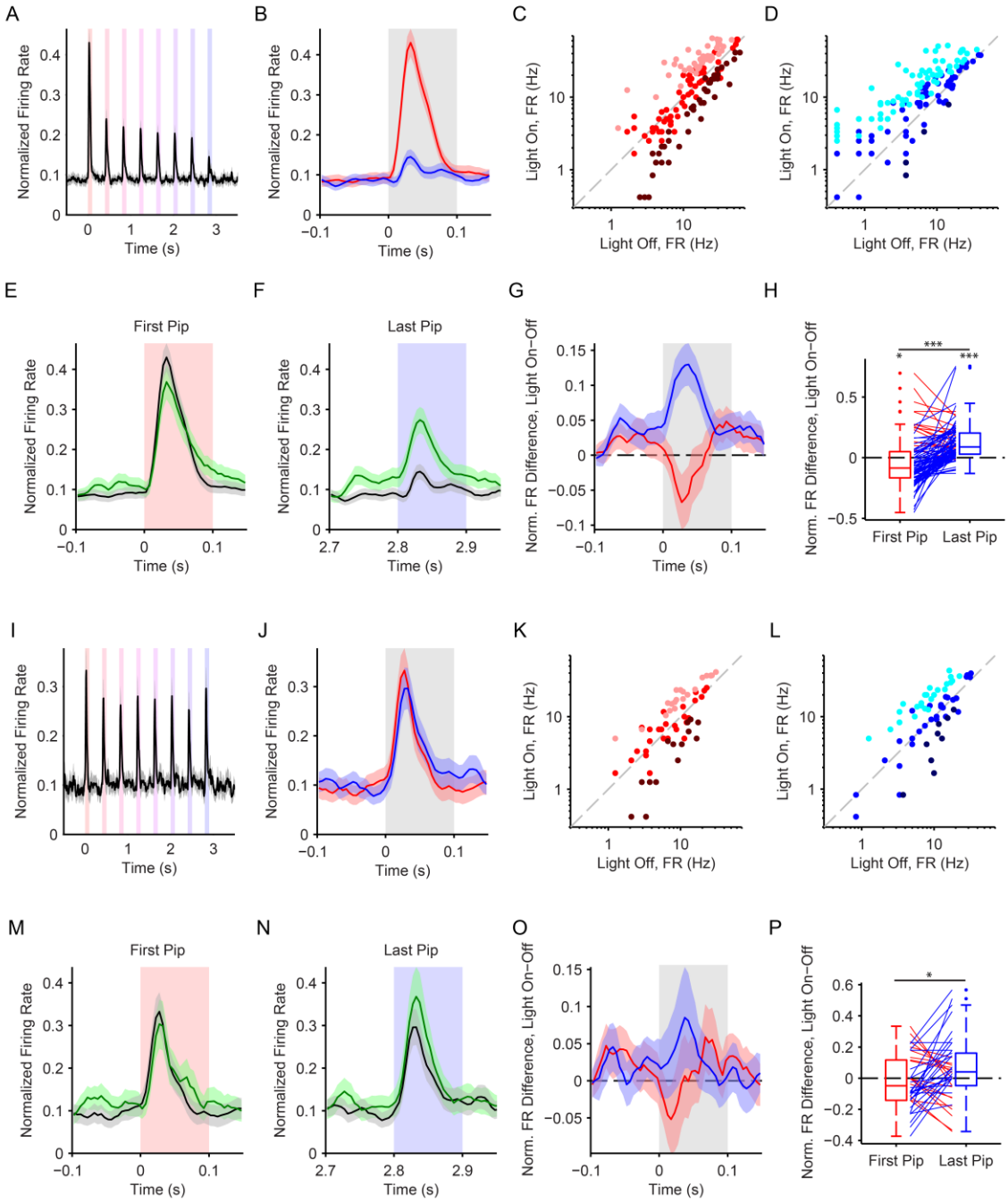

Figure 4.7. Effects of optogenetic modulation of SOMs on adaptive and non-adaptive neurons. A-H) Adaptive neuronal responses. I-P) Non-adaptive neuronal responses. A and I) Population average PSTH of normalized firing responses to tone train. B and J) Overlay of the population average PSTHs of normalized firing rate in response to the first (red) and last (blue) tone pip. C, D, K and L) Firing rate in response to the first (C and K) and last (D and L) tone pip with versus without optogenetic suppression. A Each dot represents a neuron-frequency pair, and it's shading indicates that the firing rate significantly increased (light), decreased (dark), or did not change (medium) for optogenetically suppressed trials. Dashed line - unity line. E, F, M and N) Population average firing rate

in response to the first (E and M) and last (F and N) tone pip with (green) and without (black) optogenetic suppression of interneurons. G and O) Overlay PSTHs of the mean of the per-neuron difference in firing rate between trials with and without optogenetic suppression interneurons for the first (red) and last (blue) pip. H and P) Summary of the per-neuron difference in firing rate between trials with and without optogenetic suppression of interneurons in the first and last tone onset response (0-50ms from tone onset). Line color indicates that the effect of suppression increased (blue) or decreased (red) from the first to last pip.

(Figure 4.7E-H). Similar to adapting responses, non-adapting responses were heterogeneously modulated by SOM suppression during the first tone pip (31% increased, 28% decreased) (Figure 4.7K). Unlike adapting responses, non-adapting responses continued to respond heterogeneously during the last tone pip (38% increased, 17% decreased) (Figure 4.7L). On average, SOM suppression of non-adapting response lead no significant change of first ($p = 0.37$) or last tone pip-evoked responses ($p = 0.06$), but the strength of SOM inhibition increased from the first to the last tone pip ($p < 0.027$) (Figure 4.7I-P).

Similar to SOMs, PV inhibition affected first and last tone pip-evoked responses differentially between adaptive and non-adaptive responses. However, the net effects of PV suppression were weaker than those of SOM suppression. Among adapting responses, PV suppression led to heterogeneous first tone pip-evoked modulation (27% increased and 28% decreased) (Figure 4.8C). For the last tone pip, many responses increased (66%) and a smaller portion decreased (8%) (Figure 4.7D). On average, PV suppression lead to significant disinhibition of both first ($p = 0.045$) and last tone pip-evoked responses ($p < 0.001$), showing that the strength of PV inhibition increased from the first to the last tone pip ($p < 0.001$) (Figure 4.7E-H). Non-adapting responses were heterogeneously modulated by PV suppression during the first tone pip (31% increased,

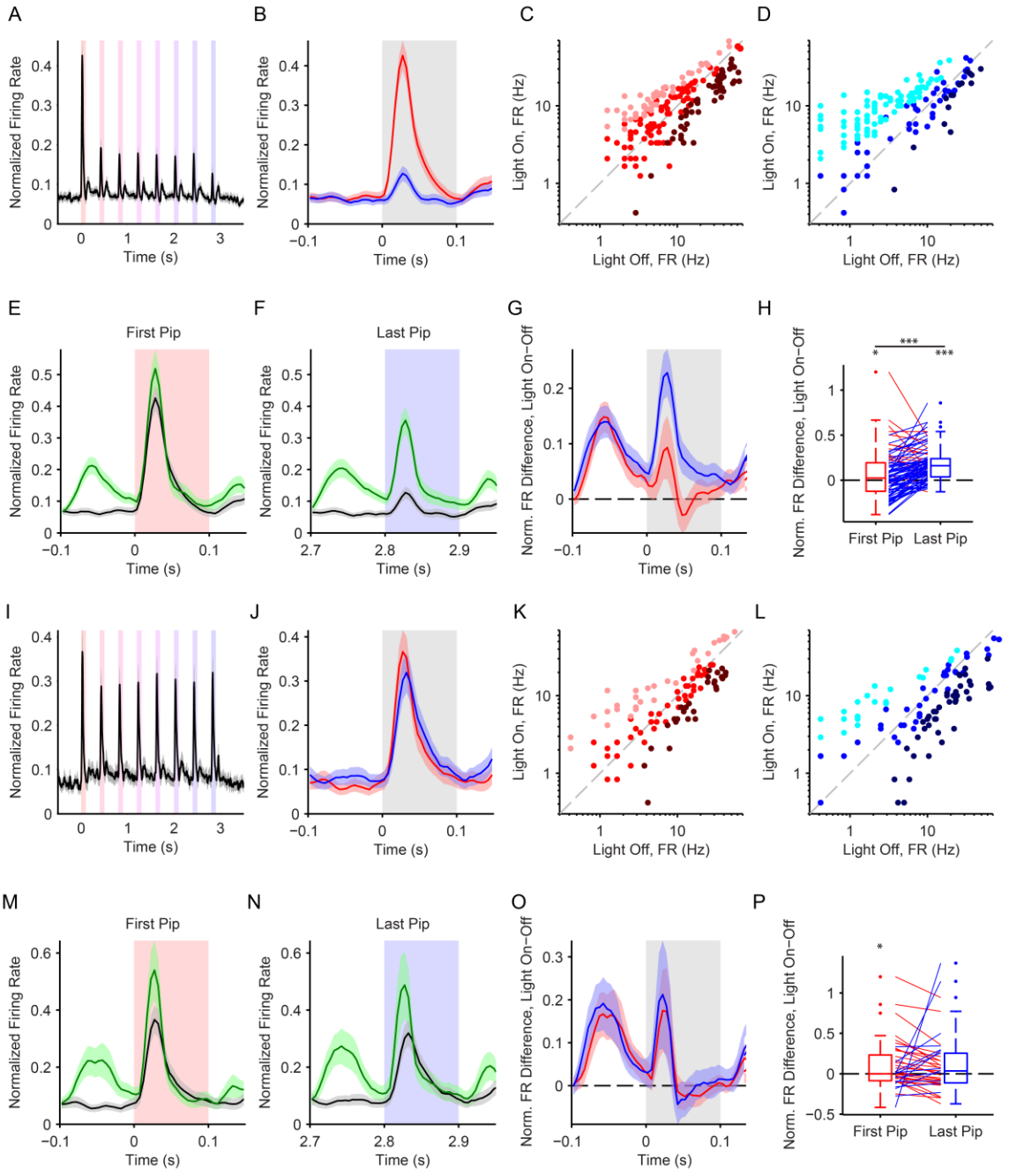

Figure 4.8. Effects of optogenetic modulation of PVs on adaptive and non-adaptive neurons. All panels as in Figure 4.7.

29% decreased) (Figure 4.7K), and inhibited more responses during the last tone pip (24% increased, 43% decreased) (Figure 4.7L). On average, PV suppression lead to significant disinhibition of first tone pip-evoked responses (p = 0.043) and no significant

modulation of last tone pip-evoked responses ($p < 0.051$). The strength of PV inhibition did not change significantly from the first to last tone pip ($p < 0.78$) (Figure 4.7I-P).

Inhibition due to SOMs and excitation due to PVs of excitatory neuronal activity predict neuronal adaptability. If inhibitory neurons contribute to adaptation, we expect that the degree of adaptation would correlate with the magnitude of response modulation due to interneuron suppression. The effect of SOM suppression between the first and last tone was weakly correlated for adapting responses ($r = 0.17$, $p = 0.036$), and not correlated for non-adapting neurons ($p = 0.91$) (Figure 4.9A, C). By contrast, the effect of PV suppression between the first and last tone was strongly correlated for both adapting responses ($r = 0.55$, $p < 0.001$) and non-adapting responses ($r = 0.55$, $p < 0.001$) (Figure 4.9B, D). These correlations demonstrate that the magnitude of SOM inhibition changes, in unpredictable directions, over the course repeated stimulation, especially for non-adaptive responses. PV inhibition, on the other hand, is largely insensitive to stimulus repetition or adaptation level, and continues to modulate tone pip responses in a similar way, regardless of stimulus repetition. Among adaptive responses, PV and SOM inhibition generally increased from the first to the last tone pip ($p < 0.001$). Among non-adaptive responses, SOM inhibition from the first to last tone pip increased modestly ($p = 0.030$), and PV inhibition was not changed ($p = 0.28$).

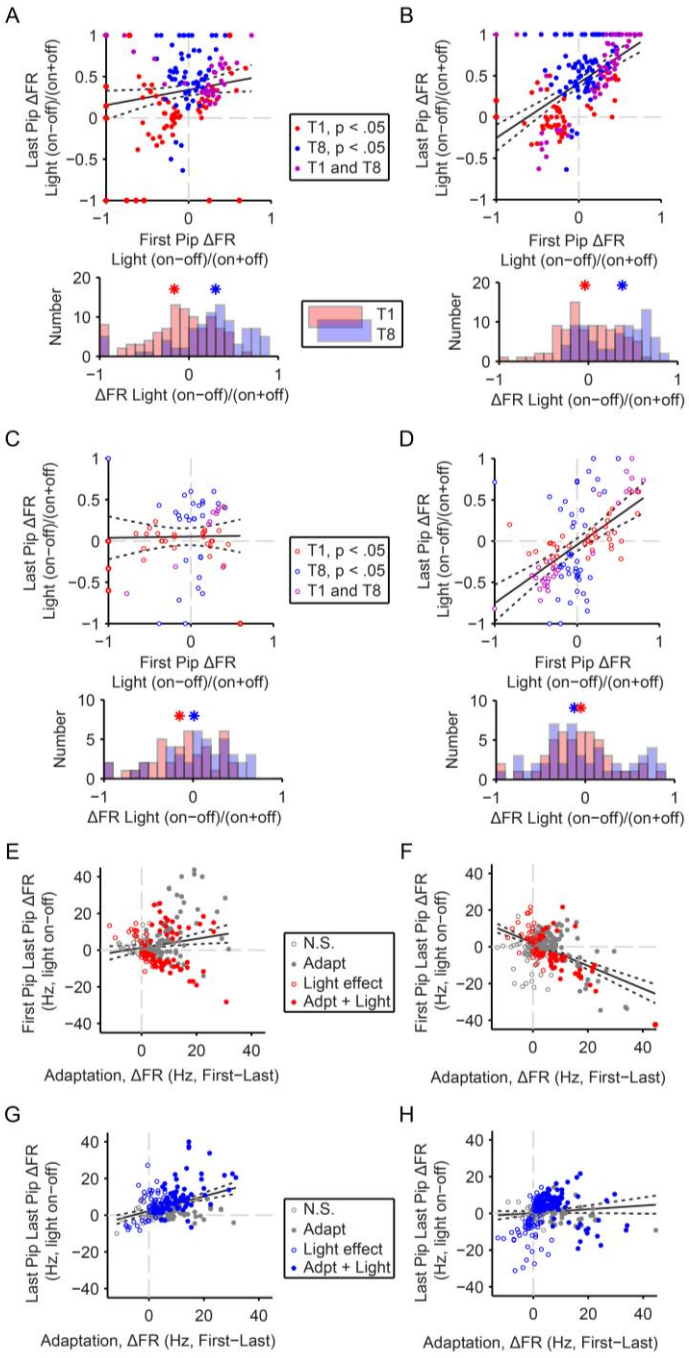

Figure 4.9. Strength of SOM inhibition correlates with magnitude of adaptation. A-D) Effect of SOM (A and C) or PV (B and D) optogenetic suppression on firing rates for adaptive (A and D) or non-adaptive (B and D) neurons in response to the first versus last tone pip. Optogenetic effects are measured as the index of change between the means between trials with and without optogenetic suppression. Top: Each dot represents a neuron-frequency pair, and its color indicates the ontogenetic suppression significantly modulated the responses to the first (red), last (blue) or both (purple) tone pips. Bottom: Overlay of the same values as above.

Asterisks – population mean. E-H) Effect of SOM (E and F) or PV (G and H) optogenetic suppression on firing rates for all neurons in response to the first (E and G) or last (F and H) tone pip versus the magnitude of firing rate adaptation. Optogenetic effects are measured as in A-D. Magnitude of adaptation is measured as the difference between firing rate in response to the first versus last tone. Each dot represents a neuron-frequency pair. Dot color indicates that optogenetic suppression significantly modulated (red or blue) or did not modulate (grey) the responses to the tone pips, and filled dots indicate significant adaption.

Does the effect of SOM or PV suppression predict the strength of adaptation? Indeed, we found that the magnitude of adaptation was correlated with the strength of SOM inhibition for the first tone ($r = 0.17$, $p = 0.011$), but especially strongly for the last tone ($r = 0.39$, $p < 0.001$) (Figure 4.9E, G). By contrast, the magnitude of adaptation was anticorrelated with the strength of PV inhibition for the first tone ($r = 0.49$, $p < 0.001$) and not correlated with for the last tone ($p = 0.11$) (Figure 4.9F, H). Together, these correlations show that neurons that experience stronger SOM influence are more likely to adapt strongly, while the opposite may be true for the effect of PV modulation.

Discussion

Our study dissected the complex roles of cortical inhibitory interneurons in adaptation to repeated stimuli, finding that SOMs and PVs exerted mixed effects on excitatory neuronal responses with some generalized properties. First, we found that within many individual neurons and across the population, adaptation to repeated tones of the same frequency induced firing rate attenuation that approximately scaled responses across the frequency tuning curve. Among well-tuned neurons, we partially attribute adaptive gain-like response suppression to an increase in SOM-mediated

inhibition that was selective for the preferred frequency tones. These results are interesting in light of recent work testing how interneurons modulate frequency tuning curves of neurons in the primary auditory cortex; both PVs and SOMs can induce divisive, multiplicative or mixed modulation (Phillips and Hasenstaub, 2016; Seybold et al., 2015). These findings are surprising considering the vastly different physiology and connectivity of PVs and SOMs. Our findings show that the effects of PV and SOM inhibition diverge sharply depending on stimulus context. Perhaps recent sensory experience drives circuit dynamics toward regimes in which PV and SOM modulation begin to play distinct roles and drive more uniform modulations. Testing SOM and PV modulations under various complex stimulus conditions may reveal a pattern to disparities between PV and SOM modulation, and help define these interneurons disparate roles in sensory processing.

Across the pyramidal neuron population, suppressing either SOMs or PVs led to bidirectional modulatory effects. Multiple local inhibitory circuit pathways, such as direct monosynaptic inhibition or sign-reversing disynaptic disinhibition, may differentially influence pyramidal activity and contribute these heterogeneous effects. This heterogeneity may be surprising in light of other studies that show more uniform effects of interneurons suppression on stimulus-evoked responses. However, these results are in alignment with our previous study (Natan et al., 2015), showing that across a broad population of neurons, PV suppression causes generalized increase in tone-evoked response while SOM suppression causes an increase specific to repeated tones.

Disparities between this and other studies may be explained by methodological differences. In most studies, these effects were measured in anesthetized animals, where GABAergic signaling may be strongly modulated, but here we used awake mice which should reflect more naturalistic cortical function. Another difference is optogenetic modulation in our study began 100ms before stimulus onset, allowing network dynamics to settle into a stable regime and isolate the effects of interneuron suppression, rather than confounding optogenetic onset effects with modulated interneuron dynamics. Since our experimental methodology resembles naturalistic conditions, the bidirectional effects of PV and SOM suppression observe here are more accurate reflections inhibitory dynamics.

Pyramidal neurons differed dramatically in the magnitude of adaptation we observed over the course of the tone train. For neuronal responses displaying measureable adaptation, SOM- and PV-mediated effects generally became more inhibitory across the tone train, contributing to adaptive suppression. Despite this similarity, SOM-mediated inhibition show more evidence of sensitivity to tone repetition that PVs lack. First, the effect of PV modulation is highly correlated from first to last tone pip, for both adaptive and non-adaptive neuronal responses. This means that PVs tend to exert the same type of modulatory effect across the tone train, suggesting that PVs are not affected by stimulus-history conditions. By contrast, SOM-mediated modulations on adaptive responses are more weakly correlated from first to last tone pip, and not correlated on non-adaptive responses. This means that regardless of the

type of modulation SOMs exert during the first tone, they generally become more inhibitory after the tone train, suggesting that SOMs are strongly affected by stimulus-history conditions. Additionally, the strength of SOMs inhibitory influence on responses correlates with the magnitude of adaptation, i.e. SOMs more strongly inhibit neurons that adapt strongly. By contrast, PVs inhibitory influence on responses to the last tone are not correlated with the magnitude of adaptation, while that to the first tone are anticorrelated, i.e. PVs more strongly inhibit neurons that do not adapt, at least during the first tone pip. Together, these results link SOM inhibition with adaptation and even though PV inhibition may also grow as tone pip responses decrease, it appears that PVs inhibition is not specifically modulated by the stimulus context. These results mirror our findings described in the previous chapter and in Natan et al., 2015, which pointed to PVs merely amplifying stimulus-specific adaptation, while SOMs were directly generating it. In this study, perhaps attenuation to repeated tones is amplified by PV inhibition and directly divine by SOM inhibition.

Some aspects of this study limit the extent to which we may generalize the results. One limitation is that we only explored adaptation for a single temporal regime, with the tones pip rate of 2.5 Hz. Increasing the tone frequency would potentially lead to a faster and stronger adaptation, and may recruit different interneuron circuits. Another limitation is that optogenetic manipulation did not allow for complete shutdown of interneuron activity. Therefore, we measure the effect of modulatory changes and reduced dynamic range of evoked spiking from interneurons, rather than

measuring the consequence of entirely removing a circuit element from the network. Future studies could repeat the experiments focusing on the questions of adaptation dynamics by focusing on changes in inter-tone interval, timing and strength of optogenetic modulation.

Extending our findings from Natan et al. (Natan et al., 2015), our work adds to evidence suggesting that SOM inhibition increases with stimulus repetition. Together, our results show that PV- or SOM-mediated inhibition is comparable for 'novel' and 'deviant' tone pip. PV suppression disinhibits responses to response to novel pips, the first pip of the train in this study, and similarly disinhibits responses to deviant tone pips in oddball stimuli. SOM suppression inhibits responses to novel pips and has no effect on deviant pips. As far as our testing can show, inhibition form either neuron is insensitive to the tones novelty, as a break from silence, or deviance, as a break from regularity. Thus, the common difference between tones in the respective studies is frequent repetition of the standard tone. SOMs appear to be uniquely sensitive to tone repetition.

Future studies could focus on testing the underlying mechanisms of this phenomenon. Previously, we found that SOMs and PVs themselves exhibit SSA, however a fractional subpopulation of SOMs spiked more strongly for repeated stimuli. We suggest four potential underlying mechanisms of stimulus-specific modulation by SOMs. First, repeated activation of facilitating synapses between SOMs and local pyramidal neurons may lead to increased inhibition, relative to excitation, specific to the

stimulus, despite reduced spiking. Second, a distinct subpopulation of SOMs for which stimulus-evoked responses increase with repetition may entirely generate the observed increase in inhibition. Third, stimulus-specific reduced firing rate among SOMs may disinhibit PVs relative to pyramidal neurons, leading to increased inhibition among pyramidal neurons. Fourth, SOMs may relay a top-down or modulatory signal generated elsewhere that drives greater inhibition in specific stimulus contexts. PVs are unlikely to be involved in any of these potential mechanisms due to their depressing synapses, exclusive pyramidal targeting, homogenously adaptive responses and relative lack of direct top-down input. Testing each of these possibilities may help to reveal the underlying mechanisms and point toward the function of this circuit.

Materials and Methods

Animals. All experiments were performed in adult male mice (supplier - Jackson Laboratories; age, 12-15 weeks; weight, 22-32 g; PV-Cre mice, strain: B6;129P2-Pvalbtm1(cre)Arbr/J; SOM-Cre: Ssttm2.1(cre)Zjh/J) housed at 28° C on a 12 h light-dark cycle with water and food provided *ad libitum*. In PV-Cre mice, Cre recombinase (Cre) is expressed in parvalbumin-positive interneurons; in SOM-Cre mice, Cre is expressed in somatostatin-positive interneurons (Taniguchi et al., 2011). This study was performed in strict accordance with the recommendations in the Guide for the Care and Use of Laboratory Animals of the National Institutes of Health. All of the animals were handled according to a protocol approved by the Institutional Animal Care and Use Committee of

the University of Pennsylvania (Protocol Number: 803266). All surgery was performed under isoflurane anesthesia, and every effort was made to minimize suffering.

Viral vectors. A Modified AAV encoding Archaerhodopsin (ArchT) under FLEX promoter was used for selective suppression in PV-Cre or SOM-Cre mice (AAV-CAG-FLEX-ArchT-GFP, UNC Vector Core).

Virus injection. 2-4 weeks prior to the start of experimental recordings, a 0.5 mm diameter craniotomy was drilled over primary auditory cortex (2.6 mm caudal and 4.1 mm lateral from bregma) under aseptic conditions while the mouse was anesthetized with isoflurane. A 750 nl bolus of AAV in water was injected into A1 (1 mm ventral from pia mater) using a stereotaxic syringe pump (Pump 11 Elite Nanomite, Harvard Apparatus). The skull overlying A1 was thinned by gentle drilling. The craniotomy was covered with bone wax and a small custom head-post was secured to the skull with dental acrylic.

Electrophysiological recordings. All recordings were carried out inside a double-walled acoustic isolation booth (Industrial Acoustics). Electrodes were targeted to A1 on the basis of stereotaxic coordinates and relation to blood vessels. In electrophysiological recordings, the location was confirmed by examining the click and tone pip responses of the recorded units for characteristic responses of neurons in A1, as described previously by our group in the rat (Carruthers et al., 2013) and by other groups in the mouse (Guo et al., 2012; Linden and Schreiner, 2003; Marlin et al., 2015). Mice were placed in the recording chamber, anesthetized with isoflurane, and the head-post secured to a

custom base, immobilizing the head. Dental acrylic and bone wax was gently drilled away exposing auditory cortex, and a silicon multi-channel probe (A1x32-tri-5mm-91-121-A32, Neuronexus) was slowly lowered to between 900 µl and 1100 mm into cortex, perpendicularly to the cortical surface. Electrophysiological data from 32 channels were bandpass filtered at 10-300 Hz for LFP and current-source density (CSD) analysis or at 600-6000 Hz for spike analysis, digitized at 32 kHz and stored for offline analysis (Neuralynx). Spikes belonging to single units were clustered using commercial software (Offline Sorter, Plexon)(Carruthers et al., 2013). Putative excitatory neurons were identified based on their expected response patterns to sounds and lack of significant suppression of the spontaneous FR due to light (Lima et al., 2009; Moore and Wehr, 2013).

Acoustic stimulus. Stimuli were delivered via a magnetic speaker (Tucker-David Technologies), directed toward the mouse's head. Speakers were calibrated prior to the experiments to +- 3 dB over frequencies between 1 and 40 kHz, by placing a microphone (Brüel and Kjaer) in the location of the ear contralateral to the recorded A1 hemisphere, recording speaker output and filtering stimuli to compensate for acoustic aberrations(Carruthers et al., 2013). First, to measure tuning, a train of 50 pure tones of frequencies spaced logarithmically between 1 and 80 kHz, at 65 dB SPL relative to 20 µPa, in pseudo-random order, was presented 20 times. Each tone was 100 ms long, with an inter-stimulus interval (ISI) of 300 ms. Frequency response functions were calculated online for several multiunits. To construct the set of tone pip trains, 10 frequencies,

spaced 0.13 octaves apart, were selected to cover a portion of multiunit frequency tuning curve from preferred to non-preferred frequencies. Each tone train consisted of 8 consecutive 100ms tone pips of the same frequency separated by 300 ms ISI. The frequency of each sequential train was pseudorandom and counterbalanced. Trains were separated by 2.4 seconds of silence.

Light presentation. An optic fiber was use to direct 532 nm laser light (Shanghai Laser & Optics Century). After positioning the silicon probe, an optic fiber was placed over the surface of auditory cortex. To limit Becquerel effect artifacts due to light striking electrodes, we positioned the optical fiber parallel to the silicon probe (Han et al., 2009; Kvitsiani et al., 2013). For each train, light may be cast over A1 to suppress interneurons during the first tone, the last tone, or during the silent period 400ms before or 400ms after the tone pip train. The light onset was 100 ms prior to tone onset, and lasted for 250 ms. At 180 mW/mm^2, light pulses were intense enough to significantly modulate multiunit activity throughout all cortical layers.

Immunohistochemistry. Brains were post-fixed in paraformaldehyde (4%, PFA) and cryoprotected in 30% sucrose. Coronal sections (40µm) were cut using a cryostat (Leica CM1860), washed in PBS containing 0.1% Triton X-100 (PBST; 3 washes, 5 min), incubated at room temperature in blocking solution (for PV 10% normal goat serum and 5% bovine serum albumin in PBST; for SOM 10% normal goat serum with 0.1% sodium azide and 2% cold water fish gelatin in PBS; 3h), and then incubated in primary antibody diluted in blocking solution overnight at 4°C. The following primary antibodies were

used: anti-PV (PV 25 rabbit polyclonal, 1:500, Swant) or anti-SOM (AB5494 rabbit polyclonal, 1:200, Millopore). After incubation, sections were washed in blocking solution (3 washes, 5 min), incubated for 2hr at room temperature with secondary antibodies (Alexa 594 goat anti-rabbit IgG; for PV 1:1000 and SOM 1:400), and then washed in PBS (3 washes, 5min each). Sections were mounted using fluoromount-G (Southern Biotech) and confocal images were acquired (Leica SP5). Cells were identified in independent fluorescent channels and subsequently scored for colocalization by hand using ImageJ's cell counter plug-in. Transfection efficiency is the percent of antibody labelled neurons which are co-labelled with GFP. Transfection specificity is the percent of GFP expressing neurons which are co-labeled with the antibody.

PSTHs and tone pip response firing rate. Termed neuron-frequency pairs, each of the 10 frequencies used in the tone pip trains was considered separately for each neuron unless otherwise stated. Single neuron-frequency pair PSTHs were calculated as the mean FR across all trains of that frequency. Light-on and light-off segments were pooled across different trials. Population PSTHs were calculated by first finding the mean FR across all included frequencies per neuron and normalizing by the mean peak firing rate in response to the first tone, and then finding the mean across the included population, and errorbars show standard error. Tone-evoked FRs displayed in boxplots and scatterplots were measured for each neuron-frequency pair as the mean FR over 50 ms post tone onset. Spontaneous activity before tone pip trains was measured from 400 ms

to 350 ms before the first tone onset, and spontaneous activity after tone pip trains was measured from 400 ms to 450 ms after the last tone onset.

Linear fits across frequencies. Linear fits were calculated using the linear regression (fitlm.m, Matlab) over 10 data points, one for each of the 10 frequencies tested. For each comparison condition (first or last tone pip response, with or without optogenetic suppression) the 10 data points were separately calculated as the mean FR over all repeats fitting those conditions. Linear fit error lines indicates standard error. Population average line was calculated as the mean of each lines y value across x from 0 to 1, and errorbars show standard error.

Statistical tests. Sign rank tests were used to test if first or last tone pip-evoked FRs or spontaneous FRs were different per trial within single neurons. Rank sum tests were used to test FR differences between light conditions within single neurons. Population comparisons were tested using the student's t-test. Bonferroni correction was applied for multiple comparisons. In all Figure 4.s, single, double and triple stars indicate $p < 0.05$, 0.01 and 0.001 respectively.

Bibliography

Aizenberg, M., Mwilambwe-Tshilobo, L., Briguglio, J.J., Natan, R.G., Geffen, M.N., 2015. Bidirectional Regulation of Innate and Learned Behaviors That Rely on Frequency Discrimination by Cortical Inhibitory Neurons. PLoS Biol 13, e1002308.

Atallah, B.V., Bruns, W., Carandini, M., Scanziani, M., 2012. Parvalbumin-expressing interneurons linearly transform cortical responses to visual stimuli. Neuron 73, 159-170.

Baccus, S.A., Meister, M., 2002. Fast and slow contrast adaptation in retinal circuitry. Neuron 36, 909-919.

Carruthers, I.M., Natan, R.G., Geffen, M.N., 2013. Encoding of ultrasonic vocalizations in the auditory cortex. J Neurophysiol 109, 1912-1927.

Guo, W., Chambers, A.R., Darrow, K.N., Hancock, K.E., Shinn-Cunningham, B.G., Polley, D.B., 2012. Robustness of cortical topography across fields, laminae, anesthetic states, and neurophysiological signal types. J Neurosci 32, 9159-9172.

Hamm, J.P., Yuste, R., 2016. Somatostatin Interneurons Control a Key Component of Mismatch Negativity in Mouse Visual Cortex. Cell Rep 16, 597-604.

Han, X., Qian, X., Bernstein, J.G., Zhou, H.H., Franzesi, G.T., Stern, P., Bronson, R.T., Graybiel, A.M., Desimone, R., Boyden, E.S., 2009. Millisecond-timescale optical control of neural dynamics in the nonhuman primate brain. Neuron 62, 191-198.

Kvitsiani, D., Ranade, S., Hangya, B., Taniguchi, H., Huang, J.Z., Kepecs, A., 2013. Distinct behavioural and network correlates of two interneuron types in prefrontal cortex. Nature 498, 363-366.

Lee, S.H., Kwan, A.C., Zhang, S., Phoumthipphavong, V., Flannery, J.G., Masmanidis, S.C., Taniguchi, H., Huang, Z.J., Zhang, F., Boyden, E.S., Deisseroth, K., Dan, Y., 2012. Activation of specific interneurons improves V1 feature selectivity and visual perception. Nature 488, 379-383.

Lima, S., Hromadka, T., Znamenskiy, P., Zador, A., 2009. PINP: a new method of tagging neuronal populations for identification during in vivo electrophysiological recording. PLoS One 4, e6099.

Linden, J.F., Schreiner, C.E., 2003. Columnar transformations in auditory cortex? A comparison to visual and somatosensory cortices. Cereb Cortex 13, 83-89.

Marlin, B.J., Mitre, M., D'Amour J, A., Chao, M.V., Froemke, R.C., 2015. Oxytocin enables maternal behaviour by balancing cortical inhibition. Nature 520, 499-504.

Moore, A.K., Wehr, M., 2013. Parvalbumin-expressing inhibitory interneurons in auditory cortex are well-tuned for frequency. J Neurosci 33, 13713-13723.

Natan, R.G., Briguglio, J.J., Mwilambwe-Tshilobo, L., Jones, S.I., Aizenberg, M., Goldberg, E.M., Geffen, M.N., 2015. Complementary control of sensory adaptation by two types of cortical interneurons. eLife 4, pii: e09868.

Phillips, E.A., Hasenstaub, A.R., 2016. Asymmetric effects of activating and inactivating cortical interneurons. Elife 5.

Seybold, B.A., Phillips, E.A., Schreiner, C.E., Hasenstaub, A.R., 2015. Inhibitory Actions Unified by Network Integration. Neuron 87, 1181-1192.

Taniguchi, H., He, M., Wu, P., Kim, S., Paik, R., Sugino, K., Kvitsiani, D., Fu, Y., Lu, J., Lin, Y., Miyoshi, G., Shima, Y., Fishell, G., Nelson, S.B., Huang, Z.J., 2011. A resource of Cre driver lines for genetic targeting of GABAergic neurons in cerebral cortex. Neuron 71, 995-1013.

Wark, B., Lundstrom, B.N., Fairhall, A., 2007. Sensory adaptation. Curr Opin Neurobiol 17, 423-429.

Wilson, N.R., Runyan, C.A., Wang, F.L., Sur, M., 2012. Division and subtraction by distinct cortical inhibitory networks in vivo. Nature 488, 343-348.

5. Conclusions

In this dissertation, we described several distinct experiments that explore how neuronal activity the primary auditory cortex adapts to variations in sound stimulus contexts. In Chapter 2, we tested how stimulus temporal correlation modulates the input-response profile of neurons in the primary auditory cortex, and our linear non-linear modeling revealed that they adaptively compensate for this particular stimulus feature through gain-control. In Chapter 3, we used optogenetic methods to test how interneuron populations in the primary auditory cortex modulate responses to standard versus deviant tones, showing that inhibition from SOMs suppresses responses specifically to repeated tones while inhibition from PVs simply amplifies the differences in response magnitude. Further we found that SOMs and PVs themselves exhibit adaptation at similar levels as local pyramidal neurons. These results were incorporated into a rate model of cortical dynamics, which found that SOM interneurons play a special role in SSA. In Chapter 4, we again used optogenetic methods to more closely examine how PVs and SOMs modulate responses before and after adaptation across frequency tuning curves. We found that inhibition from SOMs increased, modulating frequency tuning in a gain-like manner, as adaptation developed and was also correlated with the magnitude of adaptation. By contrast, inhibition from PVs was largely insensitive to tone repetition or the magnitude of adaptation. Together, these

results deliver insights to the extent, mechanisms and functions of cortical sensory adaptation.

Though the approaches are quite different, these studies share a common goal of exploring how the auditory cortex adapts to persistent temporal regularities in sound stimuli. Natural sounds contain a mix of spectrally and temporally correlated features with parametrically constrained statistical variations. In order to inform how the auditory cortex encodes natural sounds, we chose to focus separately on temporal aspects of stimulus dynamics rather than spectro-temporal correlations that could confound interpretation of the results. In Chapter 2, our custom designed dynamic random cord stimuli exhibited a range in temporal correlation independent from variation in spectral modulation. In Chapters 3 and 4, oddball sequences and single frequency tone trains explore regularity across narrow frequency bands. The adaptive phenomena tested in each experiment may operate at overlapping or different timescales. Accordingly, we tested temporal amplitude modulations ranging from 200 Hz to 12.5 Hz among the dynamic random cord stimuli and only 2.5 Hz for tone trains. We found that the time constant of adaptation ranged widely across neurons from 100 ms up to 7 s for changes in temporal correlation, and similarly from 100 ms to greater than 3 seconds for tone train stimuli. We found that across these difference dynamic ranges, adaptation plays an important role in controlling cortical responses. Future studies can address the downstream mechanisms for inferring temporal dynamics in the presence of adaptation.

Our findings indicate that PVs and SOMs may both play a role in adaptation to broadband stimuli; PVs by non-selectively amplifying stimulus-response differences and SOMs by inducing gain-like adaptation across the spectrum. Interestingly, the interneurons themselves may operate on different time scales of adaptation. Through direct thalamocortical input to PVs, inhibitory feedforward circuit dynamics could mediate adaptive responses more quickly. For instance, PVs have been shown to modulate the stimulus integration time window by around 10 ms (Gabernet et al., 2005), and could produce fast acting adaptation within very short time scales. Feedback and top-down circuits, which SOMs may participate in, would generate an adaptive signal more slowly. In Chapter 3, the tone-by-tone increase in SOM mediated inhibition indicates that SOMs may operate on longer timescales. Perhaps the difference in adaptation time scales among pyramidal neurons is due to differential weighting of PV and SOM mediated inhibitory input. These findings may help to constrain future models and understanding of temporally dynamic aspects of auditory cortical responses to natural sounds.

Our findings likely generalize to other sensory modalities and cortical areas. Beyond auditory cortex, studies have described adaptation to stimulus contrast in visual (Lesica et al., 2007) and olfactory cortex (Kadohisa and Wilson, 2006). Our experiments showed that gain-control underlying contrast adaptation similarly underlies adaptation to temporal correlation. By extension, cortical receptive fields in vision, somatosensation and olfaction may also exhibit sensitivity to temporal correlations in respective stimuli, compensate through gain-control and integrate over rapid stimulus

variations over their receptive fields. Though there are variations, interneurons in primary sensory cortices largely share common circuit architecture (Douglas and Martin, 2004). Thus, the roles of PV and SOM inhibition in adaptation is likely analogous across modalities, even if the statistics of temporal modulations in natural auditory scenes differs from those of natural stimuli in other modalities. In fact, a recent study confirms that SOMs modulate cortical responses to standard and deviant visual stimuli differentially (Hamm and Yuste, 2016). Thus, we expect that our experimental findings uncover general principles and mechanisms of cortical sensory adaptation.

The adaptive properties we describe may also underlie complex adaptive phenomena beyond temporal context sensitivity in sensory cortex. Divisive normalization, considered a canonical cortical computation, describes a spatial context-specific adaptation (Carandini and Heeger, 2011); a sensory neuron's spiking response to stimuli falling within a central excitatory receptive field are normalized by the mean intensity of the stimuli falling within a broader suppressive surround subfield. Importantly, the center and surround subfields exhibit independent sensitivity to the temporal regularities of the stimulus (Durand et al., 2007). The sensitivity to temporal correlations described in Chapter 2 may constrain models of divisive normalization in this process; a receptive field's smaller excitatory and larger suppressive subfields likely each integrate rapid stimulus variation over proportional timescales. Thus it would be interesting to test how gain-control acts independently between these subfield, and controls their combined output. Such computation structure adds a spatial component to stimulus context sensitivity. Local inhibition may mediate surround suppression in

visual cortex (Haider et al., 2010). In order to carry a context sensitive normalization signal, we would expect the inhibitory surround to exhibit stimulus tuning or stimulus-specific modulation. Our findings in Chapters 3 and 4 indicate that SOMs exhibit stimulus-specific modulation while PVs are largely insensitive to stimulus context. Combined with SOMs' finer stimulus tuning, evidence points to SOMs as a reasonable candidate for mediating surround suppression. If this is found to be the case, SOMs would be critical for spatial, in addition to temporal, context sensitivity. In Sum, our experimental findings may help shape the models and mechanisms of canonical computations in the brain.

As essential components in cortical circuits, interneurons are involved with myriad cortical functions. Since our findings point to these interneurons, particularly SOMs, playing a role in context-specific adaptation, how else might they impact sensory functions? Behavior, attention and emotional states have each been shown to modulate gain in sensory cortex stimulus responses (Mineault et al., 2016; Pourtois et al., 2013). Our findings suggest that SOMs are the more likely interneuronal subtype to support these state-dependent gain modulations, especially through top-down circuits.

Our results in Chapters 3 and 4 indicate that both PVs and SOMs could underlie behavioral habituation to regularly presented stimuli, since they both increase relative suppression to repeated tones. Adaptation through interneurons may be a necessary mechanism for long term cortical plasticity and sensory learning. Days after repeated exposure to a tone of a specific frequency, pyramidal neurons and SOMs in primary auditory cortex exhibited altered sensitivity to that stimulus in a context specific matter

(Kato et al., 2015); If the prior tones had predicted reward in a behavioral task, pyramidal sensitivity was enhanced while SOM sensitivity was diminished, suggesting that SOMs are involved in stimulus reward learning. If the prior tones were non-predictive in a passive task, pyramidal sensitivity was diminished while SOM sensitivity was enhanced suggesting SOMs are involved in habituation. This context-sensitive plasticity resembles our findings in Chapter 3 and suggest that stimulus-specific SOM inhibition at the time of initial stimulus exposure may set up the necessary conditions for neuronal plasticity that allows for habituation and reward-learning. In combination with recent findings, our results suggest that SOMs may play a distinct role from other interneurons in cortical sensory function.

Our findings further suggest that interneurons shape sensory perception through adaptive inhibition. As described in Chapter 1, perception can be modulated by adaptive processes and interneurons. Since we have shown that interneurons shape adaptation, we can extrapolate that the specific roles that SOMs and PVs could differentially impact perception. As PVs and SOMs reshape tuning curves differentially during the course of adaptation, broadband modulation by PVs may improve neurometric and behavioral detection, while specific inhibition by SOMs may drive improved discrimination. It is possible that these interneurons control adaptive modulations in concert in order to produce maximally useful information about the stimulus and support performance.

Our findings also suggest that neurological damage, disorders or psychoactive drugs effecting interneuron signaling would lead to altered or malfunctioning sensory adaptation. By extension, these conditions would directly impact the regulation of

cortical encoding of stimulus dynamic range, resolution, and salience. These changes may be observed as altered sensory perception such as tinnitus and other auditory hallucinations as well as deafness or loss of hearing acuity, which are common symptoms of many cortical disorders. Thus, adaptive dysfunction due to disorders affecting interneuron in adaptation may underlie clinical symptoms. Not surprisingly, pharmacological compounds that target inhibitory signaling appear to reduce these symptoms (Richardson et al., 2012). Our finding may eventually guide medicine toward targeting specific interneuron subtypes, such as PVs and SOMs, for more finely tuned treatments.

Bibliography

Carandini, M., Heeger, D.J., 2011. Normalization as a canonical neural computation. Nat Rev Neurosci 13, 51-62.

Douglas, R.J., Martin, K.A., 2004. Neuronal circuits of the neocortex. Annu Rev Neurosci 27, 419-451.

Durand, S., Freeman, T.C., Carandini, M., 2007 Temporal properties of surround suppression in cat primary visual cortex. Vis Neurosci 24, 679-690.

Gabernet, L., Jadhav, S.P., Feldman, D.E., Carandini, M., Scanziani, M., 2005. Somatosensory integration controlled by dynamic thalamocortical feed-forward inhibition. Neuron 48, 315-327.

Haider, B., Krause, M.R., Duque, A., Yu, Y., Touryan, J., Mazer, J.A., McCormick, D.A., 2010. Synaptic and network mechanisms of sparse and reliable visual cortical activity during nonclassical receptive field stimulation. Neuron 65, 107-121.

Hamm, J.P., Yuste, R., 2016. Somatostatin Interneurons Control a Key Component of Mismatch Negativity in Mouse Visual Cortex. Cell Rep 16, 597-604.

Kadohisa, M., Wilson, D.A., 2006. Separate encoding of identity and similarity of complex familiar odors in piriform cortex. Proc Natl Acad Sci U S A 103, 15206-15211.

Kato, H.K., Gillet, S.N., Isaacson, J.S., 2015. Flexible Sensory Representations in Auditory Cortex Driven by Behavioral Relevance. Neuron 88, 1027-1039.

Lesica, N.A., Jin, J., Weng, C., Yeh, C.I., Butts, D.A., Stanley, G.B., Alonso, J.M., 2007. Adaptation to stimulus contrast and correlations during natural visual stimulation. Neuron 55, 479-491.

Mineault, P.J., Tring, E., Trachtenberg, J.T., Ringach, D.L., 2016. Enhanced Spatial Resolution During Locomotion and Heightened Attention in Mouse Primary Visual Cortex. J Neurosci 36, 6382-6392.

Pourtois, G., Schettino, A., Vuilleumier, P., 2013. Brain mechanisms for emotional influences on perception and attention: what is magic and what is not. Biol Psychol 92, 492-512.

Richardson, B.D., Brozoski, T.J., Ling, L.L., Caspary, D.M., 2012. Targeting inhibitory neurotransmission in tinnitus. Brain Res 1485, 77-87.